Compact FDTD and Full Wave Finite Difference (FWFD)

Two novel finite difference techniques for solving eigenvalue problems in Electromagnetics

Ali Asi

B.Sc., Electrical Eng., Iran University of Science and Technology, 1988
M.Sc., Electrical Eng., Tehran University, 1990

A thesis submitted to the University of Manitoba in partial fulfillment of the requirements for a degree of Doctor of Philosophy in Electrical Engineering

Department of Electrical and Computer Engineering
University of Manitoba
Winnipeg, Manitoba, Canada R3T-5V6
Ali_Asi@UManitoba.CA

ISBN 0-612-12964-0

Canada

Name Ali Asi

Dissertation Abstracts International is arranged by broad, general subject categories. Please select the one subject which most nearly describes the content of your dissertation. Enter the corresponding four-digit code in the spaces provided.

Compact FDTD and Full Wave Finite Difference (FW FD) | 0544 | U·M·I

SUBJECT TERM | SUBJECT CODE

Subject Categories

THE HUMANITIES AND SOCIAL SCIENCES

COMMUNICATIONS AND THE ARTS
Architecture 0729
Art History 0377
Cinema 0900
Dance 0378
Fine Arts 0357
Information Science 0723
Journalism 0391
Library Science 0399
Mass Communications 0708
Music 0413
Speech Communication 0459
Theater 0465

EDUCATION
General 0515
Administration 0514
Adult and Continuing 0516
Agricultural 0517
Art 0273
Bilingual and Multicultural 0282
Business 0688
Community College 0275
Curriculum and Instruction 0727
Early Childhood 0518
Elementary 0524
Finance 0277
Guidance and Counseling 0519
Health 0680
Higher 0745
History of 0520
Home Economics 0278
Industrial 0521
Language and Literature 0279
Mathematics 0280
Music 0522
Philosophy of 0998
Physical 0523
Psychology 0525
Reading 0535
Religious 0527
Sciences 0714
Secondary 0533
Social Sciences 0534
Sociology of 0340
Special 0529
Teacher Training 0530
Technology 0710
Tests and Measurements 0288
Vocational 0747

LANGUAGE, LITERATURE AND LINGUISTICS
Language
- General 0679
- Ancient 0289
- Linguistics 0290
- Modern 0291

Literature
- General 0401
- Classical 0294
- Comparative 0295
- Medieval 0297
- Modern 0298
- African 0316
- American 0591
- Asian 0305
- Canadian (English) 0352
- Canadian (French) 0355
- English 0593
- Germanic 0311
- Latin American 0312
- Middle Eastern 0315
- Romance 0313
- Slavic and East European 0314

PHILOSOPHY, RELIGION AND THEOLOGY
Philosophy 0422
Religion
- General 0318
- Biblical Studies 0321
- Clergy 0319
- History of 0320
- Philosophy of 0322

Theology 0469

SOCIAL SCIENCES
American Studies 0323
Anthropology
- Archaeology 0324
- Cultural 0326
- Physical 0327

Business Administration
- General 0310
- Accounting 0272
- Banking 0770
- Management 0454
- Marketing 0338

Canadian Studies 0385
Economics
- General 0501
- Agricultural 0503
- Commerce-Business 0505
- Finance 0508
- History 0509
- Labor 0510
- Theory 0511

Folklore 0358
Geography 0366
Gerontology 0351
History
- General 0578
- Ancient 0579
- Medieval 0581
- Modern 0582
- Black 0328
- African 0331
- Asia, Australia and Oceania 0332
- Canadian 0334
- European 0335
- Latin American 0336
- Middle Eastern 0333
- United States 0337

History of Science 0585
Law 0398
Political Science
- General 0615
- International Law and Relations 0616
- Public Administration 0617

Recreation 0814
Social Work 0452
Sociology
- General 0626
- Criminology and Penology 0627
- Demography 0938
- Ethnic and Racial Studies 0631
- Individual and Family Studies 0628
- Industrial and Labor Relations 0629
- Public and Social Welfare 0630
- Social Structure and Development 0700
- Theory and Methods 0344

Transportation 0709
Urban and Regional Planning 0999
Women's Studies 0453

THE SCIENCES AND ENGINEERING

BIOLOGICAL SCIENCES
Agriculture
- General 0473
- Agronomy 0285
- Animal Culture and Nutrition 0475
- Animal Pathology 0476
- Food Science and Technology 0359
- Forestry and Wildlife 0478
- Plant Culture 0479
- Plant Pathology 0480
- Plant Physiology 0817
- Range Management 0777
- Wood Technology 0746

Biology
- General 0306
- Anatomy 0287
- Biostatistics 0308
- Botany 0309
- Cell 0379
- Ecology 0329
- Entomology 0353
- Genetics 0369
- Limnology 0793
- Microbiology 0410
- Molecular 0307
- Neuroscience 0317
- Oceanography 0416
- Physiology 0433
- Radiation 0821
- Veterinary Science 0778
- Zoology 0472

Biophysics
- General 0786
- Medical 0760

EARTH SCIENCES
Biogeochemistry 0425
Geochemistry 0996
Geodesy 0370
Geology 0372
Geophysics 0373
Hydrology 0388
Mineralogy 0411
Paleobotany 0345
Paleoecology 0426
Paleontology 0418
Paleozoology 0985
Palynology 0427
Physical Geography 0368
Physical Oceanography 0415

HEALTH AND ENVIRONMENTAL SCIENCES
Environmental Sciences 0768
Health Sciences
- General 0566
- Audiology 0300
- Chemotherapy 0992
- Dentistry 0567
- Education 0350
- Hospital Management 0769
- Human Development 0758
- Immunology 0982
- Medicine and Surgery 0564
- Mental Health 0347
- Nursing 0569
- Nutrition 0570
- Obstetrics and Gynecology 0380
- Occupational Health and Therapy 0354
- Ophthalmology 0381
- Pathology 0571
- Pharmacology 0419
- Pharmacy 0572
- Physical Therapy 0382
- Public Health 0573
- Radiology 0574
- Recreation 0575
- Speech Pathology 0460
- Toxicology 0383

Home Economics 0386

PHYSICAL SCIENCES
Pure Sciences
Chemistry
- General 0485
- Agricultural 0749
- Analytical 0486
- Biochemistry 0487
- Inorganic 0488
- Nuclear 0738
- Organic 0490
- Pharmaceutical 0491
- Physical 0494
- Polymer 0495
- Radiation 0754

Mathematics 0405
Physics
- General 0605
- Acoustics 0986
- Astronomy and Astrophysics 0606
- Atmospheric Science 0608
- Atomic 0748
- Electronics and Electricity 0607
- Elementary Particles and High Energy 0798
- Fluid and Plasma 0759
- Molecular 0609
- Nuclear 0610
- Optics 0752
- Radiation 0756
- Solid State 0611

Statistics 0463

Applied Sciences
Applied Mechanics 0346
Computer Science 0984
Engineering
- General 0537
- Aerospace 0538
- Agricultural 0539
- Automotive 0540
- Biomedical 0541
- Chemical 0542
- Civil 0543
- Electronics and Electrical 0544
- Heat and Thermodynamics 0348
- Hydraulic 0545
- Industrial 0546
- Marine 0547
- Materials Science 0794
- Mechanical 0548
- Metallurgy 0743
- Mining 0551
- Nuclear 0552
- Packaging 0549
- Petroleum 0765
- Sanitary and Municipal 0554
- System Science 0790

Geotechnology 0428
Operations Research 0796
Plastics Technology 0795
Textile Technology 0994

PSYCHOLOGY
General 0621
Behavioral 0384
Clinical 0622
Developmental 0620
Experimental 0623
Industrial 0624
Personality 0625
Physiological 0989
Psychobiology 0349
Psychometrics 0632
Social 0451

COMPACT FDTD AND FULL WAVE FINITE DIFFERENCE (FWFD)

by

ALI ASI

A Thesis submitted to the Faculty of Graduate Studies of the University of Manitoba in partial fulfillment of the requirements of the degree of

DOCTOR OF PHILOSOPHY

Dedicated to my parents,

Firouz and Pari Asi

Acknowledgements

I WISH to thank Professor L. Shafai for his invaluable counsel, unyielding optimism and enthusiasm during this research. Indeed, there are not enough words to express my heartfelt gratitude for him.

Special thanks are due to my wife, Tala, for her encouragement and support.

TABLE OF CONTENTS

Abstract

IN GENERAL, microwave devices can be split into two major categories, active and passive devices. In this thesis, an attempt is made to address one of the most important issues in the realm of passive devices, guided wave structures. A quick survey of the literature published in the last four decades reveals the fact that analysis of waveguides has always posed itself as a challenge to researchers. Noting that Maxwell's equations are a set of eight partial differential equations of six vector field quantities, $E_x, E_y, E_z, H_x, H_y, H_z$, in terms of four space and time variables, x, y, z, t, it can be understood why the ultimate solution technique for solving electromagnetic problems with any kind of complexity has yet to be found.

By definition, a waveguide is a three dimensional structure with exactly the same cross section at any arbitrary point along the z direction. In microwave engineering terminology, this is equivalent to not having any discontinuity along the direction of wave propagation. From analytical point of view, it can be proved that under these circumstances, all the information regarding this three dimensional structure can be extracted from a two dimensional analysis of its cross section. Solving the problem for this two dimensional cross section will result in an eigenvalue problem. For any eigenvalue problem, the solution should be expressed in terms of eigenvalue pairs, i.e. (λ, X), in which λ and X represent eigenvalues and eigenvectors, respectively. Interestingly, these eigenvalue and

eigenvector pairs correspond to two common terms in microwave engineering. As shown later on, eigenvalues are nothing but the points generated by crossing the dispersion curves with a horizontal line and eigenvectors, on the other hand, contain all the information needed to draw the field patterns of different field components inside a waveguide.

In this thesis, two new methods have been proposed which are capable of solving a waveguide eigenvalue problem completely and efficiently. The first method is specialized for solving the eigenvalues and is called the **COMPACT FINITE DIFFERENCE TIME DOMAIN** (Compact FDTD). The second method solves the other half of the problem, eigenvectors or field patterns, and is called the **FULL WAVE FINITE DIFFERENCE** (FWFD) technique. Other new signal processing and estimation techniques have also been proposed and investigated in a separate chapter. These signal processing techniques, **AUTO-REGRESSIVE** (AR), **AUTO-REGRESSIVE MOVING AVERAGE** (ARMA) and **PRONY,** have the potential of enhancing the efficiency of time domain methods. In addition to those, a new **SINGULAR VALUE DECOMPOSITION** (SVD) Based Prony method is also contributed. In each chapter, the simulation results of these new techniques are presented and compared to the results obtained using other standard procedures. Specifically, complicated problems containing diagonally anisotropic materials are addressed in chapters three and four.

The **CFDTD** and **FWFD** can be integrated as the numerical engine of a powerful CAD package to calculate the dispersion curves and field patterns of an inhomogeneous, anisotropic waveguide. The computational efficiency gained using these new methods, when combined with advanced signal processing techniques, can easily exceed those achievable by most other numerical techniques.

Chapter One

PROBLEM DESCRIPTION AND OBJECTIVES

I.A. Introduction

FINITE DIFFERENCE (Time Domain) method has been selected as the main numerical tool throughout this thesis. Therefore, in the first section of introduction, a few justifications for such a selection are provided followed by a comparative study between the **FD(TD)** and other methods. Then, in the second section, samples of different **M**icrowave **w**aveguides and **O**ptical **w**aveguides accompanied by the final objectives of a guided wave analysis are presented. This helps in understanding the purpose behind such an analysis. A brief formulation of the problem which is going to be analyzed is the subject of the third section. Finally, in the last section, a few common differences between a microwave guided wave analysis and an optical one are pointed out.

I.B. Why finite difference?

THE ANALYSIS of guided wave structures is one of the few subjects that constitutes the major part of microwave engineering [1]. Even now, the majority of papers published in transactions and technical journals are devoted to the applications of techniques such as the Moment, Finite Element and Spectral Domain methods; to guided wave structures such as microstrip, slot, coplanar and optical fiber transmission lines.

Due to the vast variety of available numerical techniques, an a priori insight to the capabilities and speed of each of these methods can be quite useful. There are usually sev-

eral factors which can affect one's decision for choosing a specific method for a particular problem. Among them are:

- *The topology of the structure, i.e. two or three dimensional, inhomogenity, anisotropicity, bounded or open,...*
- *Computer resources, **CPU** elapsed time and **RAM**,....*
- *Complexity and versatility of a method*

As a general rule, the more analytical processes that can be done prior to starting a numerical procedure, the less computational burden will be left for the computer to handle. Therefore, in those instances that a strong computer resource is not available, it is highly recommended that the problem be dealt with using analytical methods as much as possible. In fact, this is one of the reasons that in early stages of microwave developments, researchers attempted to reduce every complicated structure to a simple one to be solved using rigorous or analytical methods. Needless to say these rigorous, or analytical, solutions can only be found for some particular geometries under certain simplifying assumptions.

In the wake of recent advances in computer technology, a general trend towards less analytical, and naturally more numerical methods, has started. As a matter of fact, finite difference methods are among numerical methods from this category with a strong capability to deal with arbitrary geometries, i.e. *versatility*. For this class of numerical methods, the analytical pre-processing and the mathematically involved procedures before passing the problem to the computer are almost nonexistent, i.e. *less complexity*. The only

restriction which had previously limited the wide spread use of these methods is their dependency on large computer resources which were not available until recently. Table (I .1) offers a good comparison between the characteristics of different methods [2].

TABLE I .1 Comparison table between different methods

Method	Memory	CPU time	Generality	Pre-processing
Finite Difference	L	L	VG	Nil
Finite Element	L	ML	VG	S
Boundary Element	M	M	VG	S
TLM	ML	ML	VG	S
Integral Equation	SM	SM	G	M
Mode Matching	M	SM	G	M
Transverse Resonance	SM	SM	Ma	M
Method of Lines	M	S	G	L
Spectral Domain	S	S	Ma	L

L=*large,* **M**=*moderate,* **S**=*small,* **VG**=*very good,* **G**=*good,* **Ma**=*marginal.*

I.C. Guided wave analysis

GENERALLY SPEAKING, there are two major categories of guided wave structures, microwave and optical waveguides. Some of the most common configurations of both categories are illustrated in what follows. Basically, the methods presented in this thesis are capable of dealing with all these configurations.

I.C.1 Microwave integrated waveguides [4]

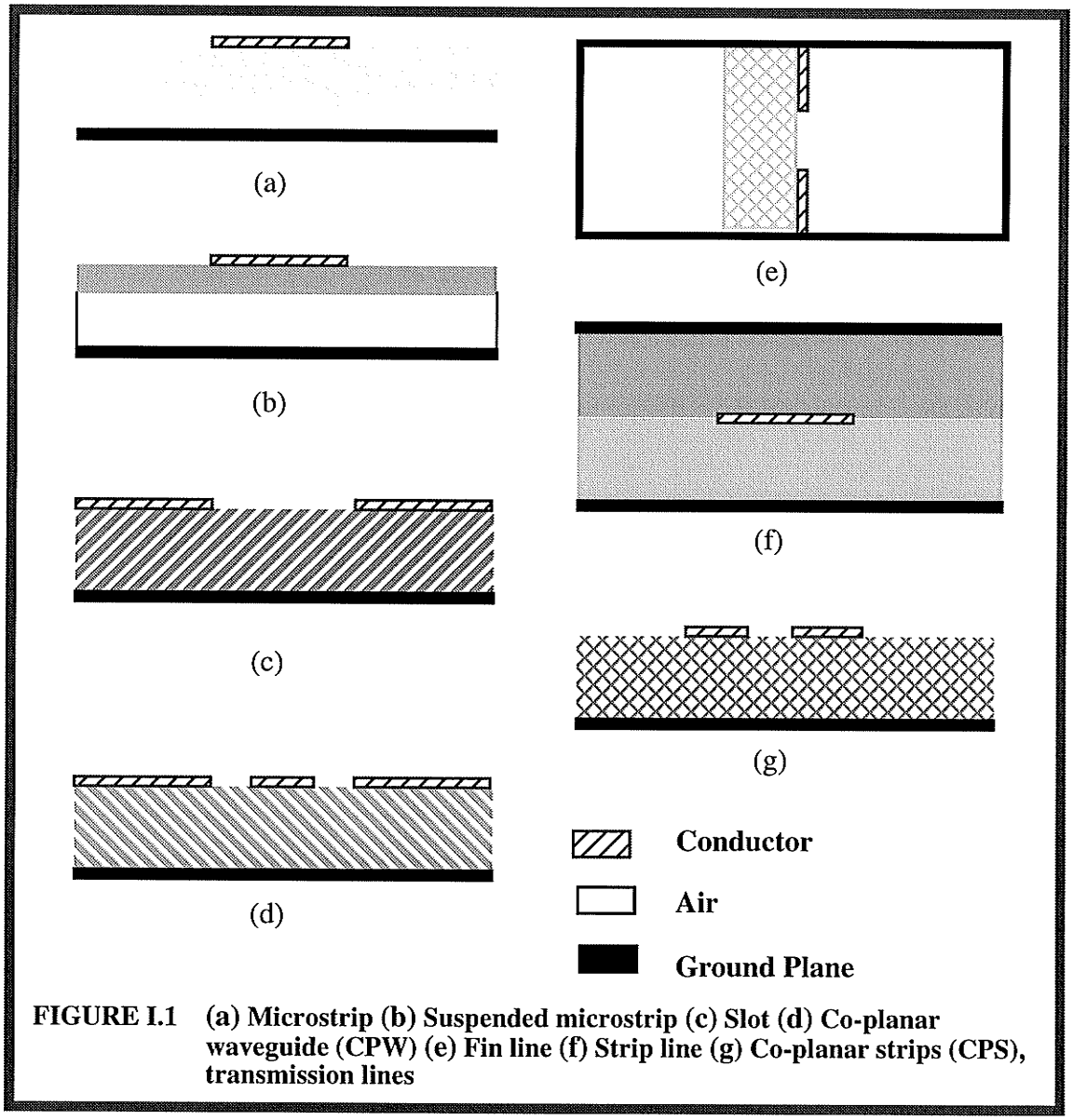

FIGURE I.1 **(a) Microstrip (b) Suspended microstrip (c) Slot (d) Co-planar waveguide (CPW) (e) Fin line (f) Strip line (g) Co-planar strips (CPS), transmission lines**

I.C.2 Optical waveguides [5]

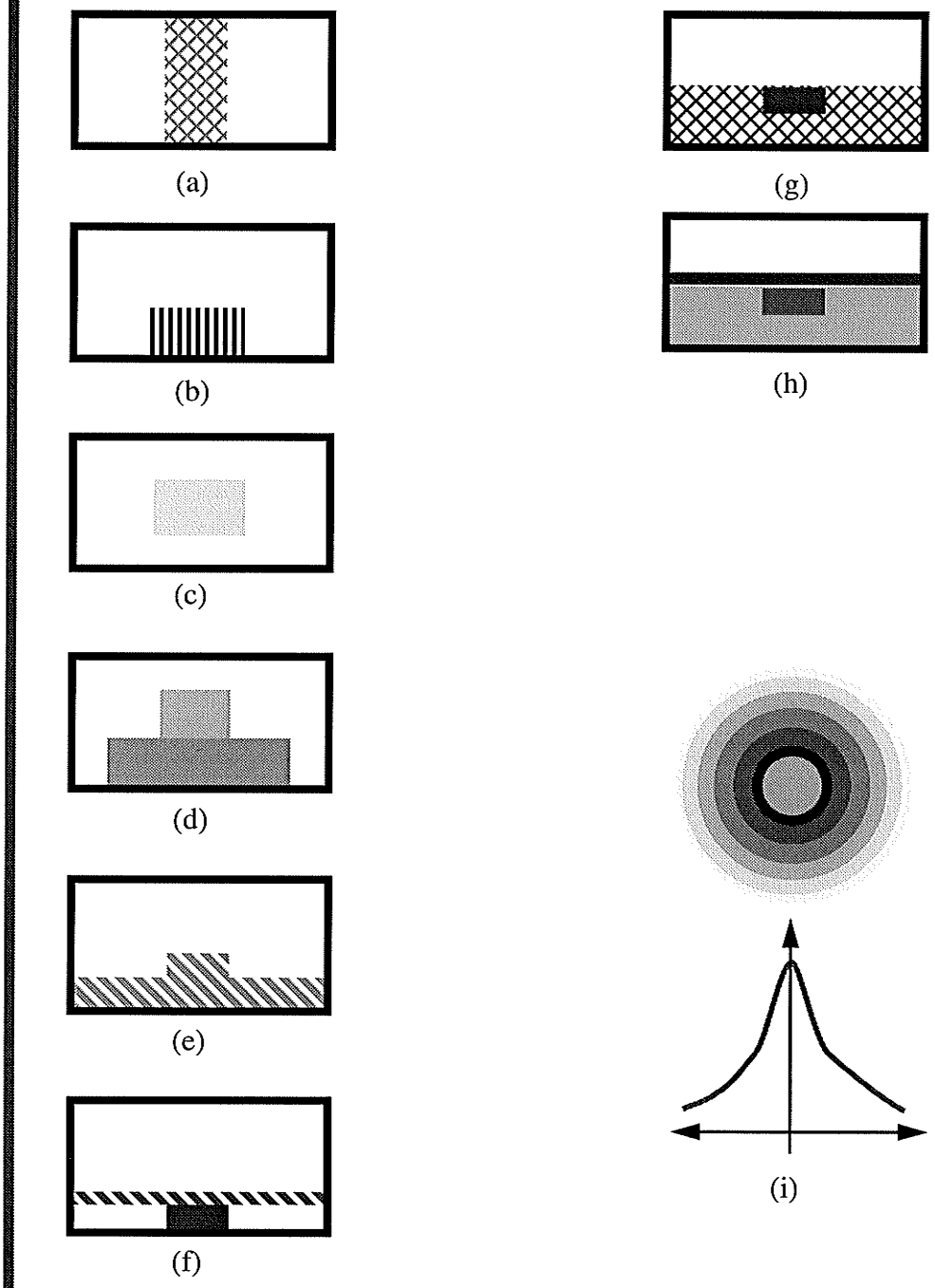

FIGURE I.2 **(a) Non-radiative dielectric (b) Dielectric image line (c) Dielectric (d) Strip dielectric, or insulated image (e) Ridge (f) Inverted strip (g) Channel or embedded strip (h) Strip slab (i) Graded index, waveguides**

I.D. Objectives of Analysis

USUALLY, the final objective of any analysis strongly depends on its very own nature. But, in general, one can summarize the most common objectives of guided wave analysis as follows:

- *Field distribution, i.e.* E_x, E_y, E_Z, H_x, H_y, H_z *patterns inside the waveguide*
- *Cut off frequencies of different modes*
- *Dispersion curve, i.e.* β *versus* ω
- *Studying the conditions to amplify a particular mode and/or attenuate the others*
- *Studying the effects of feed and output positions, type of excitation,...*
- *Studying the effects of different shielding on the modes*
- *Studying the effects of different dielectrics as the propagation media, like inhomogenity, anisotropicity, chirality, lossy,...*

Among these, maybe the first three are the basic objectives of any type of analysis. Yet, it has to be mentioned that not all numerical methods have the capability of investigating all the above items. For instance, some of the methods like perturbation method can be useful only in determining the cut off frequencies or at most the dispersion curve. On the other hand, the two methods proposed throughout this thesis are capable of answering all the above mentioned questions effectively and efficiently. Explicit solution approaches for most of the items in the aforementioned list of objectives are presented by applying the

methods to different structures. However, the power of the methods in addressing all the above mentioned objectives becomes apparent by investigating the final formulations.

I.E. Mathematical formulation of the problem

STARTING from Maxwell's equations, one can proceed to formulate the problem:

$$\vec{\nabla} \times \vec{E} = -\mu \frac{\partial \vec{H}}{\partial t} - \rho_m \vec{H} \qquad \textbf{(I.1.a)}$$

$$\vec{\nabla} \times \vec{H} = \frac{\partial \vec{D}}{\partial t} - \sigma \vec{E} \qquad \textbf{(I.1.b)}$$

$$\rho_m = 0 \qquad \sigma = 0 \qquad \textbf{in loss-less media} \qquad \textbf{(I.1.c)}$$

in which ρ_m and σ are magnetic resistivity and electric conductivity, respectively. These two parameters can properly represent magnetic and electric loss mechanism in a lossy medium. In above equations,

$$\vec{D} = \varepsilon \vec{E} \quad , \quad \varepsilon = \varepsilon_0 \varepsilon_r(x, y) = n^2(x, y) \qquad \textbf{(I.2)}$$

Taking the curl of eq. (I.1.a):

$$\vec{\nabla} \times \vec{\nabla} \times \vec{E} = -\mu \varepsilon \frac{\partial^2 \vec{E}}{\partial t^2} \qquad \textbf{(I.3)}$$

Using the well known curl of curl expansion from vector analysis:

$$\vec{\nabla}\left(\vec{\nabla} \cdot \vec{E}\right) - \vec{\nabla}^2 \vec{E} = -\mu \varepsilon \frac{\partial^2 \vec{E}}{\partial t^2} \qquad \textbf{(I.4)}$$

From Guass's law in source free media, i.e. $\vec{\nabla} \cdot \vec{D} = \rho = 0$:

$$\vec{\nabla} \cdot \vec{D} = 0 \tag{I.5}$$

$$\vec{\nabla} \cdot \left(\varepsilon_r \vec{E} \right) = 0 \tag{I.6}$$

$$\vec{\nabla} \cdot \left(n^2 \vec{E} \right) = 0 \tag{I.7}$$

$$n^2 \vec{\nabla} \cdot \vec{E} + \vec{E} \cdot \vec{\nabla} n^2 = 0 \tag{I.8}$$

$$\vec{\nabla} \cdot \vec{E} = -\vec{E} \cdot \frac{\vec{\nabla} n^2}{n^2} \tag{I.9}$$

$$\vec{\nabla} \ln\left(n^2 \right) = \frac{\vec{\nabla} n^2}{n^2} \tag{I.10}$$

$$\boxed{\vec{\nabla} \cdot \vec{E} = -\vec{E} \cdot \vec{\nabla} \ln\left(n^2 \right)} \tag{I.11}$$

Finally, substituting eq. (I.11) into eq. (I.4) yields:

$$\vec{\nabla}^2 \vec{E} - \mu\varepsilon \frac{\partial^2 \vec{E}}{\partial t^2} = \vec{\nabla}\left(\vec{\nabla} \cdot \vec{E} \right) = -\vec{\nabla}\left(\vec{E} \cdot \vec{\nabla} \ln n^2 \right) \tag{I.12}$$

$$\boxed{\vec{\nabla}^2 \vec{E} - n^2 \mu\varepsilon_0 \frac{\partial^2 \vec{E}}{\partial t^2} = -\vec{\nabla}\left(\vec{E} \cdot \vec{\nabla} \ln n^2 \right)} \quad ; \quad n^2 = \varepsilon_r(x, y) \tag{I.13}$$

Equation (I.13) is the governing wave equation for any inhomogeneous guided wave structure regardless of its operating frequency. For the homogeneous case, the right hand side of eq. (I.13) is equal to zero. Hence:

$$\vec{\nabla}^2\vec{E} - n^2\mu\varepsilon_0\frac{\partial^2\vec{E}}{\partial t^2} = \vec{0} \qquad ; \qquad n^2 = \varepsilon_r(x,y) \qquad \textbf{(I.14)}$$

CAUTION: *One must be reminded that the inhomogeneous vectorial equation (I.13) is not decomposable into three x, y, z components!!!*

I.F. Microwave waveguide analysis versus the optical one

EVEN a quick survey of the microwave and optical waveguide literatures reveals the fact that there are distinctions between their analyses. While, the governing equations, (I.1.a) and (I.1.b) or (I.13) are the same for both media, this double standard in treating them differently seems questionable. This question and the rational behind this distinction is addressed in this section. Let's rephrase the question once more:

"What are the major differences between the analysis techniques of microwave and optical guided wave structures?"

The first major distinction is due to different fabrication procedures dominant in microwave and optical frequency bands. Practically, almost all waveguides operating in microwave frequency bands are constructed from several distinct regions of homogeneity, whereas in the optical frequency bands the dominant configuration belongs to the class of **G**raded **I**ndex type of **O**ptical **W**aveguides, as shown in Fig. I.2 (j). In addition, due to high conductor losses at higher frequencies, usually no conductor is used as a transmission medium at optical frequencies. As it has been explained in §I.E., for a complete analysis, either eq. (I.13) for the inhomogeneous waveguide or eq. (I.14) for the homogeneous one, has to be solved. In fact, for the homogeneous case, the governing equation is a well

known one, the so-called **Helmholtz** equation. Instead, the difficulty will arise when one intends to solve the inhomogeneous case. This is exactly one of the points that distinguishes the analysis of microwave waveguides and graded index optical waveguides. The reason is that, usually, at microwave frequency bands, one is dealing with homogeneous waveguides or waveguides which can be divided into several homogeneous regions. And, in each region of homogeneity, one can simply analyze the problem using eq. (I.14) and then using methods like **M**ode **M**atching, impose the boundary conditions on the unknown constants of the field equations. The same procedure is still valid for step index optical waveguides, as of Figs. I.2 (a) to (i). On the other hand, the **G**raded **I**ndex **O**ptical **F**ibers constitute an important class of optical waveguides and therefore require special attention. Since, the variation of permittivity index inside graded index optical waveguides is a smooth and continuous function of position, they cannot be split into several regions of homogeneity. Hence, in general, one has to solve a fairly complicated system of equations. Quite interestingly, from the **FD(TD)** point of view, both these two classes of problems can be handled easily. This is one of the most interesting features of an **FD(TD)** algorithm that once it is written, it can deal with more complex situations as easily as with simpler ones.

The other major distinction lays in the fact that optical waveguides are usually being considered as open structures. While, in the case of microwave waveguides, a surrounding conductor is usually present that shields the structure. Although this shield is mainly used for isolating the fields inside and outside of the structure, it also facilitates the numerical computation of the field. In contrast, for most optical waveguides, the region for numerical solution is surrounded by absorbing walls. Note that the surrounding rectangles in

Figs. (a) to (i) do not necessarily represent **PEC**s (Perfect Electric Conductors). Modeling **A**bsorbing **B**oundary **C**onditions [6] has always been a challenging problem for researchers. Since the objective of this thesis is not in developing new kinds of absorbing boundary conditions, it will not be discussed in further details.

So far, from analytical point of view, two factors in favor of the microwave waveguide analysis have been pointed out. However, an important property makes the analysis of optical waveguides easier than the microwave ones. This is due to an assumption, which is valid only for optical waveguide structures. It is called the ***scalar approximation*** in optics.

I.F.1 Scalar approximation in optics

AN OPTICAL waveguide consists of different layers of dielectrics with different refractive indexes. One with the higher index, the core, is located at the center of the guide and the other, the cladding, acts as the shielding layer for the core. Luckily, in optics we usually are dealing with structures whose refractive index varies smoothly (2%) along the transverse direction, i.e. **Weakly Guided Structures**. Under these circumstances, one can assume that the right hand side of equation (I.13) equals zero, allowing the **Scalar Approximation in Optics** [7]. A careful examination of Maxwell's equations in such a guiding structure shows that the z components of both electric and magnetic fields approach zero. This in turn means that the field distribution inside the waveguide tends to follow a **Q**uasi-**TEM** pattern.

On the other hand, according to a known theorem in Electromagnetic theory, only a scalar helmholtz equation suffices to describe the behavior of all the field components of a **TEM** field distribution. Assuming propagation along the direction, this equation can be written as:

$$\left[\nabla_t^2 + k^2\varepsilon_r^2(x,y) - \beta^2\right]\Phi = 0 \qquad \textbf{(I.15.a)}$$

$$\nabla_t^2 = \frac{\partial^2}{\partial x^2} + \frac{\partial^2}{\partial y^2} \qquad \beta = k_z \qquad \textbf{(I.15.b)}$$

The field components for the **TE** mode are:

$$E_x = \Phi(x) \qquad H_y = \frac{E_x}{\eta} \qquad E_z = 0 \qquad \eta = \sqrt{\frac{\mu}{\varepsilon_0\varepsilon_r}} \qquad \textbf{(I.16)}$$

By the same token, the **TM** field components are:

$$E_y = \Phi(x) \qquad H_x = -\frac{E_y}{\eta} \qquad H_z = 0 \qquad \eta = \sqrt{\frac{\mu}{\varepsilon_0\varepsilon_r}} \qquad \textbf{(I.17)}$$

I.G. Conclusion

BASED UPON what have been cited above, it can now be understood why time consuming methods, like the **FD(TD)**, gradually become more dominant than rigorous or analytical ones; **a**) they do not require a simplified model, **b**) they do not require complex mathematical algorithms **c**) using high speed computers, the computational time for these methods can be kept quite affordable.

The followings can be listed as the common differences between a microwave waveguide analysis and an optical one.

- *In microwave analysis, one can usually find regions of homogeneity inside the waveguide and therefore solve eq. (I.14) for each of these regions. On the other hand, for graded index optical fibers, solution is usually obtained using more complicated eq. (I.13).*

- *In optical structures, scalar approximation can be used (as long as rigorous polarization study is not of any concern). While in Microwave, a vectorial analysis is a must.*

- *In optical fiber analysis, one needs an absorbing boundary condition to confine the computational region, while this requirement can be waived for most of the closed Microwave structures,i.e. Fin-lines, Strip-lines,...*

As can be seen from Figs. (I.1) and (I.2), for some of the cases, an optical waveguide can be quite similar to a microwave waveguide. However, as it was mentioned earlier, due to excessive conductor losses at higher frequencies, conducting waveguides are not usually used as a wave carrier at optical frequencies.

Chapter Two

PREVIEW OF NUMERICAL TECHNIQUES

II.A. Introduction

AS WAS pointed out in comparative table I .1, Finite Difference (**FD**) based methods are one of the most powerful and versatile techniques available, provided that computer resources do not pose limitations. With recent advances in computer technology, this is becoming less and less a problem.

FD methods can be divided into two general categories, Finite Difference Frequency Domain and Finite Difference Time Domain methods. In general, Finite Difference refers to those class of problems that are formulated by replacing all or some of the spatial derivatives with their equivalent finite difference forms. Time Domain methods refer to techniques which are based on the time domain extraction of the evolution of the fields. Needless to say that time variable, t, plays a crucial role in this formulation and is present in the final formulations, either explicitly or in terms of numerical iterations. Frequency Domain, in turn, refers to the techniques which are based on solving field equations for a certain frequency. Different categories and branches of finite difference based methods are illustrated in the following chart, Fig. II.1.

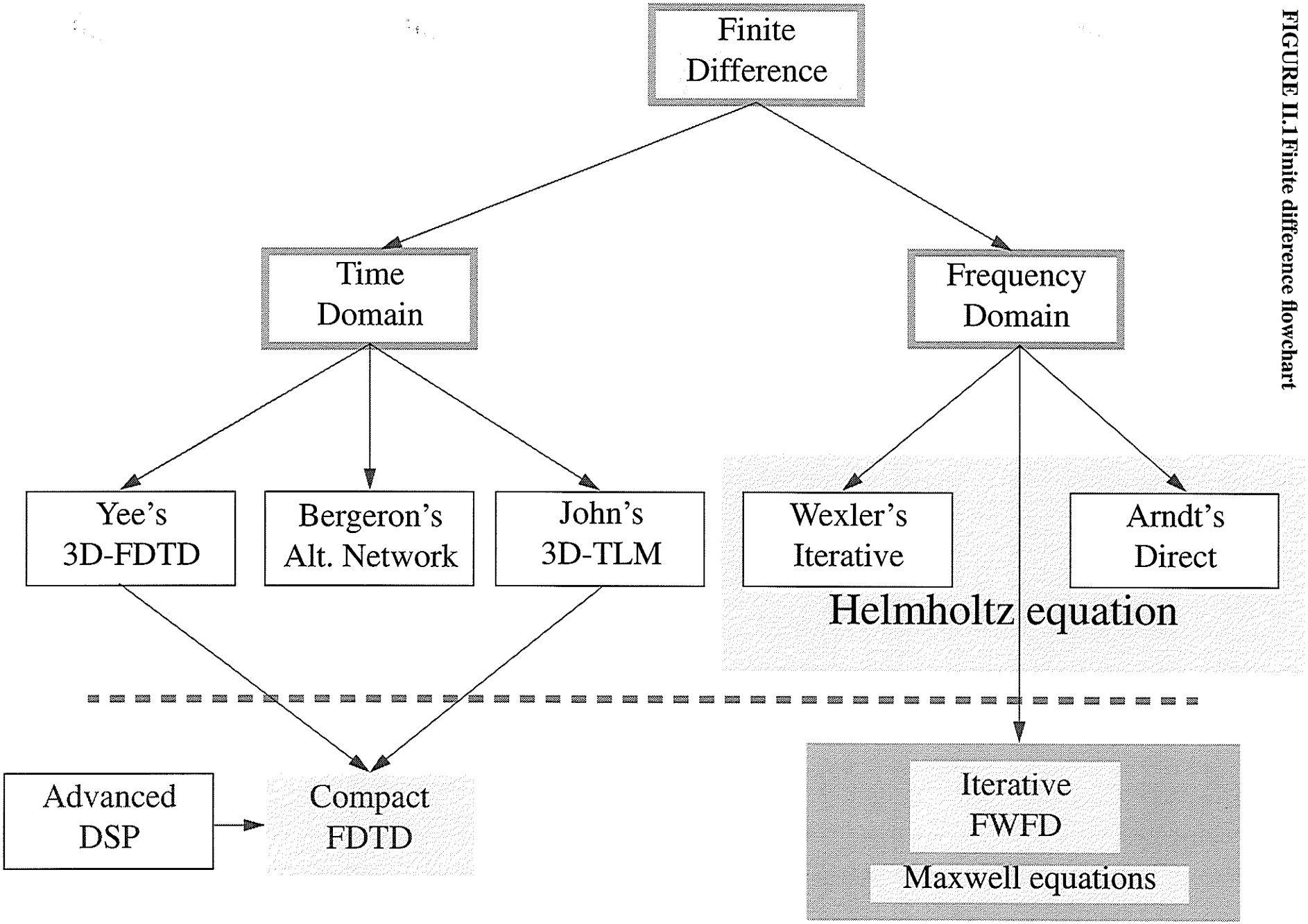

FIGURE II.1 Finite difference flowchart

II.B. Time Domain Methods

TIME DOMAIN methods constitute a major branch of the class of finite difference methods. Among methods from this category are: **TLM [8]**, **FDTD [9]**, **Bergeron**'s [10] [11]. Even though the original derivations of these three time domain methods were based on completely different physical interpretations, their equivalency has been established by several researchers [12]. Therefore, from a theoretical point of view, there is no major advantage in choosing one time domain method over another. Yet, it has to be mentioned that from a practical point of view (**CPU** time and required memory space), there are several advantages in using the **FDTD** method over any other time domain method [13].

II.B.1. Transmission line matrix (TLM) method [14]

THE TRANSMISSION Line Matrix method was first inspired by Huygen's principle and the physical nature of wave propagation [15]. When Johns first proposed this method, he simply assumed that space be modeled by a mesh of transmission lines. The equivalency is established if the physical properties of the transmission lines, characteristic impedance,..., be adjusted in a way that the effective behavior of the wave propagation in the resultant slow wave structure follows the same pattern as the actual wave in the corresponding media. According to the Huygen's principle in optics, in the course of propagation of a wave, each point on the wave-front of a wavelet acts like a new source of spherical waves. The upcoming wave-front is nothing but the envelope of the wave-fronts to all these new spherical waves. To simulate this algorithm on a computer, first, space and time must be

discretized. This procedure can be performed in different coordinate systems. For convenience, here, only the derivation in the cartesian coordinate system is presented. Fig. II.2 depicts the wave propagation mechanism in a mesh grid in the cartesian coordinate system. Suppose that one of the nodes is excited by a unit voltage pulse. Since all four branches connected to a specific node have the same properties, the incident power will be split equally between the lines. Knowing that the initial pulse was launched with a unit power, each of the reflected pulses in the four branches will have $1/4$ of the unit power. So, each of them will have an amplitude equal to $1/2$ the unit voltage.

FIGURE II.2 TLM wave propagation mechanism (a) Incident unit impulse impinges on a node (b) The resultant reflected impulses (c) The numbering sequence of the branches in each node

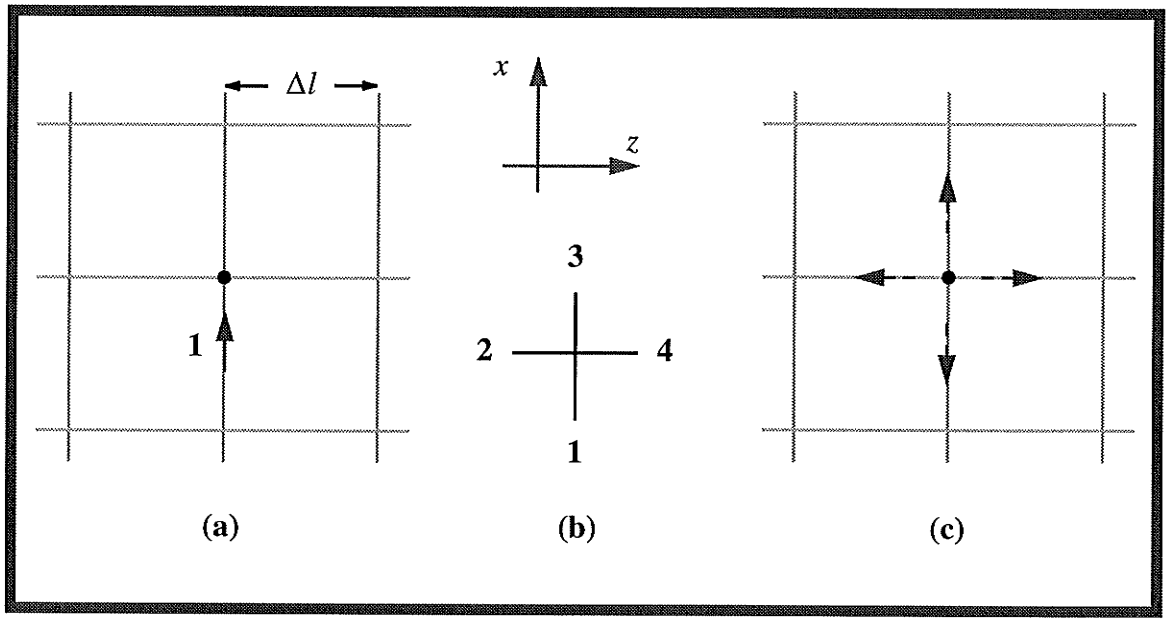

Now, having the amplitudes of all the reflected waves, the only remaining unknowns are their phases. These can also be determined from a very straightforward mathematical analysis. As it is clearly shown in Fig. II.2, in each node, there are three identical transmis-

sion lines connected to the incoming line with the same unit normalized impedance. The three outgoing lines appear in parallel, terminating the incoming line in a normalized impedance of $1/3$. Hence,

$$\Gamma_i = \frac{\frac{1}{3} - 1}{\frac{1}{3} + 1} = -\frac{1}{2} \tag{II.1}$$

and the transmission coefficient for each outgoing line is

$$T_i = 1 + \Gamma_i = \frac{1}{2} \tag{II.2}$$

and therefore, the reflected wave at the branch 1 is 180° degrees out of phase with respect to the other three scattered waves and also the initial excitation pulse. The concluded results so far, can easily be extended to a more general formulation, in which the node excitations are not just unit impulses. Let us concentrate on a more general case in which many nodes can be excited simultaneously. The voltage ${}_kV_n^l$ stands for the incident voltage if $l = i$ and reflected voltage if $l = r$; n and k stand for the branch and iteration numbers, respectively. Using superposition in linear systems,

$${}_{k+1}V_n^r = \frac{1}{2}\left[\sum_{m=1}^{4} {}_kV_m^i\right] - {}_kV_n^i \tag{II.3}$$

This situation can be conveniently formulated in a scattering matrix which relates the reflected voltages at the $(k+1)\,\Delta t$ th step to the incident voltages at the $k\Delta t$ th step:

$$_{k+1}\begin{bmatrix} V_1 \\ V_2 \\ V_3 \\ V_4 \end{bmatrix}^r = \frac{1}{2}\begin{bmatrix} -1 & 1 & 1 & 1 \\ 1 & -1 & 1 & 1 \\ 1 & 1 & -1 & 1 \\ 1 & 1 & 1 & -1 \end{bmatrix} \bullet {}_{k+1}\begin{bmatrix} V_1 \\ V_2 \\ V_3 \\ V_4 \end{bmatrix}^i \qquad \textbf{(II.4)}$$

It is obvious that any impulse emerging (reflected) from a node at position (z, x) will act as an incident impulse for the adjacent node at the next time step. Therefore,

$$_{k+1}V_1^i(z,x) = {}_kV_3^r(z,x-1) \qquad \textbf{(II.5.a)}$$

$$_{k+1}V_2^i(z,x) = {}_kV_4^r(z-1,x) \qquad \textbf{(II.5.b)}$$

$$_{k+1}V_3^i(z,x) = {}_kV_1^r(z,x+1) \qquad \textbf{(II.5.c)}$$

$$_{k+1}V_4^i(z,x) = {}_kV_2^r(z+1,x) \qquad \textbf{(II.5.d)}$$

By repeating the two algorithms expressed in eqs. (II.4) and (II.5.a)-(II.5.d), a wave propagation mechanism can be simulated by a digital computer. But, still, one may be skeptical about the precise relationship that holds between this algorithm and the actual electromagnetic wave propagation, which is formally a solution to Helmholtz equation. To investigate the validity of this method and also establish an accurate mathematical model, we write the telegraph equations for a mesh of transmission lines. Fig. II.3 depicts one unit cell of such a mesh.

FIGURE II.3 Details of a unit cell structure constructing a TLM mesh

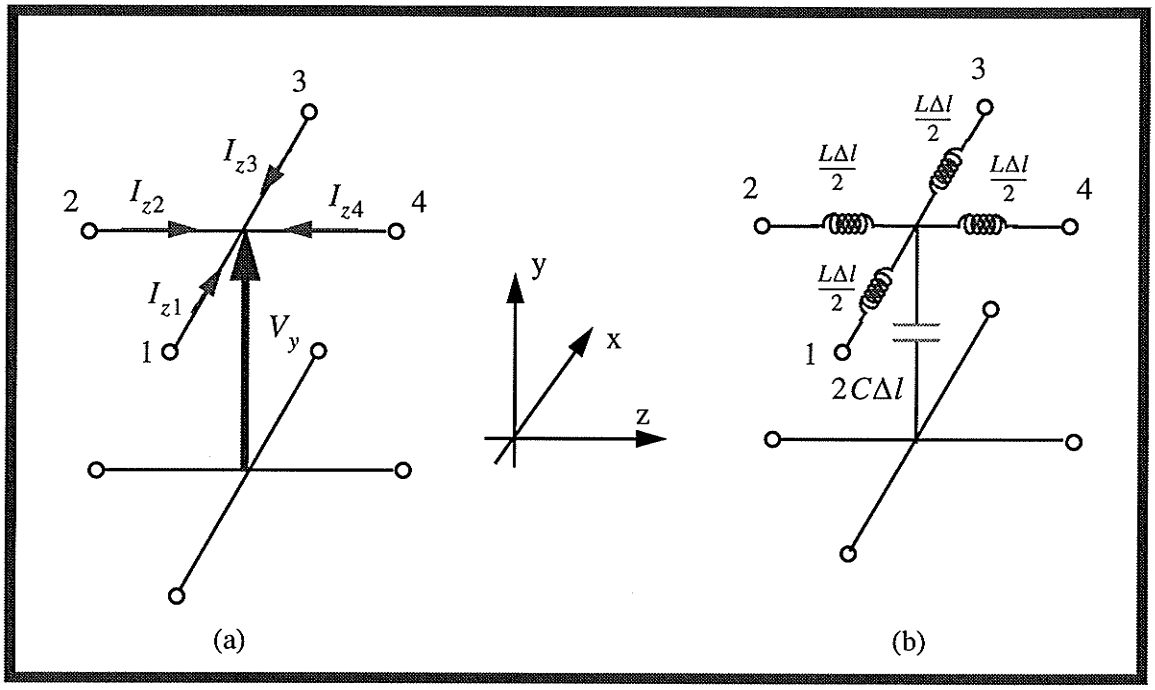

The derived equations can be written in partial differential, not partial difference, form only if the mesh grid is infinitesimally small, i.e. $\Delta l \rightarrow 0$. Assuming that this condition is met, one can proceed to:

$$\frac{\partial V_y}{\partial x} = -L\frac{\partial (I_{x1} - I_{x3})}{\partial t} \qquad \textbf{(II.6.a)}$$

$$\frac{\partial V_y}{\partial z} = -L\frac{\partial (I_{z2} - I_{z4})}{\partial t} \qquad \textbf{(II.6.b)}$$

$$\frac{\partial (I_{x1} - I_{x3})}{\partial t} + \frac{\partial (I_{z2} - I_{z4})}{\partial t} = -2C\frac{\partial V_y}{\partial t} \qquad \textbf{(II.6.c)}$$

These expressions can also be combined to yield the following Helmholtz wave equation,

$$\frac{\partial^2 V_y}{\partial x^2} + \frac{\partial^2 V_y}{\partial y^2} = 2LC\frac{\partial^2 V_y}{\partial t^2} \qquad \textbf{(II.7)}$$

Therefore, this fact has just been proved that the mechanism generated by iterating eqs. (II.4) and (II.5.a)-(II.5.d) can simulate any wave propagation phenomena which has a similar formula to eq. (II.7). The H_{m0} can serve as a good example which can be easily modeled by the **TLM** shunt-connected network. For this mode, Maxwell's equations can be re-written as:

$$\frac{\partial E_y}{\partial x} = -\mu\frac{\partial H_z}{\partial t} \qquad \textbf{(II.8.a)}$$

$$\frac{\partial E_y}{\partial z} = -\mu\frac{\partial H_x}{\partial t} \qquad \textbf{(II.8.b)}$$

$$\frac{\partial H_x}{\partial z} + \frac{\partial H_z}{\partial x} = -\varepsilon\frac{\partial E_y}{\partial t} \qquad \textbf{(II.8.c)}$$

After taking time derivative of both sides of eq. (II.8.c) and substituting for $\frac{\partial H_z}{\partial t}$ and $\frac{\partial H_x}{\partial t}$ in terms of partial derivatives of E_y (from eqs. (II.8.a) & (II.8.b)), one obtains:

$$\frac{\partial^2 E_y}{\partial x^2} + \frac{\partial^2 E_y}{\partial y^2} = \mu\varepsilon\frac{\partial^2 E_y}{\partial t^2} \qquad \textbf{(II.9)}$$

Thus, an H_{m0} mode inside a waveguide can be simulated by a TLM shunt-connected network on a digital computer. Now that this equivalency is established, it seems to be a good idea to derive the exact relationships that hold between the model parameters and the actual electromagnetic field components. A direct comparison between equations (II.6.a)-

(II.6.c) & (II.8.a)-(II.8.c) can be made with the following equivalences between parameters:

$$E_y \equiv V_y \tag{II.10.a}$$

$$H_z \equiv -(I_{x3} - I_{x1}) \tag{II.10.b}$$

$$H_x \equiv -(I_{z2} - I_{z4}) \tag{II.10.c}$$

$$\mu \equiv L \tag{II.10.d}$$

$$\varepsilon \equiv 2C \tag{II.10.e}$$

From the transmission line theory, the speed of the wave propagation and the parameters of the medium, assuming free space $\mu_r = 1$, $\varepsilon_r = 1$ are related to each other according to the following equation:

$$\frac{1}{\sqrt{\mu\varepsilon}} = \frac{1}{\sqrt{LC}} = c \tag{II.11}$$

Now, when this transmission line is placed in a shunt-connected network, the resultant structure will exhibit a slow wave structure behavior represented by:

$$v = \frac{1}{\sqrt{2LC}} = \frac{c}{\sqrt{2}} \tag{II.12}$$

II.B.2. Bergeron's method

THE OTHER TIME domain technique which is somehow similar to **TLM** is the **A**lternative **N**etwork or Bergeron's method. This model which was first proposed by Yoshida, Fukai and Fukuoka [11] is based on the equations which were already obtained by Bergeron. The basic idea behind this method is very close to the one of TLM. In fact, both methods utilize the traveling wave concept. Their differences are:

- *The way that unit cells are defined is different. Instead of having two different shunt and series connected networks as in the **TLM**, only shunt connected network is introduced. But, two different electric and magnetic nodes are defined in the structure. In the electric nodes, voltage represents the electric field while in the magnetic nodes, it represents the magnetic field component.*

- *In Bergeron's method, the voltage and current variables directly model the electromagnetic fields. On the other hand, the TLM is based on the decomposition of each voltage and current variable into two incident and reflected components.*

- *The application of just shunt connected network in Bergeron's method will result in some mismatching behavior between the voltage and current variables. To remove this, a gyrator has to be utilized between any two connected nodes in the unit cell structure.*

Most of the other properties of the Bergeron and **TLM** models are similar to each other and there is no particular advantage in using one over the other. Therefore, no further detailed derivation is presented here. Later on, only the justifications that make the **FDTD** more preferable than **TLM** for this study will be presented.

II.B.3. Finite difference time domain (FDTD) method

UNLIKE THE two preceding methods which are based on some physical interpretation of the wave propagation mechanism, the **FDTD** method is based on a very straightforward mathematical procedure and normally does not require any a priori physical interpretation in order to derive the basic formulas. **FDTD** results from replacing space and time derivatives in Maxwell's equations by their corresponding finite difference equivalences.

II.B.3.a. Formulation

STARTING FROM Maxwell's equations, expanding eqs. (I.1.a) and (I.1.b) will result in:

$$\frac{\partial H_x}{\partial t} = \frac{1}{\mu}\left(\frac{\partial E_y}{\partial z} - \frac{\partial E_z}{\partial y} - \rho_m H_x\right) \qquad \textbf{(II.13.a)}$$

$$\frac{\partial H_y}{\partial t} = \frac{1}{\mu}\left(-\frac{\partial E_x}{\partial z} + \frac{\partial E_z}{\partial x} - \rho_m H_y\right) \qquad \textbf{(II.13.b)}$$

$$\frac{\partial H_z}{\partial t} = \frac{1}{\mu}\left(\frac{\partial E_x}{\partial y} - \frac{\partial E_y}{\partial x} - \rho_m H_z\right) \qquad \textbf{(II.13.c)}$$

$$\frac{\partial E_x}{\partial t} = \frac{1}{\varepsilon}\left(-\frac{\partial H_y}{\partial z} + \frac{\partial H_z}{\partial y} - \sigma E_x\right) \qquad \textbf{(II.13.d)}$$

$$\frac{\partial E_y}{\partial t} = \frac{1}{\varepsilon}\left(\frac{\partial H_x}{\partial z} - \frac{\partial H_z}{\partial x} - \sigma E_y\right) \qquad \textbf{(II.13.e)}$$

$$\frac{\partial E_z}{\partial t} = \frac{1}{\varepsilon}\left(-\frac{\partial H_x}{\partial y} + \frac{\partial H_y}{\partial x} - \sigma E_z\right) \qquad \textbf{(II.13.f)}$$

A quick inspection of eqs. (II.13.a) to (II.13.f) shows that these equations constitute a system of coupled differential equations in terms of six vector field components, $E_x, E_y, E_z, H_x, H_y, H_z$, as functions of four independent variables, x, y, z, t. This makes the task of discretizing the above equations to their finite difference forms a peculiar one. Specifically, care has to be taken in discretizing the differential operators if a final iterative algorithm is desired. It was **Yee** who first proposed a method to accomplish this task. Although, it has should mentioned that his algorithm is not the only way to obtain a practical algorithm.

At this stage, all the derivatives with respect to time and space must be replaced by their corresponding finite difference forms. But, there are several different ways to discretize a derivative operator, such as the forward, backward and central difference formulas. Following are some basic definitions and notations required for the rest of the discussion.

$$(i, j, k) = (i\Delta x, j\Delta y, k\Delta z) \tag{II.14}$$

$$F^n(i, j, k) = F(i\Delta x, j\Delta y, k\Delta z, n\Delta t) \tag{II.15}$$

$$\frac{\partial F^n(i, j, k)}{\partial t} = \frac{F^{n+\frac{1}{2}}(i, j, k) - F^{n-\frac{1}{2}}(i, j, k)}{\Delta t} + O\left(\Delta t^2\right) \tag{II.16}$$

$$\frac{\partial F^n(i, j, k)}{\partial x} = \frac{F^n\left(i+\frac{1}{2}, j, k\right) - F\left(i-\frac{1}{2}, j, k\right)}{\Delta x} + O\left(\Delta x^2\right) \tag{II.17.a}$$

$$\frac{\partial F^n(i, j, k)}{\partial y} = \frac{F^n\left(i, j+\frac{1}{2}, k\right) - F\left(i, j-\frac{1}{2}, k\right)}{\Delta y} + O\left(\Delta y^2\right) \tag{II.17.b}$$

$$\frac{\partial F^n(i,j,k)}{\partial z} = \frac{F^n\left(i,j,k+\frac{1}{2}\right) - F\left(i,j,k-\frac{1}{2}\right)}{\Delta z} + O\left(\Delta z^2\right) \qquad \textbf{(II.17.c)}$$

Eq. (II.16) is the central difference representation for the time derivative operator. Eqs. (II.17.a), (II.17.b) and (II.17.c) are, respectively, the expressions for central, forward and backward difference formulas for the spatial derivative operators.

At the next step, Yee defined the spatial locations of electric and magnetic field vectors half a unit cell length apart in space. Also, he evaluated $\vec{E}$ and $\vec{H}$ at alternative half time steps. Fig. II.4 illustrates a unit cell of Yee's lattice. Using this unit cell and the finite difference expressions for time and space derivative operators, eqs (II.18.a)-(II.18.f) can easily be obtained. These are the governing equations of a three dimensional **FDTD** algorithm for an inhomogeneous medium, i.e. permittivity, permeability, magnetic resistance and electric conductance can be functions of space coordinates.

FIGURE II.4 Conventional Yee's **3D**-lattice

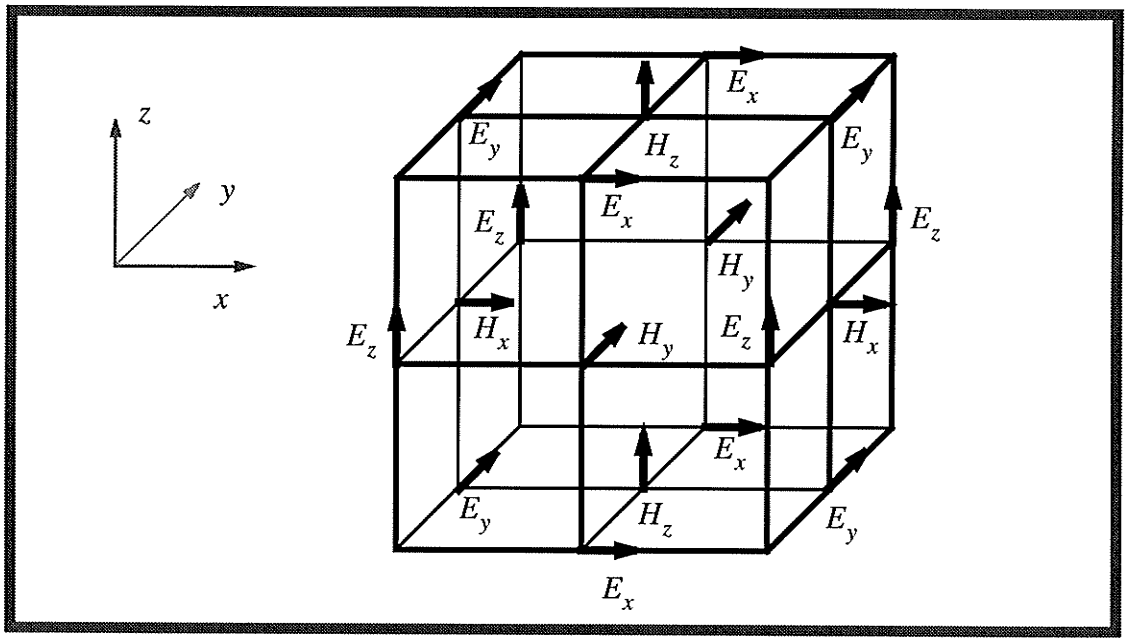

Now that all derivative operators have been replaced by their finite difference forms, one can start from any instant of time, after assuming some initial and boundary conditions, proceed to obtain the values of electric and magnetic fields at any instant of time and any position in space. Needless to say, it is to the advantage of the required calculation time if one can assume larger time (Δt) and space (Δx, Δy, Δz) steps in Yee's lattice. The bigger these step sizes are, the larger domain in both space and time can be covered. But, there are several theoretical barriers that are against increasing the step sizes unconditionally.

- ***Accuracy**: Equations (II.16), (II.17.a)-(II.17.c) are valid only when step sizes approach zero ($\Delta l \to 0$ and $\Delta t \to 0$), i.e. **fine grid** assumption.*
- *Stability factor*
- *Numerical dispersion*

The exact meaning of stability factor and numerical dispersion will be explained in what follows.

$$H_x^{n+\frac{1}{2}}\left(i,j+\frac{1}{2},k+\frac{1}{2}\right)=\frac{1-\dfrac{\rho_m\left(i,j+\frac{1}{2},k+\frac{1}{2}\right)\Delta t}{2\mu\left(i,j+\frac{1}{2},k+\frac{1}{2}\right)}}{1+\dfrac{\rho_m\left(i,j+\frac{1}{2},k+\frac{1}{2}\right)\Delta t}{2\mu\left(i,j+\frac{1}{2},k+\frac{1}{2}\right)}}\cdot H_x^{n-\frac{1}{2}}\left(i,j+\frac{1}{2},k+\frac{1}{2}\right)+\frac{\Delta t}{\mu\left(i,j+\frac{1}{2},k+\frac{1}{2}\right)}$$

$$\cdot\left[1+\frac{\rho_m\left(i,j+\frac{1}{2},k+\frac{1}{2}\right)\Delta t}{2\mu\left(i,j+\frac{1}{2},k+\frac{1}{2}\right)}\right]^{-1}\cdot\left\{\frac{E_y^n\left(i,j+\frac{1}{2},k+1\right)-E_y^n\left(i,j+\frac{1}{2},k\right)}{\Delta z}+\frac{E_z^n\left(i,j,k+\frac{1}{2}\right)-E_z^n\left(i,j+1,k+\frac{1}{2}\right)}{\Delta y}\right\}$$

(II.18.a)

$$H_y^{n+\frac{1}{2}}\left(i+\frac{1}{2},j,k+\frac{1}{2}\right)=\frac{1-\dfrac{\rho_m\left(i+\frac{1}{2},j,k+\frac{1}{2}\right)\Delta t}{2\mu\left(i+\frac{1}{2},j,k+\frac{1}{2}\right)}}{1+\dfrac{\rho_m\left(i+\frac{1}{2},j,k+\frac{1}{2}\right)\Delta t}{2\mu\left(i+\frac{1}{2},j,k+\frac{1}{2}\right)}}\cdot H_y^{n-\frac{1}{2}}\left(i+\frac{1}{2},j,k+\frac{1}{2}\right)+\frac{\Delta t}{\mu\left(i+\frac{1}{2},j,k+\frac{1}{2}\right)}$$

$$\cdot\left[1+\frac{\rho_m\left(i+\frac{1}{2},j,k+\frac{1}{2}\right)\Delta t}{2\mu\left(i+\frac{1}{2},j,k+\frac{1}{2}\right)}\right]^{-1}\cdot\left\{\frac{E_z^n\left(i+1,j,k+\frac{1}{2}\right)-E_z^n\left(i,j,k+\frac{1}{2}\right)}{\Delta x}+\frac{E_x^n\left(i+\frac{1}{2},j,k\right)-E_x^n\left(i+\frac{1}{2},j,k+1\right)}{\Delta z}\right\}$$

(II.18.b)

$$H_z^{n+\frac{1}{2}}\left(i+\frac{1}{2},j+\frac{1}{2},k\right)=\frac{1-\dfrac{\rho_m\left(i+\frac{1}{2},j+\frac{1}{2},k\right)\Delta t}{2\mu\left(i+\frac{1}{2},j+\frac{1}{2},k\right)}}{1+\dfrac{\rho_m\left(i+\frac{1}{2},j+\frac{1}{2},k\right)\Delta t}{2\mu\left(i+\frac{1}{2},j+\frac{1}{2},k\right)}}\cdot H_z^{n-\frac{1}{2}}\left(i+\frac{1}{2},j+\frac{1}{2},k\right)+\frac{\Delta t}{\mu\left(i+\frac{1}{2},j+\frac{1}{2},k\right)}$$ **(II.18.c)**

$$\cdot\left[1+\frac{\rho_m\left(i+\frac{1}{2},j+\frac{1}{2},k\right)\Delta t}{2\mu\left(i+\frac{1}{2},j+\frac{1}{2},k\right)}\right]^{-1}\cdot\left\{\frac{E_x^n\left(i+\frac{1}{2},j+1,k\right)-E_x^n\left(i+\frac{1}{2},j,k\right)}{\Delta y}+\frac{E_y^n\left(i,j+\frac{1}{2},k\right)-E_y^n\left(i+1,j+\frac{1}{2},k\right)}{\Delta x}\right\}$$

$$E_x^{n+1}\left(i+\frac{1}{2},j,k\right)=\frac{1-\dfrac{\sigma\left(i+\frac{1}{2},j,k\right)\Delta t}{2\varepsilon\left(i+\frac{1}{2},j,k\right)}}{1+\dfrac{\sigma\left(i+\frac{1}{2},j,k\right)\Delta t}{2\varepsilon\left(i+\frac{1}{2},j,k\right)}}\cdot E_x^n\left(i+\frac{1}{2},j,k\right)+\frac{\Delta t}{\varepsilon\left(i+\frac{1}{2},j,k\right)}\cdot\left[1+\frac{\sigma\left(i+\frac{1}{2},j,k\right)\Delta t}{2\varepsilon\left(i+\frac{1}{2},j,k\right)}\right]^{-1}$$ **(II.18.d)**

$$\cdot\left\{\frac{H_z^{n+\frac{1}{2}}\left(i+\frac{1}{2},j+\frac{1}{2},k\right)-H_z^{n+\frac{1}{2}}\left(i+\frac{1}{2},j-\frac{1}{2},k\right)}{\Delta y}+\frac{H_y^{n+\frac{1}{2}}\left(i+\frac{1}{2},j,k-\frac{1}{2}\right)-H_y^{n+\frac{1}{2}}\left(i+\frac{1}{2},j,k+\frac{1}{2}\right)}{\Delta z}\right\}$$

$$E_y^{n+1}\left(i,j+\frac{1}{2},k\right) = \frac{1-\dfrac{\sigma\left(i,j+\frac{1}{2},k\right)\Delta t}{2\varepsilon\left(i,j+\frac{1}{2},k\right)}}{1+\dfrac{\sigma\left(i,j+\frac{1}{2},k\right)\Delta t}{2\varepsilon\left(i,j+\frac{1}{2},k\right)}} \cdot E_y^{n}\left(i,j+\frac{1}{2},k\right) + \frac{\Delta t}{\varepsilon\left(i,j+\frac{1}{2},k\right)} \cdot \left[1+\frac{\sigma\left(i,j+\frac{1}{2},k\right)\Delta t}{2\varepsilon\left(i,j+\frac{1}{2},k\right)}\right]^{-1} \qquad \textbf{(II.18.e)}$$

$$\cdot \left\{ \frac{H_x^{\,n+\frac{1}{2}}\left(i,j+\frac{1}{2},k+\frac{1}{2}\right) - H_x^{\,n+\frac{1}{2}}\left(i,j+\frac{1}{2},k-\frac{1}{2}\right)}{\Delta z} + \frac{H_z^{\,n+\frac{1}{2}}\left(i-\frac{1}{2},j+\frac{1}{2},k\right) - H_y^{\,n+\frac{1}{2}}\left(i+\frac{1}{2},j+\frac{1}{2},k\right)}{\Delta x} \right\}$$

$$E_z^{n+1}\left(i,j,k+\frac{1}{2}\right) = \frac{1-\dfrac{\sigma\left(i,j,k+\frac{1}{2}\right)\Delta t}{2\varepsilon\left(i,j,k+\frac{1}{2}\right)}}{1+\dfrac{\sigma\left(i,j,k+\frac{1}{2}\right)\Delta t}{2\varepsilon\left(i,j,k+\frac{1}{2}\right)}} \cdot E_z^{n}\left(i,j,k+\frac{1}{2}\right) + \frac{\Delta t}{\varepsilon\left(i,j,k+\frac{1}{2}\right)} \cdot \left[1+\frac{\sigma\left(i,j,k+\frac{1}{2}\right)\Delta t}{2\varepsilon\left(i,j,k+\frac{1}{2}\right)}\right]^{-1} \qquad \textbf{(II.18.f)}$$

$$\cdot \left\{ \frac{H_y^{\,n+\frac{1}{2}}\left(i+\frac{1}{2},j,k+\frac{1}{2}\right) - H_y^{\,n+\frac{1}{2}}\left(i-\frac{1}{2},j,k+\frac{1}{2}\right)}{\Delta x} + \frac{H_x^{\,n+\frac{1}{2}}\left(i,j-\frac{1}{2},k+\frac{1}{2}\right) - H_x^{\,n+\frac{1}{2}}\left(i,j+\frac{1}{2},k+\frac{1}{2}\right)}{\Delta y} \right\}$$

II.B.3.b. Numerical Stability

IN SOLVING differential equations using numerical methods, there is usually an upper limit for the step sizes. Beyond this numerical limit, the algorithm is unstable and results in excessive errors. Note that this error is not due to any physical phenomenon, and is just the result of an improper choice of the step size. For the three dimensional **FDTD**, it has been shown that the upper limit can be determined from the following equation.

$$\Delta t \leq \frac{1}{c_{max}}\left[\frac{1}{\Delta x^2}+\frac{1}{\Delta y^2}+\frac{1}{\Delta z^2}\right]^{-\frac{1}{2}} \qquad \textbf{(II.19)}$$

$$\Delta t \leq \frac{\Delta l}{c_{max}\sqrt{3}} \qquad \Delta x = \Delta y = \Delta z = \Delta l \qquad \textbf{(II.20)}$$

where c_{max} is the maximum phase velocity of the electromagnetic wave within the medium. For homogeneous free space, it is simply the speed of light. For the two dimensional case, one has:

$$\Delta t \leq \frac{1}{c_{max}}\left[\frac{1}{\Delta x^2}+\frac{1}{\Delta y^2}\right]^{-\frac{1}{2}} \qquad \textbf{(II.21)}$$

$$\Delta t \leq \frac{\Delta l}{c_{max}\sqrt{2}} \qquad \Delta x = \Delta y = \Delta l \qquad \Delta z \to 0 \qquad \textbf{(II.22)}$$

It is customary to call the ratio $s = \frac{c\Delta t}{\Delta l}$ the stability factor. Therefore, the stability factor for a three dimensional **FDTD** lattice must be less than $1/\sqrt{3}$, while for the two dimensional lattice, it should be less than $1/\sqrt{2}$.

II.B.3.c. Dispersion Analysis

THE NUMERICAL algorithm represented by eqs. (II.18.a)-(II.18.f) introduces dispersions to the wave propagation within numerical lattice. This is called the numerical dispersion in contrast to the medium dispersion which is just a result of the inhomogeneous and/or anisotropic properties of the medium. In order to investigate the properties of numerical dispersion, one can consider the plane wave propagation in free space. In this case, free space is considered as a homogeneous medium and therefore there is no contribution due to "medium properties" in the total dispersion.

Starting from Maxwell's curl equations (I.1.a)-(I.1.b), and following a procedure similar to the one explained in section I.E., one finds the three dimensional lossy Helmholtz equation as, assuming $\rho_m = 0$:

$$\frac{\partial^2 E_z}{\partial x^2} + \frac{\partial^2 E_z}{\partial y^2} + \frac{\partial^2 E_z}{\partial z^2} = \mu\varepsilon \frac{\partial^2 E_z}{\partial t^2} + \mu\sigma \frac{\partial E_z}{\partial t} \tag{II.23}$$

The second derivative operator can easily be discretized by implementing central difference operator (II.17.a) twice:

$$\frac{\partial^2 F^n(i,j,k)}{\partial x^2} \approx \frac{F^n\left(i+\frac{1}{2},j,k\right) - 2F^n(i,j,k) + F^n\left(i-\frac{1}{2},j,k\right)}{\Delta x^2} \tag{II.24}$$

$$\frac{\partial^2 F^n(i,j,k)}{\partial t^2} \approx \frac{F^{n+\frac{1}{2}}(i,j,k) - 2F^n(i,j,k) + F^{n-\frac{1}{2}}(i,j,k)}{\Delta t^2} \tag{II.25}$$

The second derivative operators with respect to y and z can also be discretized in the same fashion. Substituting eqs. (II.24) and (II.25) into eq. (II.23) yields:

$$\frac{E_z^n\left(i+\frac{1}{2},j,k\right)-2E_z^n(i,j,k)+E_z^n\left(i-\frac{1}{2},j,k\right)}{\Delta x^2} + \frac{E_z^n\left(i,j+\frac{1}{2},k\right)-2E_z^n(i,j,k)+E_z^n\left(i,j-\frac{1}{2},k\right)}{\Delta y^2} + \frac{E_z^n\left(i,j,k+\frac{1}{2}\right)-2E_z^n(i,j,k)+E_z^n\left(i,j,k-\frac{1}{2}\right)}{\Delta z^2} = \frac{E_z^{n+\frac{1}{2}}(i,j,k)-2E_z^n(i,j,k)+E_z^{n-\frac{1}{2}}(i,j,k)}{\Delta t^2} + \mu_0\frac{E_z^{n+\frac{1}{2}}(i,j,k)-E_z^{n-\frac{1}{2}}(i,j,k)}{\Delta t} \quad \textbf{(II.26)}$$

On the other hand, the standard solution to a lossy scalar Helmholtz equation has the following general form:

$$E_z = e^{\Upsilon(x\sin\theta\cos\phi + y\sin\theta\sin\phi + z\cos\theta) + j\omega t} \quad \textbf{(II.27)}$$

in which $\Upsilon = -\alpha - j\beta$, where α and β represent attenuation and propagation constants of the wave, respectively. Substituting (II.27) into (II.26) results in:

$$\left[\frac{1}{\Delta x}\sinh\left(\frac{\Delta x\Upsilon\sin\theta\cos\phi}{2}\right)\right]^2 + \left[\frac{1}{\Delta y}\sinh\left(\frac{\Delta y\Upsilon\sin\theta\sin\phi}{2}\right)\right]^2 + \left[\frac{1}{\Delta z}\sinh\left(\frac{\Delta z\Upsilon\cos\theta}{2}\right)\right]^2 = j\frac{\mu\sigma}{\Delta t}\frac{\sin(\omega\Delta t)}{4} - \frac{\mu\varepsilon}{\Delta t^2}\left[\sin\frac{\omega\Delta t}{2}\right]^2 \quad \textbf{(II.28)}$$

For the special lossless case, eq. (II.28) can be simplified to:

$$\left[\frac{1}{\Delta x}\sinh\left(\frac{k_x\Delta x}{2}\right)\right]^2 + \left[\frac{1}{\Delta y}\sinh\left(\frac{k_y\Delta y}{2}\right)\right]^2 + \left[\frac{1}{\Delta z}\sinh\left(\frac{k_z\Delta z}{2}\right)\right]^2 = \left[\frac{1}{c\Delta t}\sin\left(\frac{\omega\Delta t}{2}\right)\right]^2 \quad \textbf{(II.29)}$$

$$k_x = \beta \sin\theta \cos\phi$$

$$k_y = \beta \sin\theta \sin\phi \qquad c = \frac{1}{\sqrt{\mu\varepsilon}}$$

$$k_x = \beta \cos\theta$$

Eq. (II.29) is called the numerical dispersion equation for the three dimensional **FDTD** lattice. It clearly demonstrates the fact that there is a transcendental relationship between β and ω, i.e. numerically dispersive. This numerical dispersion is a characteristic of the **FDTD** lattice; there is no other dispersion present in the free space medium under study. In fact, in this case the "medium dispersion" equation is:

$$\beta = \frac{\omega}{c} \qquad \textbf{(II.30)}$$

It is customary to call a medium non-dispersive whenever a linear relationship holds between β and ω.

Careful inspection of eq. (II.29) shows that numerical dispersion is generally a function of wavelength, direction of propagation and grid sizes (in both time and space domains). When all step sizes approach zero ($\Delta x, \Delta y, \Delta z, \Delta t \rightarrow 0$), eq. (II.29) becomes exactly the same as eq. (II.30). Thus, the smaller the grid size, the less numerical dispersion is introduced to the simulation lattice. But, as it has already been stated, this has a destructive effect on CPU elapsed time. In conclusion, one has to choose the grid sizes as small as possible while keeping the computational time affordable. Usually, it is recommended [16] that the grid size be taken not larger than 0.1λ, if numerical dispersion less than 1% is to be achieved.

II.C. Frequency domain methods

ACCORDING TO THE terminology used in this thesis, frequency domain methods are those which are based on removing the time variable in the final formulations. This removal can be accomplished by applying the Fourier transform on the time derivative operator, i.e. $\frac{\partial}{\partial t} \rightarrow j\omega$. This transformation, automatically, shifts the whole technique to frequency domain. Traditionally, these frequency domain techniques have been based on the Helmholtz equation. There are, at least, two classes of Finite Difference Frequency Domain techniques that are pertinent to our discussion, see Fig. II.1. Other derivations usually fit into one of the following two categories [17][18][19].

II.C.1 Beaubien-Wexler's iterative approach [20]

IN GENERAL, it can be proved (appendix A:) that at certain frequencies, namely cut-off, all electromagnetic waves can be decomposed into two orthogonal **TE** and **TM** modes. Under these circumstances, Maxwell's equations can be written in terms of a scalar field potential Φ [21].

For the TM modes:

$$\vec{E}_t = -\frac{\gamma}{k_c^2}\nabla_t \Phi \qquad \textbf{(II.31.a)}$$

$$E_z = \Phi \qquad \textbf{(II.31.b)}$$

$$\vec{H}_t = -\left(\frac{j\omega\varepsilon}{k_c^2}\right)\hat{a}_z \times \nabla_t \Phi \qquad \textbf{(II.31.c)}$$

$$H_z = 0 \qquad \textbf{(II.31.d)}$$

and for the TE modes:

$$\vec{E}_t = \frac{j\omega\mu}{k_c^2}\hat{a}_z \times \nabla_t \Phi \qquad \textbf{(II.32.a)}$$

$$E_z = 0 \qquad \textbf{(II.32.b)}$$

$$\vec{H}_t = -\frac{\gamma}{k_c^2}\nabla_t \Phi \qquad \textbf{(II.32.c)}$$

$$H_z = \Phi \qquad \textbf{(II.32.d)}$$

in which Φ should satisfy the scalar Helmholtz equation subject to relevant boundary conditions:

$$\left(\nabla_t^2 + k_c^2\right)\Phi = 0 \qquad \textbf{(II.33)}$$

in which $k_c = k^2 - k_z^2 = k^2 + \gamma^2$ is the cutoff wave number. Assuming that only waveguides surrounded by **PEC** (Perfect Electric Conductor) walls are of major concern, Φ should satisfy Dirichlet and Neumann boundary conditions:

$$\Phi = 0 \qquad \textbf{(II.34)}$$

for the TM mode and,

$$\frac{\partial \Phi}{\partial n} = 0 \qquad \textbf{(II.35)}$$

for the TE mode. Replacing the transverse Laplace operator by its discretized form yields, Fig. (II.5):

$$\nabla_t^2 \Phi = \left(\frac{\partial^2}{\partial x^2} + \frac{\partial^2}{\partial y^2}\right)\Phi = \frac{\Phi_{i+1,j} - 2\Phi_{i,j} + \Phi_{i-1,j}}{(\Delta x)^2} + \frac{\Phi_{i,j+1} - 2\Phi_{i,j} + \Phi_{i,j-1}}{(\Delta y)^2} \qquad \textbf{(II.36)}$$

in which $\Phi = \Phi(x, y) = \Phi_{i,j}$.

Assuming a uniform grid in both directions, $\Delta x = \Delta y = h$, eq. (II.33) converts to:

$$-\Phi_{i+1,j} - \Phi_{i-1,j} - \Phi_{i,j+1} - \Phi_{i,j-1} + (4-\lambda)\,\Phi_{i,j} = 0 \qquad \textbf{(II.37)}$$

This is called a five point finite difference operator, and generally can be expressed in the following form:

$$b_{i,j}^{i,j-1} \cdot \Phi_{i,j-1} + b_{i,j}^{i-1,j} \cdot \Phi_{i-1,j} + b_{i,j}^{i,j} \cdot \Phi_{i,j} + b_{i,j}^{i+1,j} \cdot \Phi_{i+1,j} + b_{i,j}^{i,j+1} \cdot \Phi_{i,j+1} = 0 \qquad \textbf{(II.38)}$$

where, for the internal points, $b_{i,j}^{i,j-1} = b_{i,j}^{i-1,j} = b_{i,j}^{i+1,j} = b_{i,j}^{i,j+1} = -1$ and $b_{i,j}^{i,j} = 4-\lambda$. The eigenvalue λ is also defined as:

$$\lambda = (k_c h)^2 \qquad \textbf{(II.39)}$$

FIGURE II.5 The finite difference grid

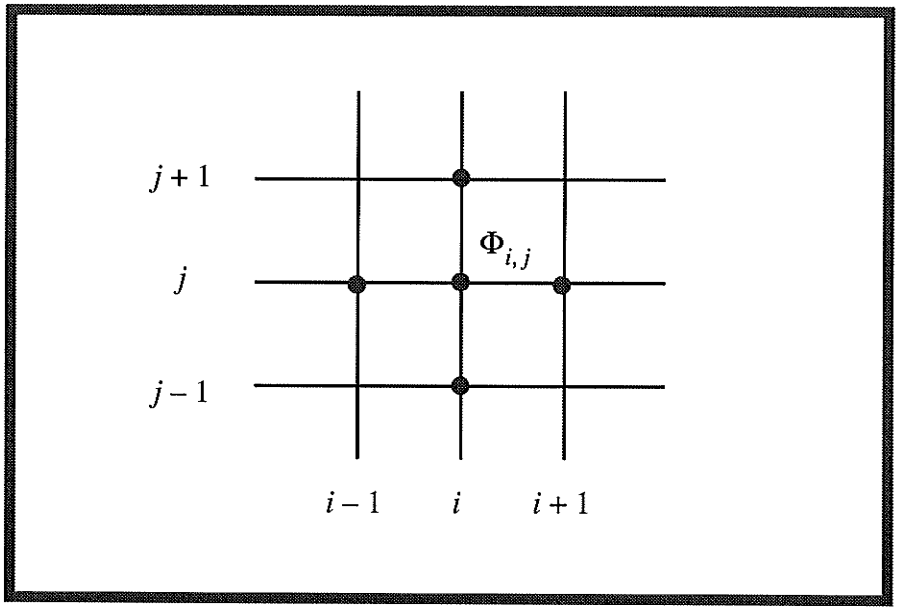

Now, assuming a rectangular grid with M and N mesh grid nodes in the x and y directions, respectively, the following eigenvalue system of equations can be generated:

$$[A - \lambda I]_{MN \times MN} [\Phi]_{MN \times 1} = [0]_{MN \times 1} \quad \textbf{(II.40)}$$

or,

$$[B]_{MN \times MN} [\Phi]_{MN \times 1} = [0]_{MN \times 1} \quad \textbf{(II.41)}$$

in which $B = A - \lambda I$. For a non-trivial solution to eq. (II.41), the determinant of matrix B must be zero. This can be achieved only for certain discrete values of λ called eigenvalues. The problem is that these eigenvalues are not known beforehand. Two approaches can be chosen to solve the problem, either direct or iterative methods. On the other hand, according to eq. (II.37), only five non-zero elements exist corresponding to each row of the B matrix. This renders the final system of equations highly sparse. According to the Linear Algebra theory, iterative methods are generally much more efficient compared to direct methods when it comes to sparse matrices. This results in shorter computational time. Also, in iterative methods, one row of the matrix is needed at a time, whereas in direct methods the entire matrix must be calculated and stored in computer memory. This makes direct methods inefficient compared to iterative methods both in CPU time and RAM memory. Based upon this analysis, iterative schemes have been favored for solving the above eigenvalue problems.

The algorithm starts with an initial guess for the eigenvalue λ and eigenvector Φ. Generally speaking, these guessed values are inaccurate. As long as the initial guess is not

too far from the correct one, a variational relation known as the Rayleigh quotient can be implemented:

$$\lambda^{(r+1)} = \frac{\Phi^{(r)T} A \Phi^{(r)}}{\Phi^{(r)T} \Phi^{(r)}} \tag{II.42}$$

where r and T represent iteration number and vector transpose operator respectively. In the same manner, Rayleigh quotient can be implemented after each iteration to reach a better estimate of the eigenvalue. Finally, iteration can be terminated whenever the following convergence tests are met:

$$\left|\lambda^{(r+1)} - \lambda^{(r)}\right| \le \varepsilon_{\lambda} \tag{II.43.a}$$

$$\left\|\Phi^{(r+1)} - \Phi^{(r)}\right\| \le \varepsilon_{\Phi} \tag{II.43.b}$$

$$R = \sqrt{\frac{(B\Phi)^{T} B\Phi}{\Phi^{T}\Phi}} \le \varepsilon_{R} \tag{II.43.c}$$

Depending on the objectives of the analysis, any or all of the above criteria can be checked before terminating the iterations. For instance, if the dispersion curve is desired, eq. (II.43.a) can be enforced, whereas for field pattern analysis, eq. (II.43.b) seems more appropriate. Eq. (II.43.c) might be more meaningful if the final convergence of the mathematical system is desired. However, under ideal circumstances, and upon reaching the convergence, all three criteria should be vanishingly small.

To review the mathematical concept of convergence, suppose a successive over-relaxation method is implemented to achieve faster convergence:

$$\Phi_{i,j}^{(r+1)} = (1-\omega)\,\Phi_{i,j}^{(r)} + \frac{\omega}{(4-\lambda)}\left[\Phi_{i,j-1}^{(r+1)} + \Phi_{i-1,j}^{(r+1)} + \Phi_{i,j+1}^{(r)} + \Phi_{i+1,j}^{(r)}\right] \qquad \textbf{(II.44)}$$

assuming that scanning of the numerical space is done from left to right and from bottom to top. Eq. (II.44) is valid only for internal nodes. For nodes in the neighborhood of the boundary, some of the coefficients would be different, depending on the **TE** or **TM** mode analysis. For the **TM** mode, matrix B is symmetric. This is not the case for the **TE** mode due to Neumann boundary conditions that can deteriorate the convergence properties of the final algorithm.

In any case, there are several strategies that can be adopted to ensure convergence of the final algorithm. One of them [22] is based on multiplying the B matrix by its transpose to achieve a symmetric positive definite matrix. From eq. (II.41), and pre-multiplying by B^T, one obtains:

$$B^T(B\Phi) = 0 \qquad \textbf{(II.45)}$$

$$C\Phi = 0 \qquad \textbf{(II.46)}$$

where $C = B^T B$. It can be proved that B and C share the same eigenvalues.

$$det(C) = det\left(B^T\right) det(B) = (det(B))^2 \qquad \textbf{(II.47)}$$

The main advantage of using C instead of B is in the fact that C is a positive definite matrix when λ is not an eigenvalue, and positive semi-definite when λ is an eigenvalue. Suppose, x is an arbitrary matrix with at least one nonzero element:

$$x^T x > 0 \qquad \textbf{(II.48)}$$

and also assume that for each x, there exists a y that satisfies the following equation:

$$x = By \tag{II.49}$$

It is obvious that y is a real matrix, provided that B is non-singular, an assumption which is valid when λ is not an eigenvalue. Replacing (II.49) in (II.48) gives:

$$y^T B^T B y = y^T C y \geq 0 \tag{II.50}$$

As indicated earlier, C is not only a positive semi-definite matrix, but also symmetric:

$$C^T = \left(B^T B\right)^T = B^T B = C \tag{II.51}$$

It is known that successive over-relaxation is guaranteed to converge for a positive semi-definite matrix [23]. Therefore, the aforementioned procedure is a reliable method even for higher order modes.

Since this method is meant to be an iterative one, not all the elements of B are known in advance and therefore, the multiplication $C = B^T B$ cannot be performed directly. A thorough investigation of how this multiplication works on a highly sparse matrix such as the one generated by eq. (II.37), results in a thirteen point finite difference [22], in contrast with the original finite difference which was based on a five point operator. Again, assuming that scanning is done from left to right and from bottom to top:

$$\Phi_{i,j}^{(r+1)} = (1-\omega)\,\Phi_{i,j}^{(r)} - \frac{\omega}{c_{i,j}^{i,j}}\Big[c_{i,j}^{i,j-2}\Phi_{i,j-2}^{(r+1)} + c_{i,j}^{i-1,j-1}\Phi_{i-1,j-1}^{(r+1)} \qquad \textbf{(II.52)}$$

$$+ c_{i,j}^{i,j-1}\Phi_{i,j-1}^{(r+1)} + c_{i,j}^{i+1,j-1}\Phi_{i+1,j-1}^{(r+1)} + c_{i,j}^{i-2,j}\Phi_{i-2,j}^{(r+1)} + c_{i,j}^{i-1,j}\Phi_{i-1,j}^{(r+1)}$$

$$+ c_{i,j}^{i+1,j}\Phi_{i+1,j}^{(r)} + c_{i,j}^{i+2,j}\Phi_{i+2,j}^{(r)} + c_{i,j}^{i-1,j+1}\Phi_{i-1,j+1}^{(r)} + c_{i,j}^{i,j+1}\Phi_{i,j+1}^{(r)}$$

$$+ c_{i,j}^{i+1,j+1}\Phi_{i+1,j+1}^{(r)} + c_{i,j}^{i,j+2}\Phi_{i,j+2}^{(r)}\Big]$$

$$c_{i,j}^{i,j+2} = b_{i,j+1}^{i,j} \cdot b_{i,j+1}^{i,j+2} \qquad \textbf{(II.53)}$$

$$c_{i,j}^{i-1,j+1} = b_{i,j+1}^{i,j} \cdot b_{i,j+1}^{i-1,j+1} + b_{i-1,j}^{i,j} \cdot b_{i-1,j}^{i-1,j+1}$$

$$c_{i,j}^{i,j+1} = b_{i,j+1}^{i,j} \cdot b_{i,j+1}^{i,j+1} + b_{i,j}^{i,j} \cdot b_{i,j}^{i,j+1}$$

$$c_{i,j}^{i+1,j+1} = b_{i,j+1}^{i,j} \cdot b_{i,j+1}^{i+1,j+1} + b_{i+1,j}^{i,j} \cdot b_{i+1,j}^{i+1,j+1}$$

$$c_{i,j}^{i-2,j} = b_{i-1,j}^{i,j} \cdot b_{i-1,j}^{i-2,j}$$

$$c_{i,j}^{i-1,j} = b_{i-1,j}^{i,j} \cdot b_{i-1,j}^{i-1,j} + b_{i,j}^{i,j} \cdot b_{i,j}^{i-1,j}$$

$$c_{i,j}^{i,j} = \left(b_{i,j+1}^{i,j}\right)^2 + \left(b_{i-1,j}^{i,j}\right)^2 + \left(b_{i,j}^{i,j}\right)^2 + \left(b_{i+1,j}^{i,j}\right)^2 + \left(b_{i,j-1}^{i,j}\right)^2$$

$$c_{i,j}^{i+1,j} = b_{i,j}^{i,j} \cdot b_{i,j}^{i+1,j} + b_{i+1,j}^{i,j} \cdot b_{i+1,j}^{i+1,j}$$

$$c_{i,j}^{i+2,j} = b_{i+1,j}^{i,j} \cdot b_{i+1,j}^{i+2,j}$$

$$c_{i,j}^{i-1,j-1} = b_{i-1,j}^{i,j} \cdot b_{i-1,j}^{i-1,j-1} + b_{i,j-1}^{i,j} \cdot b_{i,j-1}^{i-1,j-1}$$

$$c_{i,j}^{i,j-1} = b_{i,j}^{i,j} \cdot b_{i,j}^{i,j-1} + b_{i,j-1}^{i,j} \cdot b_{i,j-1}^{i,j-1}$$

$$c_{i,j}^{i+1,j-1} = b_{i+1,j}^{i,j} \cdot b_{i+1,j}^{i+1,j-1} + b_{i,j-1}^{i,j} \cdot b_{i,j-1}^{i+1,j-1}$$

$$c_{i,j}^{i,j-2} = b_{i,j-1}^{i,j} \cdot b_{i,j-1}^{i,j-2}$$

FIGURE II.6 Thirteen point finite difference mesh

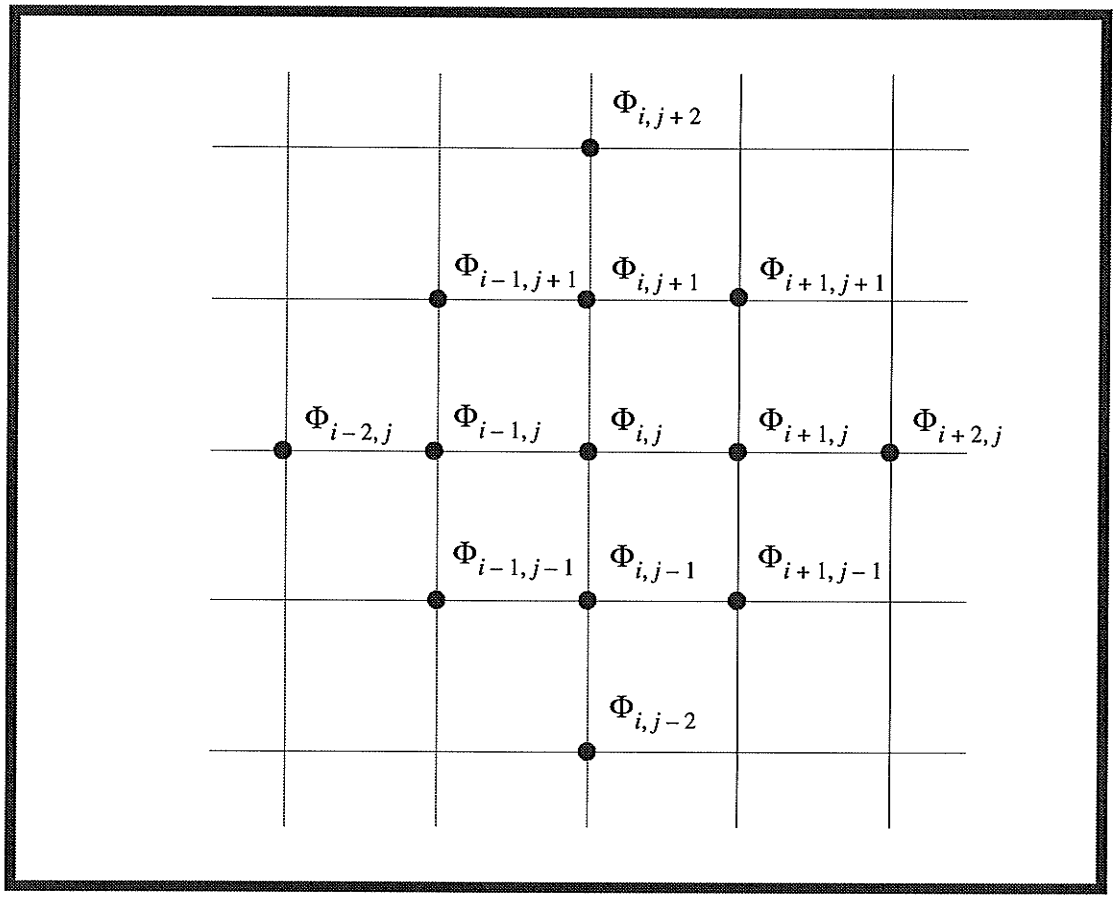

In summary, eq. (II.52) can be written as:

$$\Phi^{(r+1)} = \Psi_{\omega,\lambda}\Phi^{(r)} = \Psi^{r}_{\omega,\lambda}\Phi^{(0)} \qquad \textbf{(II.54)}$$

where the subscripts in operator Ψ refer to its dependence on ω and λ.

Since the set of eigenvectors spans a complete vector space, any vector can be expressed in terms of a linear combination of orthonormal eigenvectors. Let's decompose $\Phi^{(0)}$, the first eigenvector guesses, into a summation of eigenvectors:

$$\Phi^{(0)} = a_1 x_1 + a_2 x_2 + \ldots + a_N x_N \qquad \textbf{(II.55)}$$

in which, the eigenvectors x_i are those of C, or to be more accurate ψ. Since, the eigenvectors constitute an orthonormal set, after $r+1$ iterations, one obtains:

$$\Phi^{(r+1)} = a_1\mu_1^r x_1 + a_2\mu_2^r x_2 + \ldots + a_N\mu_N^r x_N \qquad \textbf{(II.56)}$$

where μ_i is the corresponding eigenvalue to x_i. For this iteration to be stable, the modulus of all eigenvalues should be less than unity. Suppose that μ_1 has the biggest modulus. Therefore:

$$\Phi^{(r+1)} = \lim_{r\to\infty} a_1\mu_1^r x_1 \qquad \textbf{(II.57)}$$

and the only possible way that this iteration can result in a unique stable solution, the fact that was already proven, is by assuming $\mu_1 = 1$. Of course, this happens, if and only if the correct value of λ_1 is substituted into eq. (II.44) or (II.52). If λ_1 deviates slightly from the correct value, so does μ_1, and as a result the iterations either blow up or converge to zero, depending on $|\mu_1|$ being greater or less than unity. On the other hand, the interesting point is that even for the wrong λ_1 s, eq. (II.57) has the tendency to converge to the correct shape of Φ, even though the amplitude will not be accurate until the correct eigenvalue is substituted. This fact, can be very useful whenever only the field pattern is sought, i.e. FWFD.

II.C.2. Arndt's direct approach

THE NEXT approach which is more general, but less efficient, is due to Arndt et al. [24]. It is general, because it is not restricted to cut-off frequencies. One major drawback of the Beaubien-Wexler approach is the fact that it is derived from the assumption that the modes are decomposable into TE and TM modes. It can be proved that this is only valid for the following special cases:

- *Homogeneous waveguides and entire range of the frequency spectrum*
- *Inhomogeneous waveguides operating only at cut-off frequency, appendix A:*

As can be seen, the general case of inhomogeneous waveguide operating in an arbitrary frequency is missing from the aforementioned list. Under these circumstances, modes are generally present in their hybrid form, meaning all six vector field components are present. Now, let's investigate more carefully why the Beaubien-Wexler approach can not be implemented for this general case, and determine if there is any possibility of modifications:

- ***It is based on a TE and TM mode decomposition which is not generally valid.***

Comment: Even for the general case, the homogeneous Helmholtz equation for H field components holds, similar to eq. (I.14). But, remember that for the electric field components, E, the inhomogeneous Helmholtz equation (I.13) must be used, which leads to excessively complicated equations, correlating all electric field components. There-

fore, as long as the dispersion curve analysis is desired, not the field patterns; the homogeneous Helmholtz equation in terms of one of the magnetic field components can be expanded into its finite difference form and used to extract the eigenvalues. But, as will be explained in the next paragraph, this approach does not lead to a unique solution and hence is prone to the appearance of spurious modes.

- ***At least the knowledge of two field components is required to determine the total field uniquely.***

Comment: As it is demonstrated by Harrington [25], every hybrid field configuration can be expressed as a superposition of two electric and magnetic vector potentials. On the other hand, each of these vector potentials can only generate one type of TE or TM field, and hence the presence of both is necessary to provide a hybrid field. By a simple analogy, Φ in Beaubien-Wexler's formulation can be viewed as the z component of the generating potential. It is a scalar function because we are only considering the TE_z and/or TM_z which are both in the z direction. Now, if the general Inhomogeneous case is desired, at least two potentials, or equivalently two field components have to be solved simultaneously. But, the presence of two field components was not predicted in the original Beaubien-Wexler formulation.

Arndt's approach [24] was developed by keeping both of the aforementioned points in mind. As usual, it starts from the Homogeneous Helmholtz equations:

$$\nabla_t^2 H_x^{(\nu)} + k_\nu^2 H_x^{(\nu)} = 0 \qquad \textbf{(II.58)}$$

and;

$$\nabla_t^2 H_y^{(\nu)} + k_\nu^2 H_y^{(\nu)} = 0 \qquad \textbf{(II.59)}$$

where $k_\nu^2 = \omega^2 \mu \varepsilon_\nu + \gamma^2$ and $\nu = 1, 2, 3, 4$ represents region numbers, Fig. (II.7).

FIGURE II.7 Adaptive finite difference scheme

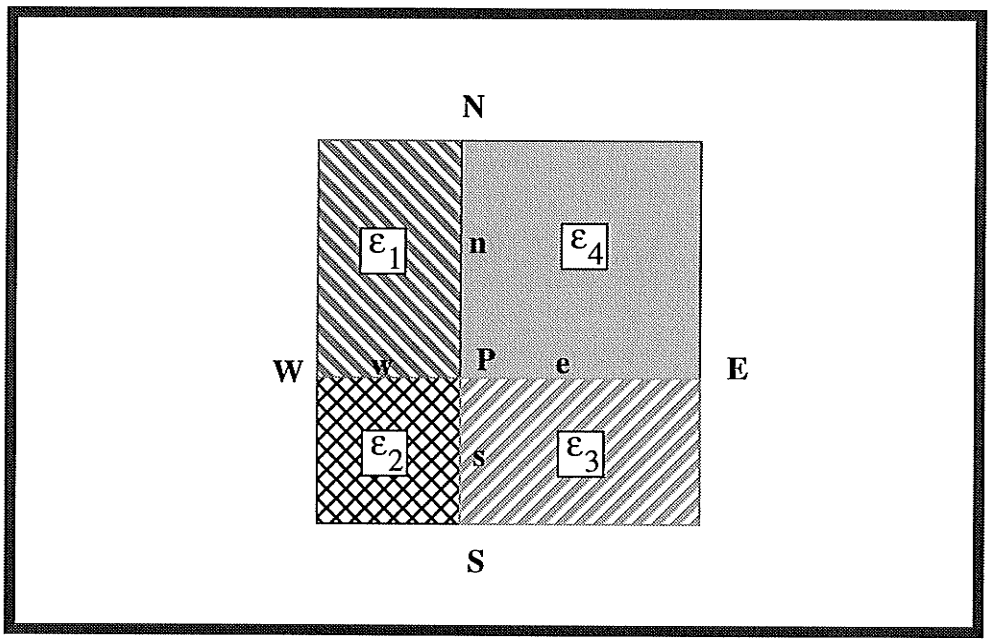

Now, these equations have to be expanded in an inhomogeneous medium. Assume that each inhomogeneous medium can be discretized into a finite number of homogeneous ones. At the worst case, the central node P can be placed on the interface between four

different homogeneous media. Expanding eqs. (II.58) and (II.59) results in each of these sub-regions as:

Region 1: $$-\frac{n}{w}H_W-\frac{w}{n}H_N+\left(\frac{w}{n}+\frac{n}{w}\right)H_P-\frac{1}{2}wnk_1^2H_P+w\frac{\partial H}{\partial y}\bigg|_1-n\frac{\partial H}{\partial x}\bigg|_1=0 \quad \textbf{(II.60.a)}$$

Region 2: $$-\frac{s}{w}H_W-\frac{w}{s}H_S+\left(\frac{w}{s}+\frac{s}{w}\right)H_P-\frac{1}{2}wsk_2^2H_P-w\frac{\partial H}{\partial y}\bigg|_2-s\frac{\partial H}{\partial x}\bigg|_2=0 \quad \textbf{(II.60.b)}$$

Region 3: $$-\frac{s}{e}H_E-\frac{e}{s}H_S+\left(\frac{e}{s}+\frac{s}{e}\right)H_P-\frac{1}{2}esk_3^2H_P-e\frac{\partial H}{\partial y}\bigg|_3+s\frac{\partial H}{\partial x}\bigg|_3=0 \quad \textbf{(II.60.c)}$$

Region 4: $$-\frac{n}{e}H_E-\frac{e}{n}H_N+\left(\frac{n}{e}+\frac{e}{n}\right)H_P-\frac{1}{2}enk_4^2H_P+e\frac{\partial H}{\partial y}\bigg|_4+n\frac{\partial H}{\partial x}\bigg|_4=0 \quad \textbf{(II.60.d)}$$

where H stands for H_x or H_y. The existence of partial derivative operators in the finite difference formulations of (II.60.a)-(II.60.d) can be explained in lieu of the inhomogenity between neighboring regions. As was explained in section II.C.1, in five point finite difference operator the potential, or the field, at the central node must be expressed in terms of its four neighboring points. On the other hand, according to Fig. II.7, only two of these neighbors fall on the same region each time. The other two points must be extrapolated using the first term of taylor's series; hence the presence of these partial derivatives come to the picture. But, a digital computer is only capable of dealing with partial differences, not derivatives. Therefore, to remove them, additional equations are needed. These extra equations can be supplied by imposing boundary conditions. In fact, by imposing the boundary conditions, another purpose which is assuring the unique solution of maxwell's equations, can also be served.

When solving for H_x in eqs. (II.60.a)-(II.60.d):

$$E_{z1} = E_{z2} \qquad \frac{-1}{\varepsilon_1}\frac{\partial H_x}{\partial y}\bigg|_1 + \frac{1}{\varepsilon_2}\frac{\partial H_x}{\partial y}\bigg|_2 + \frac{1}{\varepsilon_1}\frac{\partial H_y}{\partial x}\bigg|_1 - \frac{1}{\varepsilon_2}\frac{\partial H_y}{\partial x}\bigg|_2 = 0 \qquad \textbf{(II.61.a)}$$

$$E_{z3} = E_{z4} \qquad \frac{1}{\varepsilon_3}\frac{\partial H_x}{\partial y}\bigg|_3 + \frac{-1}{\varepsilon_4}\frac{\partial H_x}{\partial y}\bigg|_4 + \frac{-1}{\varepsilon_3}\frac{\partial H_y}{\partial x}\bigg|_3 + \frac{1}{\varepsilon_4}\frac{\partial H_y}{\partial x}\bigg|_4 = 0 \qquad \textbf{(II.61.b)}$$

$$H_{z1} = H_{z2} \qquad \frac{\partial H_x}{\partial x}\bigg|_1 - \frac{\partial H_x}{\partial x}\bigg|_2 + \frac{\partial H_y}{\partial y}\bigg|_1 - \frac{\partial H_y}{\partial y}\bigg|_2 = 0 \qquad \textbf{(II.61.c)}$$

$$H_{z3} = H_{z4} \qquad \frac{\partial H_x}{\partial x}\bigg|_3 - \frac{\partial H_x}{\partial x}\bigg|_4 + \frac{\partial H_y}{\partial y}\bigg|_3 - \frac{\partial H_y}{\partial y}\bigg|_4 = 0 \qquad \textbf{(II.61.d)}$$

$$H_{z1} = H_{z4} \qquad \frac{\partial H_x}{\partial x}\bigg|_1 - \frac{\partial H_x}{\partial x}\bigg|_4 + \frac{\partial H_y}{\partial y}\bigg|_1 - \frac{\partial H_y}{\partial y}\bigg|_4 = 0 \qquad \textbf{(II.61.e)}$$

When solving for H_y in eqs. (II.60.a)-(II.60.d):

$$E_{z1} = E_{z4} \qquad \frac{-1}{\varepsilon_1}\frac{\partial H_x}{\partial y}\bigg|_1 + \frac{1}{\varepsilon_4}\frac{\partial H_x}{\partial y}\bigg|_4 + \frac{1}{\varepsilon_1}\frac{\partial H_y}{\partial x}\bigg|_1 - \frac{1}{\varepsilon_4}\frac{\partial H_y}{\partial x}\bigg|_4 = 0 \qquad \textbf{(II.62.a)}$$

$$E_{z2} = E_{z3} \qquad \frac{1}{\varepsilon_3}\frac{\partial H_x}{\partial y}\bigg|_3 + \frac{-1}{\varepsilon_2}\frac{\partial H_x}{\partial y}\bigg|_2 + \frac{-1}{\varepsilon_3}\frac{\partial H_y}{\partial x}\bigg|_3 + \frac{1}{\varepsilon_2}\frac{\partial H_y}{\partial x}\bigg|_2 = 0 \qquad \textbf{(II.62.b)}$$

$$H_{z1} = H_{z4} \qquad \frac{\partial H_x}{\partial x}\bigg|_1 - \frac{\partial H_x}{\partial x}\bigg|_4 + \frac{\partial H_y}{\partial y}\bigg|_1 - \frac{\partial H_y}{\partial y}\bigg|_4 = 0 \qquad \textbf{(II.62.c)}$$

$$H_{z2} = H_{z3} \qquad \frac{\partial H_x}{\partial x}\bigg|_3 - \frac{\partial H_x}{\partial x}\bigg|_2 + \frac{\partial H_y}{\partial y}\bigg|_3 - \frac{\partial H_y}{\partial y}\bigg|_2 = 0 \qquad \textbf{(II.62.d)}$$

$$H_{z1} = H_{z2} \qquad \frac{\partial H_x}{\partial x}\bigg|_2 - \frac{\partial H_x}{\partial x}\bigg|_1 + \frac{\partial H_y}{\partial y}\bigg|_2 - \frac{\partial H_y}{\partial y}\bigg|_1 = 0 \qquad \textbf{(II.62.e)}$$

And finally, by cancelling the partial derivative operators, the final equations are derived, eqs. (II.65.a) and (II.65.b). One interesting point about these equations is the inter-dependency of x and y components of the field. In other words, H_x in a mesh point

is a function of both H_x and H_y at its four neighboring points. This observation is in close agreement with the predictions on page 58.

Writing these equations for each individual node results in the following matrix equation:

$$\begin{bmatrix} (X) & (YX) \\ (XY) & (Y) \end{bmatrix} \begin{bmatrix} (H_x) \\ (H_y) \end{bmatrix} = -\gamma^2 \begin{bmatrix} (H_x) \\ (H_y) \end{bmatrix} \qquad \textbf{(II.63)}$$

in which (X) and (Y) stand for the coefficient matrices of H_x and H_y terms. Also, (XY) and (YX) refer to the mutual coupling $H_y \rightarrow H_x$ and $H_x \rightarrow H_y$, respectively. Finally, by rewriting this last equation:

$$[\,(A) - \lambda\,(I)\,]\,[\chi] = 0 \qquad \textbf{(II.64)}$$

where:

$$\lambda = -\gamma^2$$

$$[\chi] = \left[H_{x1}\ H_{x2}\ \ldots\ H_{xN}\ H_{y1}\ H_{y2}\ \ldots\ H_{yN}\right]^T$$

Finally, one of the eigen-solver packages, like EISPACK [26] can be employed to extract the eigenvalues of eq. (II.64).

$$\frac{2}{w(w+e)}H_{xW}+\frac{2}{e(w+e)}H_{xE}+\frac{2}{n(w+e)}\left(\frac{w\varepsilon_2}{s\varepsilon_1+n\varepsilon_2}+\frac{e\varepsilon_3}{n\varepsilon_3+s\varepsilon_4}\right)H_{xN}+\frac{2}{s(w+e)}\left(\frac{w\varepsilon_1}{s\varepsilon_1+n\varepsilon_2}+\frac{e\varepsilon_4}{n\varepsilon_3+s\varepsilon_4}\right)H_{xS} \qquad \textbf{(II.65.a)}$$
$$-\frac{2}{w+e}\left(\frac{\varepsilon_1}{s\varepsilon_1+n\varepsilon_2}\left(\frac{w}{s}+\frac{s}{w}\right)+\frac{\varepsilon_2}{s\varepsilon_1+n\varepsilon_2}\left(\frac{w}{n}+\frac{n}{w}\right)+\frac{\varepsilon_3}{n\varepsilon_3+s\varepsilon_4}\left(\frac{e}{n}+\frac{n}{e}\right)+\frac{\varepsilon_4}{n\varepsilon_3+s\varepsilon_4}\left(\frac{e}{s}+\frac{s}{e}\right)\right)H_{xP}$$
$$+\omega^2\mu\left(\frac{n+s}{w+e}\right)\left(\frac{w\varepsilon_1\varepsilon_2}{s\varepsilon_1+n\varepsilon_2}+\frac{e\varepsilon_3\varepsilon_4}{n\varepsilon_3+s\varepsilon_4}\right)H_{xP}+\gamma^2H_{xP}-\frac{2}{w+e}\left(\frac{\varepsilon_1-\varepsilon_2}{s\varepsilon_1+n\varepsilon_2}\right)H_{yW}-\frac{2}{w+e}\left(\frac{\varepsilon_3-\varepsilon_4}{n\varepsilon_3+s\varepsilon_4}\right)H_{yE}$$
$$-\frac{2}{w+e}\left(\frac{\varepsilon_2}{s\varepsilon_1+n\varepsilon_2}-\frac{\varepsilon_3}{n\varepsilon_3+s\varepsilon_4}\right)H_{yN}-\frac{2}{w+e}\left(\frac{\varepsilon_4}{n\varepsilon_3+s\varepsilon_4}-\frac{\varepsilon_1}{s\varepsilon_1+n\varepsilon_2}\right)H_{yS}=0$$

$$\frac{2}{w(n+s)}\left(\frac{s\varepsilon_3}{e\varepsilon_2+w\varepsilon_3}+\frac{n\varepsilon_4}{e\varepsilon_1+w\varepsilon_4}\right)H_{yW}+\frac{2}{e(n+s)}\left(\frac{n\varepsilon_1}{e\varepsilon_1+w\varepsilon_4}+\frac{s\varepsilon_2}{e\varepsilon_2+w\varepsilon_3}\right)H_{yE}+\frac{2}{n(n+s)}H_{yN}+\frac{2}{s(n+s)}H_{yS} \qquad \textbf{(II.65.b)}$$
$$-\frac{2}{n+s}\left(\frac{\varepsilon_1}{e\varepsilon_1+w\varepsilon_4}\left(\frac{e}{n}+\frac{n}{e}\right)+\frac{\varepsilon_2}{e\varepsilon_2+w\varepsilon_3}\left(\frac{e}{s}+\frac{s}{e}\right)+\frac{\varepsilon_3}{e\varepsilon_2+w\varepsilon_3}\left(\frac{w}{s}+\frac{s}{w}\right)+\frac{\varepsilon_4}{e\varepsilon_1+w\varepsilon_4}\left(\frac{w}{n}+\frac{n}{w}\right)\right)H_{yP}$$
$$+\omega^2\mu\left(\frac{w+e}{n+s}\right)\left(\frac{n\varepsilon_1\varepsilon_4}{e\varepsilon_1+w\varepsilon_4}+\frac{s\varepsilon_2\varepsilon_3}{e\varepsilon_2+w\varepsilon_3}\right)H_{yP}+\gamma^2H_{yP}+\frac{2}{n+s}\left(\frac{\varepsilon_3}{e\varepsilon_2+w\varepsilon_3}-\frac{\varepsilon_4}{e\varepsilon_1+w\varepsilon_4}\right)H_{xW}$$
$$+\frac{2}{n+s}\left(\frac{\varepsilon_1}{e\varepsilon_1+w\varepsilon_4}-\frac{\varepsilon_2}{e\varepsilon_2+w\varepsilon_3}\right)H_{xE}+\frac{2}{n+s}\left(\frac{\varepsilon_4-\varepsilon_1}{e\varepsilon_1+w\varepsilon_4}\right)H_{xN}+\frac{2}{n+s}\left(\frac{\varepsilon_2-\varepsilon_3}{e\varepsilon_2+w\varepsilon_3}\right)H_{xS}=0$$

II.D. Conclusion

DIFFERENT FINITE difference methods have been discussed. They were subdivided into two major categories of time domain and frequency domain techniques. It has been stressed that all time domain methods are in essence equivalent and therefore for most of the applications are interchangeable. However, this does not mean that these methods can offer the same speed or require the same amount of **CPU** and memory resources. On the contrary, one can usually find one (or some) of these methods more efficient than the others. In the dispersion curve analysis, it can be shown that the **FDTD** is superior than other time domain finite difference methods and so it is the method of choice.

Frequency domain techniques are historically older and mathematically more involved than time domain techniques. It has also been demonstrated that the frequency domain finite difference techniques, in their present form, lack the generality and the efficiency required for a versatile CAD package.

During the following two chapters, two novel finite difference techniques will be proposed. One of them is based on a time domain scheme and the other on a frequency domain one. It will be shown that they are much more powerful and efficient than their predecessors.

Chapter Three

COMPACT FDTD

Dispersion Analysis

III.A. Introduction

ALL versions of finite difference (time and frequency domain) techniques relevant to the particular topic of this thesis (guided wave structures) were discussed in the previous chapter. Some of these methods, like the TLM and FDTD have been used for a vast array of electromagnetic applications, i.e. scattering, antennas,..., and finally eigenvalue problems. Whereas others, like finite difference methods were mainly developed to deal with eigenvalue, and particularly waveguide, problems.

In this chapter, the following objectives are pursued:

- *Demonstrate different possible strategies that have been common in time domain analysis of guided wave structures.*
- *Introduce Compact FDTD*
- *Compare Compact FDTD with classical time and frequency domain finite difference methods and prove its superiority.*

This chapter begins with the basic idea behind the frequency spectroscopy as a means of eigenvalue evaluation. The implementations of two and three dimensional **TLM** and **FDTD** constitute the subject of the succeeding sections. Finally, the Compact **FDTD** which is the main subject of this study is introduced with major emphasize on its advantages over the other methods.

III.B. Frequency spectroscopy as a means for evaluating eigenvalues

FROM GENERAL circuit theory, it is known that if the input port of a circuit is excited with a unit impulse function, the Fourier transform of the output will represent the circuit transfer function which in turn contains all the information about the network. Using the same analogy, one can excite any linear structure (or in fact any linear system of differential equations) with a unit impulse and safely assume that all the characteristics of the structure will manifest themselves in the output response.

FIGURE III.1 a) A general linear network model, (b) Corresponding waveguide model

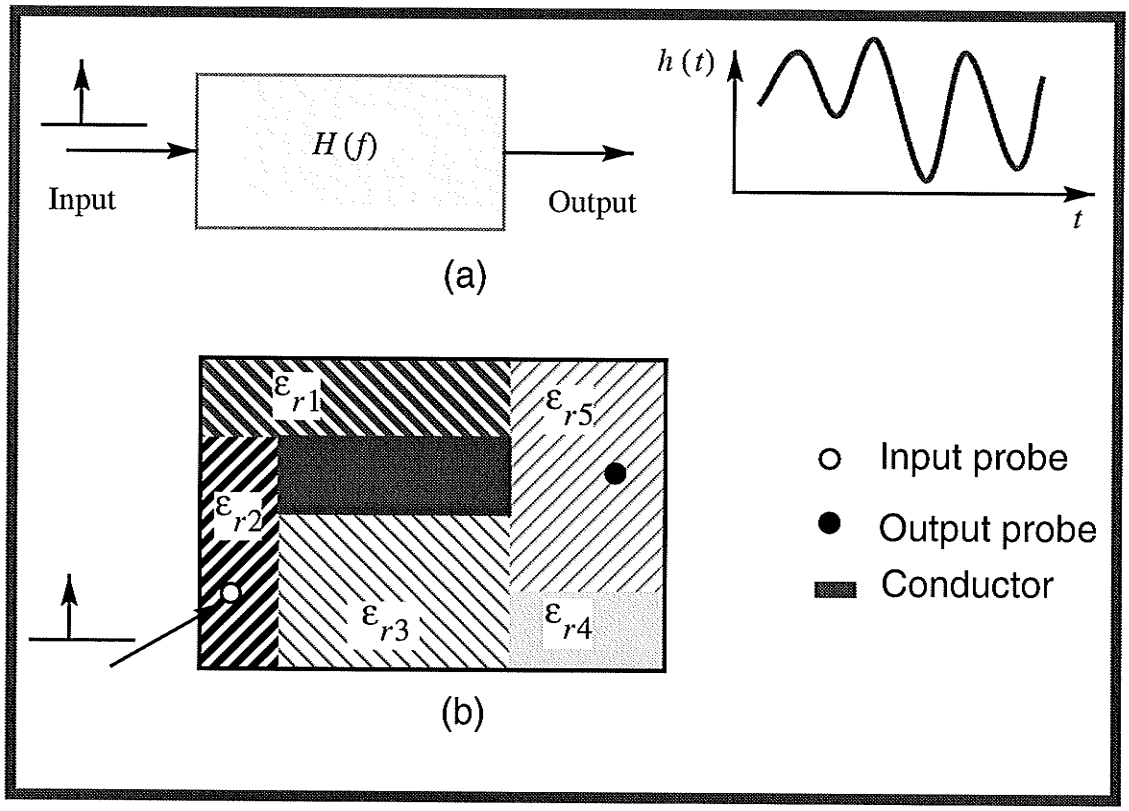

Fig. III.1(a) depicts a general linear network which is excited by a unit impulse and its corresponding response at an arbitrary point known as the output port. Fig. III.1(b) illustrates the same theory and procedure when it is applied to an inhomogeneous waveguide. In fact what is shown in this figure is the cross section of a rectangular waveguide with two probes input and output probes.

The choice of input and output ports is quite arbitrary and does not affect the locations of the poles of the transfer function in the complex frequency plane. On the other hand, certain modes can benefit from a particular probe location and have a stronger peak in the output spectrogram. This feature can be useful in the analysis of guided wave structures. For instance, one can use the symmetry property of a mode to enhance that particular mode and filter out the others. The probe type is another instrument that can be used to serve this purpose. Like practical situations, a probe can have six different configurations, its type being E or H and its alignment being in the x, y or z direction.As mentioned each propagating mode can be best excited, or attenuated, with a certain combination of the input and output probes. In a laboratory, the E probe can be made by the continuation of the central conductor of a coaxial cable, while the H probe can be constructed by a closed loop. However, from numerical computation point of view, implementation is much easier and can be accomplished by assuming the particular component as the input (or output) entry of the program.

III.B.1 Mathematical basis of frequency spectroscopy

GENERALLY SPEAKING, a waveguide can be viewed as a two dimensional resonant structure. In such a structure, the eigenvalues are cut-off frequencies, and eigenvectors are the orthonormal basis functions. According to applied mathematics terminology, these eigenvectors are also known as modes. If these modes span a complete set, then any arbitrary field distribution which satisfies the governing equations of the system, i.e. Maxwell or Helmholtz equations, can be expressed as a linear combination of these fundamental modes [35], i.e.:

$$\Psi(x, y, t) = \sum_m c_m \xi_m(x, y)\, e^{j2\pi f_m t} \qquad \textbf{(III.1)}$$

where m, c_m, $\xi_m(x, y)$ and f_m stand for modal index, modal amplitude, modal basis function and modal cut-off frequency, respectively. This represents a two dimensional wave function. In general, wave propagates in a three dimensional space, but since the wave behavior along the z direction is already known, i.e. $e^{-j\beta z}$, there is no need to enter it in the equation and make the final derivations more complex.

Eq. (III.1) is a continuous equation in terms of the time and space variables. But, we are interested in numerical computations in digital computers. Therefore, eq. (III.1) must be discretized:

$$\Psi^n(i, j) = \Psi(i\Delta x, j\Delta y, n\Delta t) \quad ; \quad n = 0, 1, 2, \ldots, N-1 \qquad \textbf{(III.2)}$$

But, from frequency spectroscopy point of view, the response in frequency domain is required. Taking DFT of the discrete time domain response results in:

$$\Im_k(i,j) = \sum_{n=0}^{N-1} \Psi^n(i,j)\, e^{-j2\pi f_k n\Delta t} \qquad \textbf{(III.3)}$$

in which $f_k = \dfrac{k}{N\Delta t}$.

Inserting eq. (III.1) in (III.3) yields:

$$\Im_k(i,j) = \sum_m c_m \xi_m(x,y) \sum_{n=0}^{N-1} e^{j2\pi f_m n\Delta t}\, e^{-j2\pi f_k n\Delta t} \qquad \textbf{(III.4)}$$

On the other hand:

$$\sum_{n=0}^{N-1} e^{j2\pi (f_m - f_k) n\Delta t} = \frac{1 - e^{j2\pi (f_m - f_k) N\Delta t}}{1 - e^{j2\pi (f_m - f_k)\Delta t}} = \frac{1 - e^{j2\pi f_m N\Delta t}}{1 - e^{j2\pi (f_m - f_k)\Delta t}} \qquad \textbf{(III.5)}$$

Eq. (III.5) is obtained using the trigonometric sum formula and $f_k N\Delta t = k$. Hence:

$$\Im_k(i,j) = \sum_m c_m \xi_m(x,y) \frac{1 - e^{j2\pi f_m N\Delta t}}{1 - e^{j2\pi (f_m - f_k)\Delta t}} \qquad \textbf{(III.6)}$$

Eq. (III.6) is quite adequate for drawing the conclusion that the poles in the frequency domain response, peaks of the spectrogram, are located at the eigenvalues of the structure, i.e. $f_k = f_m$.

III.C. TLM

THE CONCEPTS presented in section §III.B. are applicable using any time domain technique, i.e. the **TLM**, **FDTD** or **Bergeron**'s. In this section, a brief survey of the implementations of frequency spectroscopy concept using the **TLM**, as reported in the literature, are presented. In §III.C.1 the evaluation of cut-off frequencies using the **2D-TLM** is discussed. The extension of this technique to the entire dispersion curve is the subject of §III.C.2.

III.C.1 2D-TLM for evaluating cut-off frequencies

THE BASIC PRINCIPLES of a two dimensional **TLM** network have already been described in §II.B.1.. Here, the algorithms represented by eqs. (II.3) and (II.5.a)-(II.5.d) are being executed iteratively to simulate the structure shown by Fig. III.1 in the time domain. The idea of frequency spectroscopy as a numerical tool for calculating the eigenvalues of resonant structures, i.e. the cutoff frequencies of waveguides, goes back to 1971 when Johns [27][28][29] and his Ph.D. student, Akhtarzad were investigating the applications of their **TLM** method for different structures. The method was later extended to calculate the entire dispersion curve, not just cutoff frequencies, using a three dimensional application of the **TLM**. The results of their simulations have been reported in numerous publications [30][31][32][33]. There are also software packages which have been devel-

oped by Akhtarzad (in Fortran) [34] and later on by Hoefer (in Pascal) [2] to handle these simulations.

The basic weakness of this approach is in the fact that it is limited to cut off frequency calculations. A quick examination of eq. (II.7) depicts that there is no derivative with respect to the z variable present in that equation. In fact, that equation has been based on the major assumption that $\frac{\partial}{\partial z} = 0$, which in turn means $\beta = k_z = 0$. As is known, the latter is the basic criteria for defining the cut off frequency of a propagating mode.

III.C.2 3D-TLM for dispersion analysis

THE EXTENSION of the two dimensional **TLM** to three dimensions will enable one to solve for dispersion analysis. In fact, this step had also been undertaken by Akhtarzad [36] at the early stages of the **TLM** development. In this way, there is no need to assume $\beta = k_z = 0$, and therefore the analysis need not be restricted just to determination of cut-off frequencies.

It is obvious that a digital computer can only simulate a finite region of space. Therefore, the structure under study (waveguide) must be bounded along all coordinate system directions, x, y and z. The boundaries along the x and y directions can be considered as perfect electric conductors (**PEC**) provided that the waveguide is a closed one or the dimensions of the structure are much greater than the operating wavelength, i.e. high frequency assumption. One or several boundaries along the x and y directions can be considered as perfect magnetic conductors (**PMC**) in case that the study of a mode with a

particular symmetry, is desired. In this case, **PMC**s will be applied along the planes of even symmetry of the propagating mode under study. In case of odd symmetry, a **PEC** must be applied. Finally, in case of open waveguides, absorbing boundary condition must be enforced at the outer boundaries of the structure. Ideally, a waveguide possesses a cylindrical shape and so is infinite along the z direction. But, again, an infinite structure can not be modelled using the finite memory of a digital computer. To solve this problem, two different approaches have been proposed and utilized by researchers. Here, the first approach which was used in Akhtarzad's studies is presented. The second one is postponed to §III.D.

Fig. III.2 illustrates a partially filled waveguide which is surrounded by **PEC** walls along its transverse directions. As has been mentioned earlier, **PEC**s can be applied along the x and y directions as the surrounding walls of a closed waveguide or a waveguide operating at higher frequencies. But, in the z direction, the implementation of conductor walls serves another purpose. By closing the two ends of a waveguide in the z direction, it becomes a three dimensional resonant structure. The resonant frequencies of such a structure can be easily obtained at the locations of the peaks in the frequency response to a unit impulse excitation. On the other hand, the corresponding k_z (or β) can be calculated from the distance between the two conductor walls at the two ends of the waveguide along the z direction.

$$\beta = k_z = \frac{m\pi}{L} \qquad ; \quad m = 1, 2, 3, \ldots \qquad \textbf{(III.7)}$$

in which m is a positive integer and L is the length of the structure along the z direction. The values of a and b, the dimensions of the waveguide along the x and y directions

should be chosen exactly as the physical dimensions of the waveguide (in case of a closed structure) or large enough to have the least effect on the field distribution inside the structure (in case of an open structure). On the other hand, the choice of the value of L is quite arbitrary. In fact, in a complete dispersion analysis, one can start with a value of k_z (input of the problem) and then proceed to calculate L from eq. (III.7).

FIGURE III.2 Partially filled waveguide. All surrounding walls are PECs.

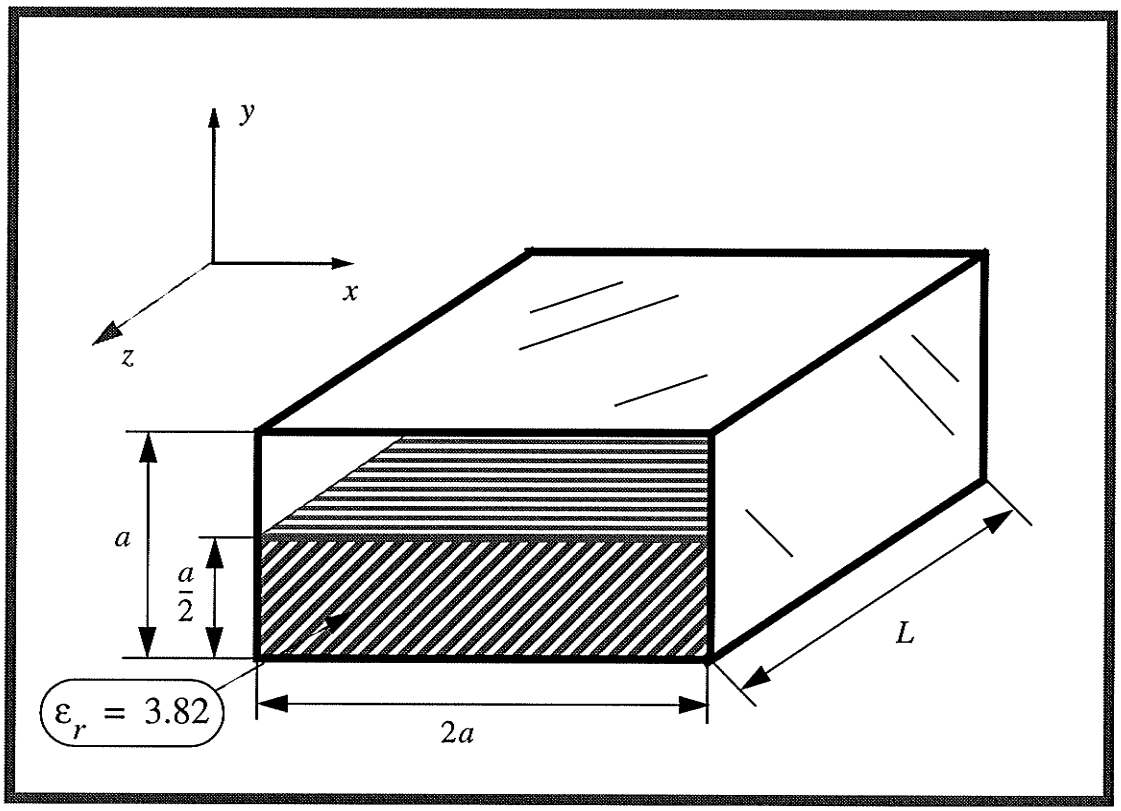

Fig. III.4 illustrates the procedure that generates a complete dispersion curve. Contrary to what will be described for classical **FD**, Fig., the dispersion curve in this case has been swept (generated) vertically. Note that for any particular value of k_z, there are several peaks in the frequency response in the desired bandwidth, ω_{r1}, ω_{r2}, ω_{r3},..... Note,

however, that the 3D-TLM is not a very reliable method for multimode analysis. Let's elaborate on this with an example. Suppose the distance between the two PEC walls is set to $L = L_1$, therefore:

$$\beta = \frac{\pi}{L_1}, \frac{2\pi}{L_1}, \frac{3\pi}{L_1}, \cdots \qquad \textbf{(III.8)}$$

FIGURE III.3 General procedure for generating a complete dispersion curve using 3D-TLM.

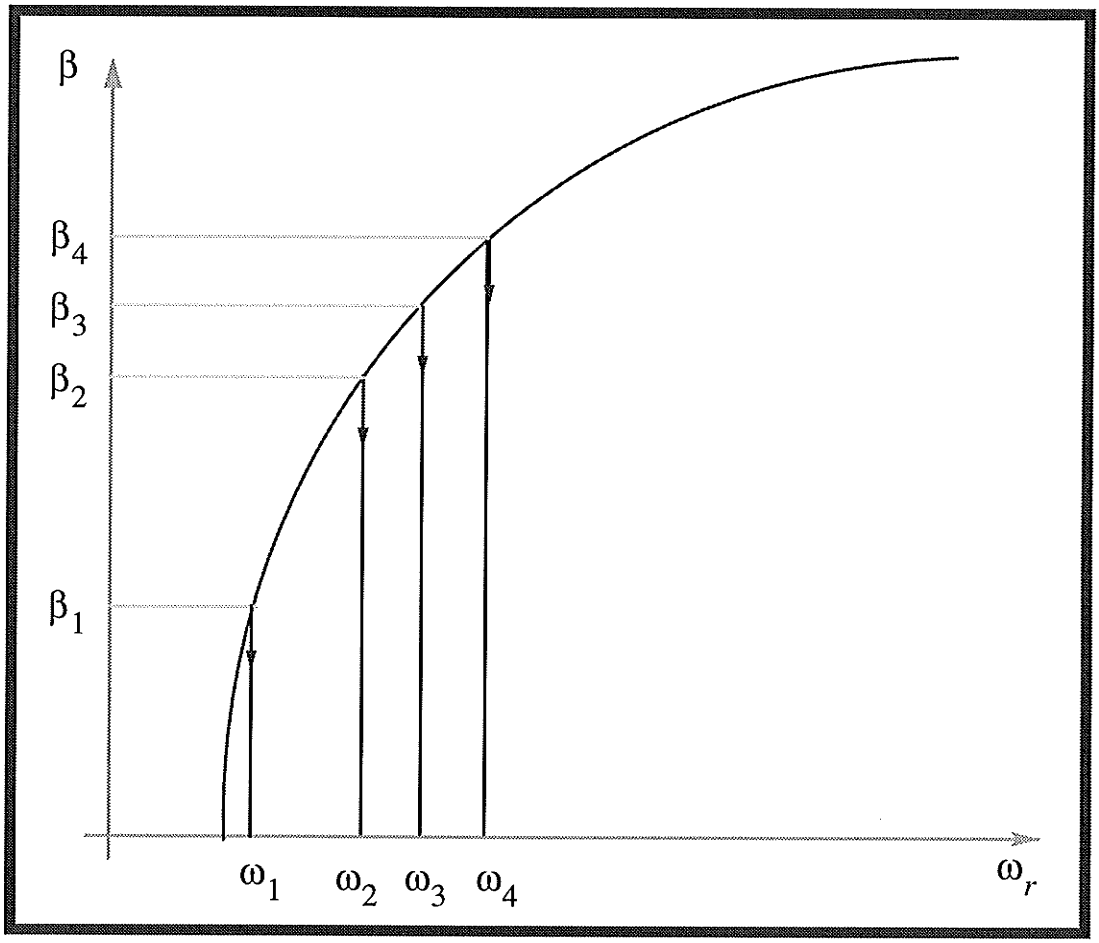

So, there can be no assurance whether a particular peak in the frequency spectrogram belongs to a second propagating mode of $\beta = \pi/L_1$ or the first mode corresponding to $\beta = (m\pi)/L_1$. Of course, intuitively, for a single mode analysis, one can always assume

that the first peak corresponds to $\beta = \pi/L_1$. Yet again, this is based on the assumption that dispersion curves are usually monotonic ascending functions, and hopefully the characteristic curve of the first mode would not intersect the second mode. Fig. III.4 presents a sample of dispersion curve that has been reported in the literature using the **3D-TLM** method.

FIGURE III.4 Dispersion curve of the structure shown in Fig. III.2 generated by changing the distance L along the z direction.

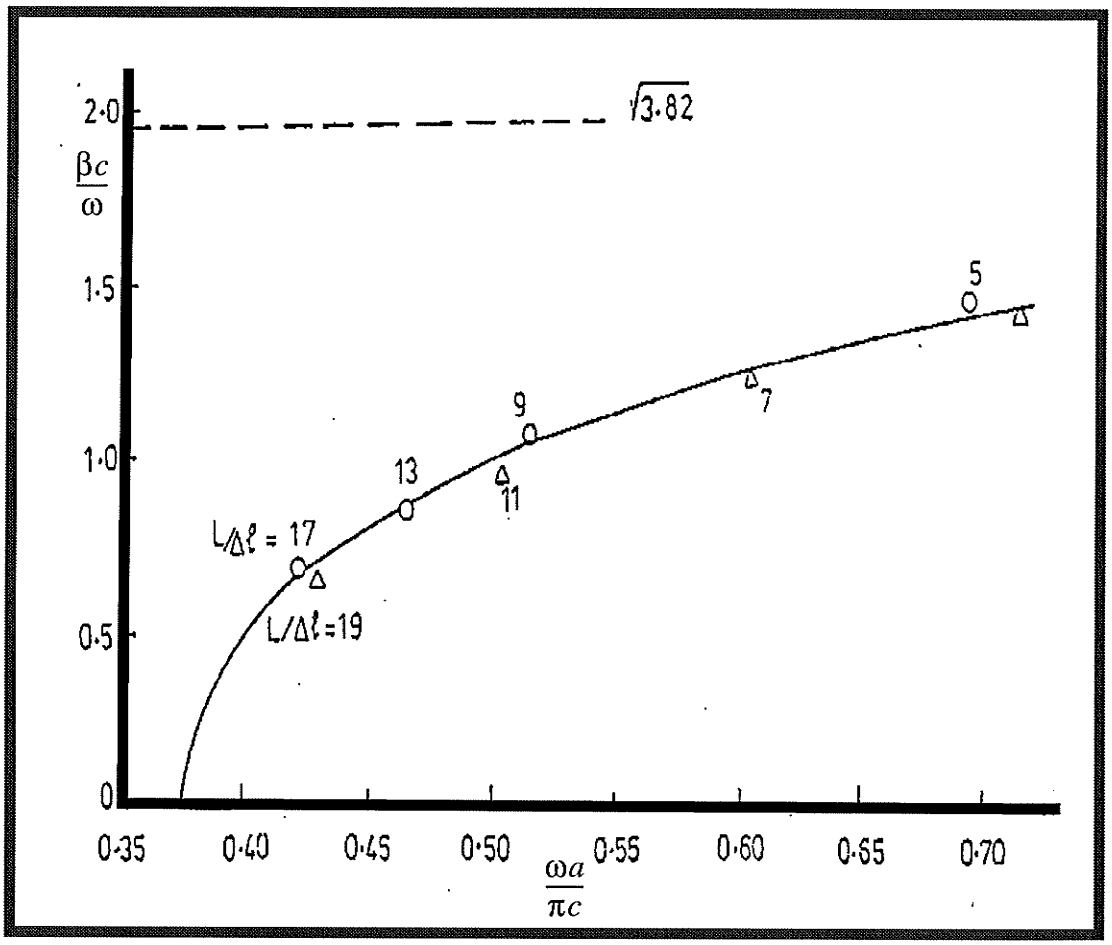

III.D. FDTD

IT HAS been stated that all time domain analyses are in essence equivalent. So, all the material presented in §III.C.1 and §III.C.2 is equally applicable using the **FDTD** method. However, it is emphasized once again that this equivalency does not extend to implementation. On the contrary, for some applications, one of these methods may be more efficient than the others. In particular it has been shown that for the dispersion curve type of analysis, the **FDTD** is more efficient than **TLM [13]**.

III.D.1 2D-FDTD for evaluating cut-off frequencies

ACCORDING TO the theorem which is discussed in appendix A:, one can assume that all the modes at cutoff frequencies are either **TE** or **TM**. And this is true even if the waveguide is inhomogeneous and/or anisotropic. Hence one can simply start a very straightforward algorithm to either discretize the set of eqs. (A.1), (A.2) and (A.3) for the **TM** type or the set of (A.4), (A.5) and (A.6) for the **TE** type modes. As can be seen, the analysis possesses a very important feature which is being a two dimensional one. But, unfortunately it is restricted just to cutoff frequency studies.

III.D.2 3D-FDTD for dispersion analysis [37]

LIKE THE **3D-TLM** case, one can extend the analysis to the whole dispersion curve and for any arbitrary value of k_z at the expense of going to a three dimensional simulation. Before doing so, one question has to be addressed. How to truncate the cylindrical waveguide, which theoretically goes to infinity along the z-direction. There are two traditional answers to this question. The first one which was based on truncating the waveguide using two **PEC** planes was discussed in §III.C.2 and was based on eq. (III.7).

The second type of analysis utilizes a pair of absorbing boundary conditions (**ABC**) at the two ends of the waveguide. The method is based on launching an incident wave at one end of the waveguide and measuring the occurred phase delay on the output probe. From a theoretical point of view, the separation distance between these two **ABC**s is arbitrary provided that they are perfect; i.e., there would be no reflection back from these surfaces. Since, up to now, no perfect **ABC** has been reported, one has to consider the separation distance between these two planes as large as possible. This, in turn, reduces the destructive effect caused by the reflected waves from these imperfect absorbing surfaces. Fig. III.5 illustrates a scheme from the computational domain.

FIGURE III.5 Computational field of a 3D-FDTD

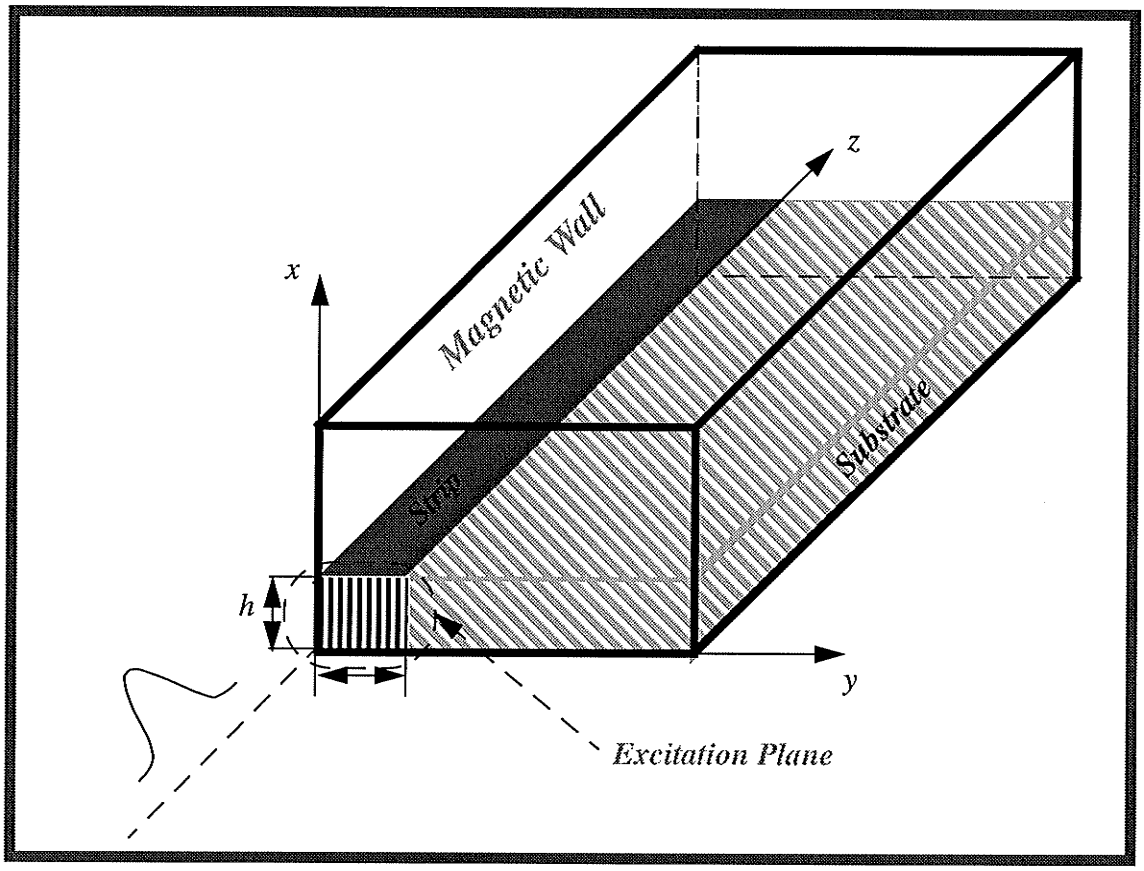

Suppose that a Gaussian pulse of the following shape excites the structure.

$$E_x(t) = e^{\left[-\frac{(t-t_0)^2}{T^2}\right]} \qquad \textbf{(III.9)}$$

If the output probe is located at a distance L from the input probe, then the Fourier transforms of the input and output data can be calculated from

$$E_x(\omega, z=0) = \int_{-\infty}^{\infty} E_x(t, z=0)\, e^{-j\omega t} dt \qquad \textbf{(III.10.a)}$$

$$E_x(\omega, z=L) = \int_{-\infty}^{\infty} E_x(t, z=L)\, e^{-j\omega t} dt \qquad \textbf{(III.10.b)}$$

The efficient method for evaluating eqs. (III.10.a) and (III.10.b) is the subject of chapter five. Thereafter, the dispersion and attenuation characteristics of the waveguide can be calculated from:

$$e^{-\gamma(\omega)L} = \frac{E_x(\omega, z = L)}{E_x(\omega, z = 0)} \qquad \textbf{(III.11)}$$

where

$$\gamma(\omega) = \alpha(\omega) + j\beta(\omega) \qquad \textbf{(III.12)}$$

The relative effective permittivity, $\varepsilon_{eff}(\omega)$, can also be calculated through $\beta(\omega)$ as:

$$\beta(\omega) = \omega\sqrt{\mu_0\varepsilon_0\varepsilon_{eff}(\omega)} \qquad \textbf{(III.13)}$$

Figure III.6 illustrates a sample example from the literature [37].

FIGURE III.6 The dispersion curves corresponding to the structure shown in Fig. III.5

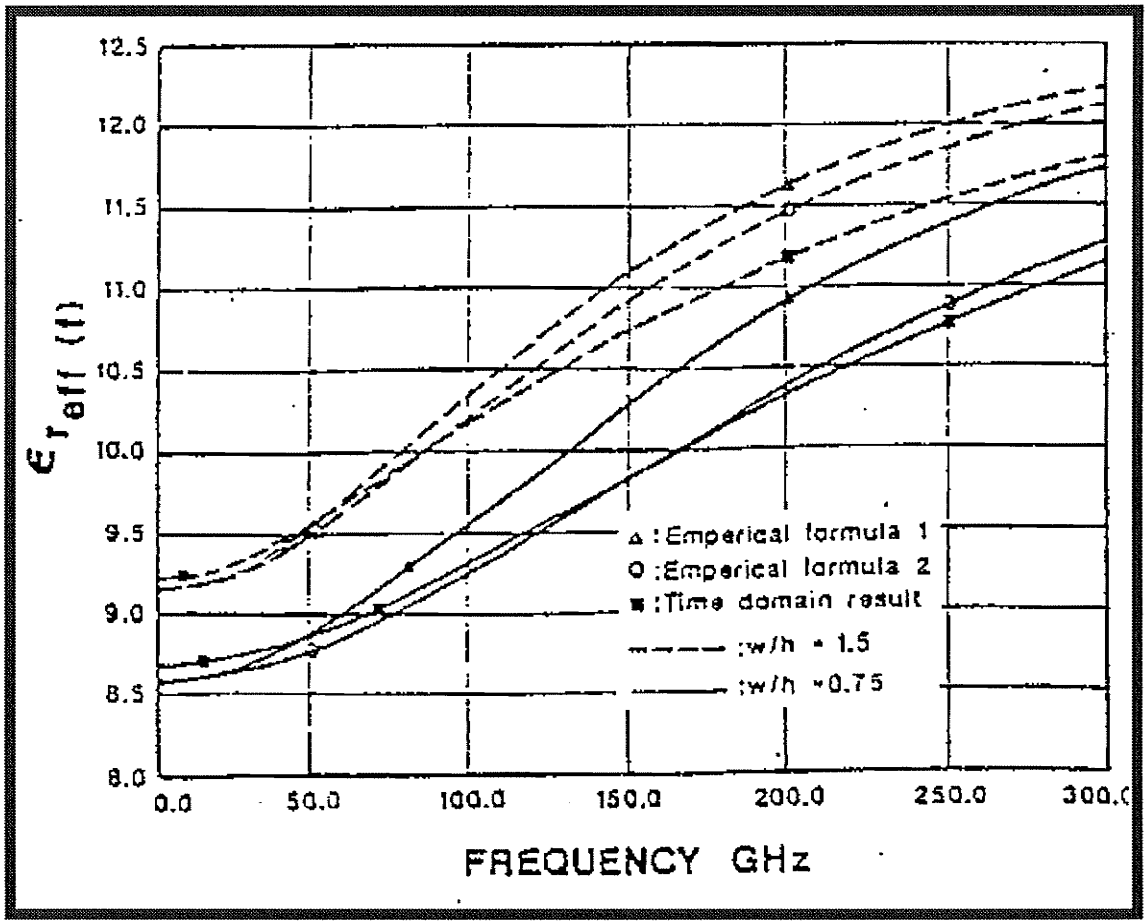

III.E. Compact FDTD [38]

THIS METHOD is one of the major contributions that has been made during this thesis. The basic motivation for developing such a method was for finding a technique with which the entire dispersion curve could be generated using just a two dimensional analysis. As will be shown, the **Compact FDTD** can successfully accomplish this task. By rendering a traditionally three dimensional analysis to a two dimensional one, a great deal of reduction in **CPU** time and memory resources is achieved.

III.E.1 Formulation

THEORETICALLY, in time domain methods the structure under study, such as a waveguide, is excited at an arbitrary location in space (input probe) and its response is recorded at another point (output probe). After taking a Fourier transform of the output, several peaks appear in the frequency domain, that correspond to the waveguide cutoff frequencies. By a quick inspection of Maxwell's equations on page 182, it can be shown that at cutoff frequencies, they decompose into two sets of uncoupled equations, each corresponding to the **TE** or the **TM** modes. Consequently, the calculation of cutoff frequencies can be carried out in a two dimensional space. However, when the entire dispersion curve analysis is the major concern, i.e. $\beta = 0$, all six vector field components in Maxwell's equations are coupled and a three dimensional analysis becomes necessary. This complicates the problem considerably and in using numerical methods, increases the computation time dramatically.

It will be shown here, however, that for axially inhomogeneous waveguides with no discontinuity along the z direction, the problem can still be reduced to a two dimensional analysis. To describe the solution technique, a waveguide region, homogeneous and free of discontinuity along its z axis, is considered. Such a waveguide will support modes that have constant propagation constant β along its axis. In Maxwell's equations, therefore one can replace the z derivatives with $-j\beta$, to efficiently reduce them to a two dimensional space in the waveguide cross section. Here, the derivation of expressions is limited to waveguides with diagonal tensor constants. Maxwell's equations are given by:

$$\vec{\nabla} \times \vec{H} = \varepsilon_0 \bar{\varepsilon} \frac{\partial \vec{E}}{\partial t} \qquad \bar{\varepsilon} = \text{Diagonal relative permittivity tensor} \qquad \textbf{(III.14)}$$

$$\vec{\nabla} \times \vec{E} = -\mu_0 \bar{\mu} \frac{\partial \vec{H}}{\partial t} \qquad \bar{\mu} = \text{Diagonal relative permeability tensor} \qquad \textbf{(III.15)}$$

where:

$$\bar{\varepsilon} = \begin{bmatrix} \varepsilon_{xx} & 0 & 0 \\ 0 & \varepsilon_{yy} & 0 \\ 0 & 0 & \varepsilon_{zz} \end{bmatrix} \quad \text{and} \quad \bar{\mu} = \begin{bmatrix} \mu_{xx} & 0 & 0 \\ 0 & \mu_{yy} & 0 \\ 0 & 0 & \mu_{zz} \end{bmatrix} \qquad \textbf{(III.16)}$$

which generates six scalar equations for six vector field components.

$$\frac{\partial H_x}{\partial t} = \frac{1}{\mu_0 \mu_{xx}} \left(-j\beta E_y - \frac{\partial E_z}{\partial y} \right) \qquad \textbf{(III.17.a)}$$

$$\frac{\partial H_y}{\partial t} = \frac{1}{\mu_0 \mu_{yy}} \left(j\beta E_x + \frac{\partial E_z}{\partial x} \right) \qquad \textbf{(III.17.b)}$$

$$\frac{\partial H_z}{\partial t} = \frac{1}{\mu_0 \mu_{zz}}\left(\frac{\partial E_x}{\partial y} - \frac{\partial E_y}{\partial x}\right) \qquad \textbf{(III.17.c)}$$

$$\frac{\partial E_x}{\partial t} = \frac{1}{\varepsilon_0 \varepsilon_{xx}}\left(j\beta H_y + \frac{\partial H_z}{\partial y}\right) \qquad \textbf{(III.17.d)}$$

$$\frac{\partial E_y}{\partial t} = \frac{1}{\varepsilon_0 \varepsilon_{yy}}\left(-j\beta H_x - \frac{\partial H_z}{\partial x}\right) \qquad \textbf{(III.17.e)}$$

$$\frac{\partial E_z}{\partial t} = \frac{1}{\varepsilon_0 \varepsilon_{zz}}\left(-\frac{\partial H_x}{\partial y} + \frac{\partial H_y}{\partial x}\right) \qquad \textbf{(III.17.f)}$$

An important distinction here is the concept of complex impulses in the time domain marching. Although it has not been used previously in the **FDTD** analysis, its introduction here does not violate the requirement of the time to frequency domain transformation. The transformation is with respect to the spatial variable and all expressions are still in the time domain. In fact, we originally proposed **COMPACT FDTD** [33] [34] using these complex impulses in the time domain. But, a more careful inspection of eqs. (III.17.a)-(III.17.f) shows that even these complex impulses can be avoided if the following change of variables is made.

$$E_x' = jE_x \qquad \textbf{(III.18.a)}$$

$$E_y' = jE_y \qquad \textbf{(III.18.b)}$$

$$H_z' = jH_z \qquad \textbf{(III.18.c)}$$

The new system of equations which are entirely based on real variables is as follows:

$$\frac{\partial H_x}{\partial t} = \frac{1}{\mu_0 \mu_{xx}}\left(-\beta E_y' - \frac{\partial E_z}{\partial y}\right) \qquad \textbf{(III.19.a)}$$

$$\frac{\partial H_y}{\partial t} = \frac{1}{\mu_0 \mu_{yy}}\left(\beta E_x' + \frac{\partial E_z}{\partial x}\right) \qquad \textbf{(III.19.b)}$$

$$\frac{\partial H_z'}{\partial t} = \frac{1}{\mu_0 \mu_{zz}}\left(\frac{\partial E_x'}{\partial y} - \frac{\partial E_y'}{\partial x}\right) \qquad \textbf{(III.19.c)}$$

$$\frac{\partial E_x'}{\partial t} = \frac{1}{\varepsilon_0 \varepsilon_{xx}}\left(-\beta H_y + \frac{\partial H_z'}{\partial y}\right) \qquad \textbf{(III.19.d)}$$

$$\frac{\partial E_y'}{\partial t} = \frac{1}{\varepsilon_0 \varepsilon_{yy}}\left(\beta H_x - \frac{\partial H_z'}{\partial x}\right) \qquad \textbf{(III.19.e)}$$

$$\frac{\partial E_z}{\partial t} = \frac{1}{\varepsilon_0 \varepsilon_{zz}}\left(-\frac{\partial H_x}{\partial y} + \frac{\partial H_y}{\partial x}\right) \qquad \textbf{(III.19.f)}$$

This, in turn, can enhance the algorithm efficiency by factors of two and (around) four, for RAM memory space and elapsed **CPU** time, respectively. In a conventional **FDTD** method, the three dimensional Yee's lattice of Fig. III.7 (a) is used to solve the respective field equations in the waveguide volume. In the present method, however, since the z variable is eliminated, the above equations are solved in the two dimensional leap frog lattice of Fig. III.7 (b), the waveguide cross section. Conceptually, this is equivalent to compressing the 3D-Yee's lattice in the direction of the arrows. It is therefore a ***Compact FDTD*** method. It is worthwhile mentioning that one of the other advantages of such a compression is doubling the numerical resolution for defining the media characteristics, i.e. the permittivity, permeability, conductivity.

FIGURE III.7 (a) Conventional Yee's 3D-lattice. Arrows indicate the direction of compression to reduce the 3D lattice to a 2D one, (b) The unit cell in the new compact FDTD.

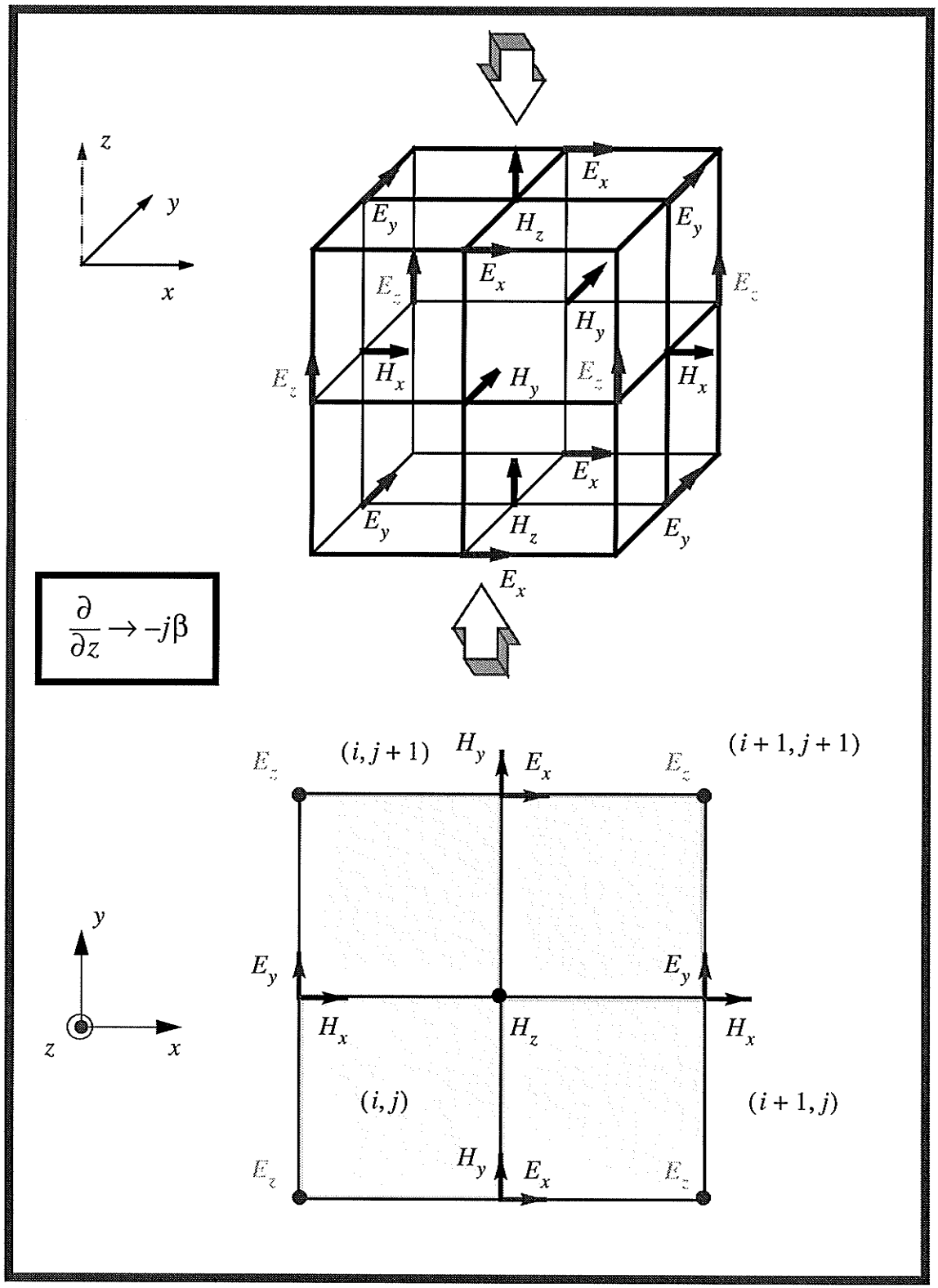

Discretizing all the derivatives using their central difference formula:

$$\frac{H_x^{n+\frac{1}{2}}\left(i,j+\frac{1}{2}\right)-H_x^{n-\frac{1}{2}}\left(i,j+\frac{1}{2}\right)}{\Delta t} \qquad \textbf{(III.20)}$$

$$= -\frac{1}{\mu_0\mu_{xx}}\left(\beta E_y^n\left(i,j+\frac{1}{2}\right)+\frac{E_z^n(i,j+1)-E_z^n(i,j)}{\Delta y}\right)$$

where for convenience, the notation of $F^n(i,j) = F(i\Delta x, j\Delta y, n\Delta t)$ is adopted. Furthermore, by performing the following normalizations, the characteristic impedance of free space is set to unity.

$$e_x = \frac{E_x'}{\sqrt{\mu_0}} \qquad \textbf{(III.21.a)}$$

$$e_y = \frac{E_y'}{\sqrt{\mu_0}} \qquad \textbf{(III.21.b)}$$

$$e_z = \frac{E_z}{\sqrt{\mu_0}} \qquad \textbf{(III.21.c)}$$

$$h_x = \frac{H_x}{\sqrt{\varepsilon_0}} \qquad \textbf{(III.21.d)}$$

$$h_y = \frac{H_y}{\sqrt{\varepsilon_0}} \qquad \textbf{(III.21.e)}$$

$$h_z = \frac{H_z'}{\sqrt{\varepsilon_0}} \qquad \textbf{(III.21.f)}$$

So, the final discretized form of Maxwell's equations which constitutes the body of a Compact **FDTD** algorithm is as follows:

$$h_x^{n+\frac{1}{2}}\left(i, j+\frac{1}{2}\right) = h_x^{n-\frac{1}{2}}\left(i, j+\frac{1}{2}\right) \qquad \textbf{(III.22.a)}$$

$$+\frac{s}{\mu_{xx}\left(i, j+\frac{1}{2}\right)}\left[-(\beta\Delta l)\, e_y^n\left(i, j+\frac{1}{2}\right) - e_z^n(i, j+1) + e_z^n(i, j)\right]$$

$$h_y^{n+\frac{1}{2}}\left(i+\frac{1}{2}, j\right) = h_y^{n-\frac{1}{2}}\left(i+\frac{1}{2}, j\right) \qquad \textbf{(III.22.b)}$$

$$+\frac{s}{\mu_{yy}\left(i+\frac{1}{2}, j\right)}\left[(\beta\Delta l)\, e_x^n\left(i+\frac{1}{2}, j\right) + e_z^n(i+1, j) - e_z^n(i, j)\right]$$

$$h_z^{n+\frac{1}{2}}\left(i+\frac{1}{2}, j+\frac{1}{2}\right) = h_z^{n-\frac{1}{2}}\left(i+\frac{1}{2}, j+\frac{1}{2}\right) \qquad \textbf{(III.22.c)}$$

$$+\frac{s}{\mu_{zz}\left(i+\frac{1}{2}, j+\frac{1}{2}\right)}\left[e_x^n\left(i+\frac{1}{2}, j+1\right) - e_x^n\left(i+\frac{1}{2}, j\right) + e_y^n\left(i, j+\frac{1}{2}\right) - e_z^n\left(i+1, j+\frac{1}{2}\right)\right]$$

$$e_x^{n+1}\left(i+\frac{1}{2}, j\right) = e_x^n\left(i+\frac{1}{2}, j\right) \qquad \textbf{(III.22.d)}$$

$$+\frac{s}{\varepsilon_{xx}\left(i+\frac{1}{2}, j\right)}\left[-(\beta\Delta l)\, h_y^{n+\frac{1}{2}}\left(i+\frac{1}{2}, j\right) + h_z^{n+\frac{1}{2}}\left(i+\frac{1}{2}, j+\frac{1}{2}\right) - h_z^{n+\frac{1}{2}}\left(i+\frac{1}{2}, j-\frac{1}{2}\right)\right]$$

$$e_y^{n+1}\left(i,j+\frac{1}{2}\right) = e_y^{n}\left(i,j+\frac{1}{2}\right) \qquad \textbf{(III.22.e)}$$

$$+\frac{s}{\varepsilon_{yy}\left(i,j+\frac{1}{2}\right)}\left[(\beta\Delta l)\,h_x^{n+\frac{1}{2}}\left(i,j+\frac{1}{2}\right)+h_z^{n+\frac{1}{2}}\left(i-\frac{1}{2},j+\frac{1}{2}\right)-h_z^{n+\frac{1}{2}}\left(i+\frac{1}{2},j+\frac{1}{2}\right)\right]$$

$$e_z^{n+1}(i,j) = e_z^{n}(i,j) \qquad \textbf{(III.22.f)}$$

$$+\frac{s}{\varepsilon_{zz}(i,j)}\left[h_x^{n+\frac{1}{2}}\left(i,j-\frac{1}{2}\right)-h_x^{n+\frac{1}{2}}\left(i,j+\frac{1}{2}\right)+h_y^{n+\frac{1}{2}}\left(i+\frac{1}{2},j\right)-h_y^{n+\frac{1}{2}}\left(i-\frac{1}{2},j\right)\right]$$

in which, $s = \frac{c\Delta l}{\Delta t} \le \left[2+\left(\frac{\beta\Delta l}{2}\right)^2\right]^{-\frac{1}{2}}$ [40] is the stability factor and $\Delta x = \Delta y = \Delta l$. By iterating the six resultant equations, the time domain response of the structure can be obtained, and by taking an **FFT** of the output data, one can easily calculate the resonant frequencies of different modes by finding the locations of the peaks in the frequency domain spectrum.

To solve the resulting equations, however, one needs to select a value for β, as input parameter, and locate the peaks at the frequency spectrum, to determine the eigenvalues for the dominant and higher order modes. The method, thus, reduces a complex three dimensional **FDTD** analysis to a number of small two dimensional ones.

Fig. III.8 depicts the systematic procedure of generating a complete dispersion curve. First, for each arbitrary value of $\beta\Delta l$, the CFDTD algorithm is executed. Next, the Fourier transform of the output time sequence is calculated. The corresponding resonant frequen-

cies, $\frac{\Delta l}{\lambda}$, are located at the peaks of these transforms. By having several of these points, the complete dispersion curve can be interpolated using techniques such as cubic splines.

FIGURE III.8 : Generation of a complete dispersion curve using compact FDTD.

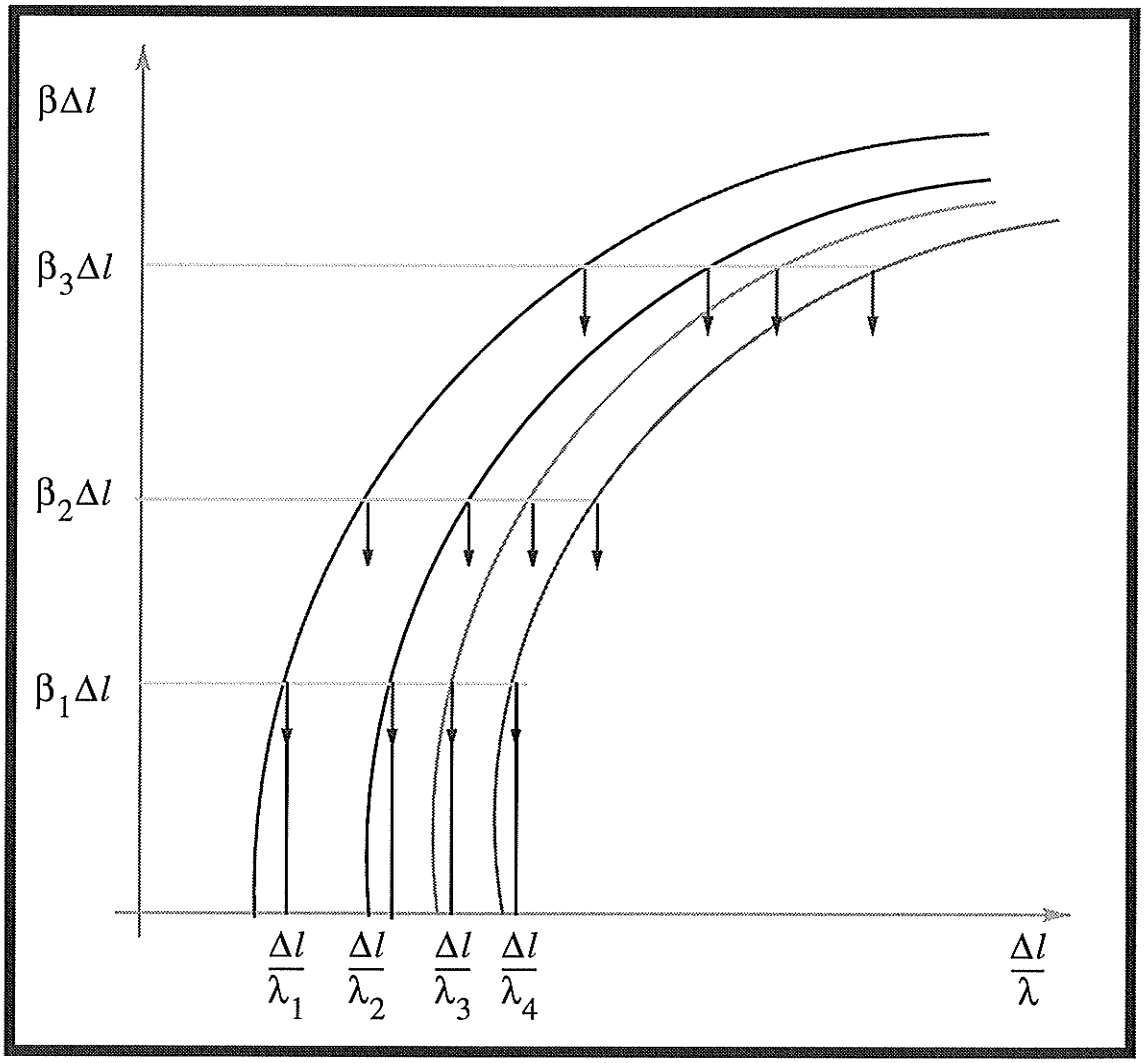

III.E.2 Applications

TO GENERATE a complete dispersion curve, generally, the time domain responses are evaluated for eleven incremental values of $\beta\Delta l$ from zero to one (or any other desired value as the upper margin). The corresponding peaks are extracted from the spectrograms of the signals and finally a natural cubic spline interpolation technique [41] is implemented to obtain a smooth dispersion curve for each mode. To illustrate the accuracy of the method several different cases, ranging from simple rectangular hollow waveguides to more complex coupled strip lines on anisotropic substrate, are considered. In each case, excellent agreement between the Compact FDTD and earlier results, with errors less than 0.5%, are achieved.

Two frequency spectra of the time domain data corresponding to two distinct values of $\beta\Delta l = 0.1, 0.3$, for a hollow rectangular waveguide, are illustrated in Fig. III.10. The dispersion curves of its first three dominant modes are depicted in Fig. III.11. The agreement between the Compact FDTD and analytical solutions obtained from the following parabolic formula is excellent and they are practically indistinguishable.

$$\beta\Delta l = \pi\sqrt{\left(\frac{2\Delta l}{\lambda}\right)^2 - \left(\frac{m}{10}\right)^2 - \left(\frac{n}{6}\right)^2} \qquad \textbf{(III.23)}$$

One interesting phenomenon in Fig. III.10 is the existence of a sharp peak at zero frequency, i.e. DC. In fact, this happened in most of the simulated cases. In two conductor structures such as boxed microstrip line, it may be attributed to the propagation of DC waves in the form of a TEM mode along the line. But, in a hollow rectangular waveguide,

a TEM or Quasi-TEM mode cannot exist and therefore propagation at DC frequency is not feasible. On the other hand, from electrostatic and magno-static point of view, Fig. III.9, one can assume a circulating electric surface current along the waveguide walls with no longitudinal component, i.e. $J_z = 0$. Such an arrangement can explain the presence of one solution to Maxwell's equations in DC frequency. Also, the following observations can be used to support the preceding theory:

- *Under cut-off condition, the zero frequency peak appears only for TE modes.*
- *If one of the waveguide walls is replaced with a PMC, a significant drop in the amplitude of the zero frequency component will be observed.*

FIGURE III.9 Circular electric surface currents along the surface of the waveguide

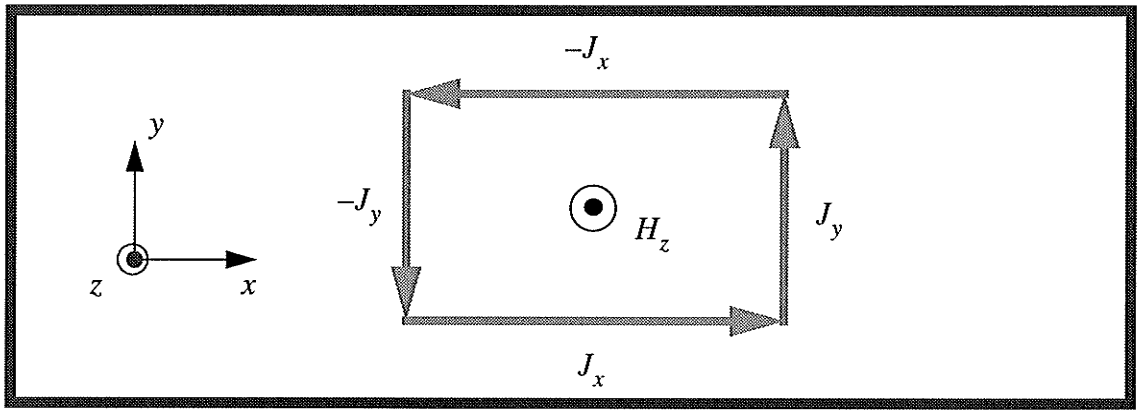

Fig. III.12 depicts a partially filled rectangular waveguide which is selected for the next example. This problem is somewhat more complicated than the hollow rectangular waveguide. But, still it can be solved analytically up to the point of a transcendental equation [25]:

For TE_x modes:

$$\frac{k_{x0}}{\mu_0}\cot\left[k_{x0}\left(\frac{a-d}{2}\right)\right] = \frac{k_{x1}}{\mu_1}\tan\left[k_{x1}\left(\frac{d}{2}\right)\right] \qquad \textbf{(III.24.a)}$$

and for the TM_x modes:

$$\frac{k_{x0}}{\varepsilon_0}\tan\left[k_{x0}\left(\frac{a-d}{2}\right)\right] = \frac{k_{x1}}{\varepsilon_1}\cot\left[k_{x1}\left(\frac{d}{2}\right)\right] \qquad \textbf{(III.24.b)}$$

where:

$$k_{x0}^2 + \left(\frac{n\pi}{b}\right)^2 + \beta^2 = k_0^2 = \omega\varepsilon_0\mu_0 \qquad \textbf{(III.24.c)}$$

$$k_{x1}^2 + \left(\frac{n\pi}{b}\right)^2 + \beta^2 = k_1^2 = \omega\varepsilon_1\mu_1 \qquad \textbf{(III.24.d)}$$

The dominant mode is the lowest order TE mode (smallest root for $n = 0$). Also, if a small amount of error can be tolerated, the following perturbational equation can be used:

$$\frac{\beta}{k_0} = \sqrt{1 + \frac{\varepsilon_1 - \varepsilon_0}{\varepsilon_0}\left[\frac{d}{a} + \frac{1}{\pi}\sin\left(\frac{\pi d}{a}\right)\right] - \left(\frac{\pi}{k_0 a}\right)^2} \qquad \textbf{(III.25)}$$

Again an excellent match between analytical techniques and CFDTD is observed.

The analysis of a Unilateral Fin-line constitutes our next example, Fig. III.13. From this point, there is usually no standard analytical solution available for the cases under study. However, using standard numerical procedures, like mode matching, its dispersion curves can be evaluated. One major distinction between this case and previous one of partially filled waveguide, is that for the present case a set of different modes, in each region, are required in order to satisfy all the boundary conditions. Whereas for the partially filled waveguide, just a single TE_x or TM_x mode will suffice to fulfil all boundary conditions.

Fig. III.13 illustrates the dispersion curve generated by CFDTD. Again this result shows a good agreement with the reported data in the literature [13]. In fact, Choi and Hoefer constructed a three dimensional resonant structure by terminating a unilateral fin-line at its two ends with two PEC walls. By adjusting the distance between these walls, they managed to tune the resonant structure for different values of β, refer to Section III.C.2 on page 73.

The next case deals with a more complicated structure consisting of an anisotropic inhomogeneous medium. Using conventional techniques, this class of problems has always been more difficult to deal with compared to isotropic media. The difficulty arises from the fact that in this case some extra correlation between electromagnetic field components will be generated. Expanding one of Maxwell's equations for both isotropic and anisotropic cases is used for further elaboration. For the isotropic case:

$$\frac{\partial H_z}{\partial y} - \frac{\partial H_y}{\partial z} = \varepsilon_0 \varepsilon_r \frac{\partial E_x}{\partial t} \qquad \textbf{(III.26)}$$

and for the anisotropic case:

$$\frac{\partial H_z}{\partial y} - \frac{\partial H_y}{\partial z} = \varepsilon_0 \varepsilon_{xx} \frac{\partial E_x}{\partial t} + \varepsilon_0 \varepsilon_{xy} \frac{\partial E_y}{\partial t} + \varepsilon_0 \varepsilon_{xz} \frac{\partial E_z}{\partial t} \qquad \textbf{(III.27)}$$

By comparing these two equations, one notices the presence of two extra terms on the right side of eq. (III.27). This can noticeably increase the mathematical preprocessing required using conventional techniques. But, from CFDTD point of view the problem can be treated simply by adding the finite difference equivalences of the added terms.

Fig. III.14 illustrates a boxed microstrip line on Sapphire. The substrate is placed such that its main dielectric axis is parallel to one of the axes of cartesian coordinate system. Under these circumstances, dielectric will behave like a diagonally anisotropic medium with the following specifications: $\varepsilon_{xx} = \varepsilon_{zz} = 9.4$ and $\varepsilon_{yy} = 11.6$. The dispersion curve of this structure, with the same geometrical specifications, had already been reported by Alexopoulos et al [42] using quasi-static, and by Hoefer et al [13] using 3D-FDTD methods. Some empirical data was also presented by Getsinger [43]. Finally, in an invited paper by Alexopoulos, a comparative study was conducted among all available data versus the results obtained using 3D-TLM method [44]. This comparative study reveals the fact that TLM results have always been an underestimation of the dispersion data obtained from other techniques. The same observation is true for the present case, i.e. 3D-TLM and 3D-FDTD underestimate CFDTD results, as shown in Table III .1. CFDTD generates more accurate results than the other two simply because it calculates the z derivative analytically.

TABLE III .1 Comparison of computed dominant mode frequencies, $f = \frac{kc}{2\pi}$ for problem of fig. III.14.

		$\beta\,(1/(mm))$				
		1.0472	**0.7854**	**0.6283**	**0.4189**	**0.3142**
Frequency (GHz)	**3D TLM**	**14.97**	**11.70**	**9.66**	**6.75**	**5.22**
	3D FDTD	**14.64**	**11.52**	**9.54**	**6.78**	**5.28**
	CFDTD	**16.092**	**12.402**	**10.158**	**7.044**	**5.406**
	Difference	**7 – 9 %**	**5.7 – 7 %**	**5 – 6 %**	**3.7 – 4 %**	**2.3 – 3.4 %**

The observed discrepancies can be attributed to three separate reasons. One is due to the approximation for the permittivity at the boundary of the two regions, where an aver-

age value between the air and substrate is used. Second, due to the inherent advantage of the present method, a double resolution mesh is used to define the dielectric constant of the medium and, consequently, the results are expected to be more accurate. Third, the z derivative in the present approach is handled analytically, while in others, this has been done numerically. Furthermore, as mentioned above, the previous results listed in Table III .1, in comparison to the **3D-TLM** and other methods, has shown consistent underestimation of the resonant frequencies at given values. It is therefore believed that our computed results are more accurate.

In these examples, 1000 iterations have achieved an acceptable solution accuracy, and extending it to more than 5000 iterations had no appreciable effect on increasing the accuracy. On a **Sun-Sparc20** computer, each 1000 iterations needed about 3 seconds of CPU time, which is sufficiently small to generate the entire dispersion curve rapidly. For instance, the dispersion curve presented in Fig. III.14 was generated using 11 incremental values of $\beta\Delta l$ from 0.1 to 1. To enhance the resolution of the FFT operation, all time domain sequences have been zero padded to eight times their actual data size. However, there are other signal processing methods that are available to serve the same purpose [39]. Also, in [40], a technique based on taking the average value between the permittivity of free space and Sapphire in the x and z directions, i.e. $\frac{\varepsilon_{xx}+1}{2}$ and $\frac{\varepsilon_{zz}+1}{2}$, were used while along the y direction the permittivity of Sapphire has been directly used, i.e. ε_{yy}. This modification, compared to what has been explained in [33] in which the average values were used along all coordinate directions, did not show any noticeable effect on the resonant frequencies. To make the output results independent of the physical dimensions

of the structure, the input and output quantities of the analysis are presented in their normalized forms. Consequently, we define $\beta\Delta l$ as the normalized propagation constant and $\frac{\Delta l}{\lambda}$ as the normalized frequency. Since these normalized parameters are dimensionless, they are independent of the actual physical dimensions of the structures and hence the analysis is general as long as the ratios between different structural dimensions are kept constant.

In microwave engineering, it is desirable to have a waveguide that exhibits a linear dispersion characteristics. Fig. III.14 shows that by introducing a conductor at the center of a partially Sapphire-filled rectangular waveguide, this goal for the first dominant mode was indeed achieved. However, at higher frequencies and therefore higher order modes, the famous parabolic shape of the results for a hollow rectangular waveguide, similar to those of Fig. III.11, gradually appears and deteriorates the perfect linear shape of the higher order modes.

Fig. III.15 illustrates the dispersion curves of even and odd modes for a coupled microstrip line laid on Sapphire. In fact, half of the structure was analyzed for each case. This was achieved by placing a PEC (for odd mode) or PMC (for even mode) wall instead of the dash-line. The results are in good agreement with those reported using TLM [44].

In all above analysis, reducing the grid size and/or increasing the number of iterations can enhance the accuracy. Also as the $\Delta l/\lambda$ decreases, the higher number of iterations is required to achieve the same degree of accuracy. This is due to the fact that as $\Delta l/\lambda$ departs from the origin in the positive direction, its shadow moves in the negative direc-

tion along the fourier frequency axis. For lower values of $\Delta l/\lambda$, the side lobe generated by the negative frequency component can interfere with the main lobe of the positive component. Specially, this problem is quite noticeable when the study of the modes in a Quasi-TEM structure is concerned. In such a structure, the value of $\Delta l/\lambda = 0$ corresponds to the value $\beta\Delta l = 0$. On the other hand, in the structures that do not support Q-TEM (usually structures with one or no conductor), the $\beta\Delta l = 0$ case corresponds to a non-zero positive values of $\Delta l/\lambda > 0$, and therefore the aforementioned problem do not exist or quite alleviated.

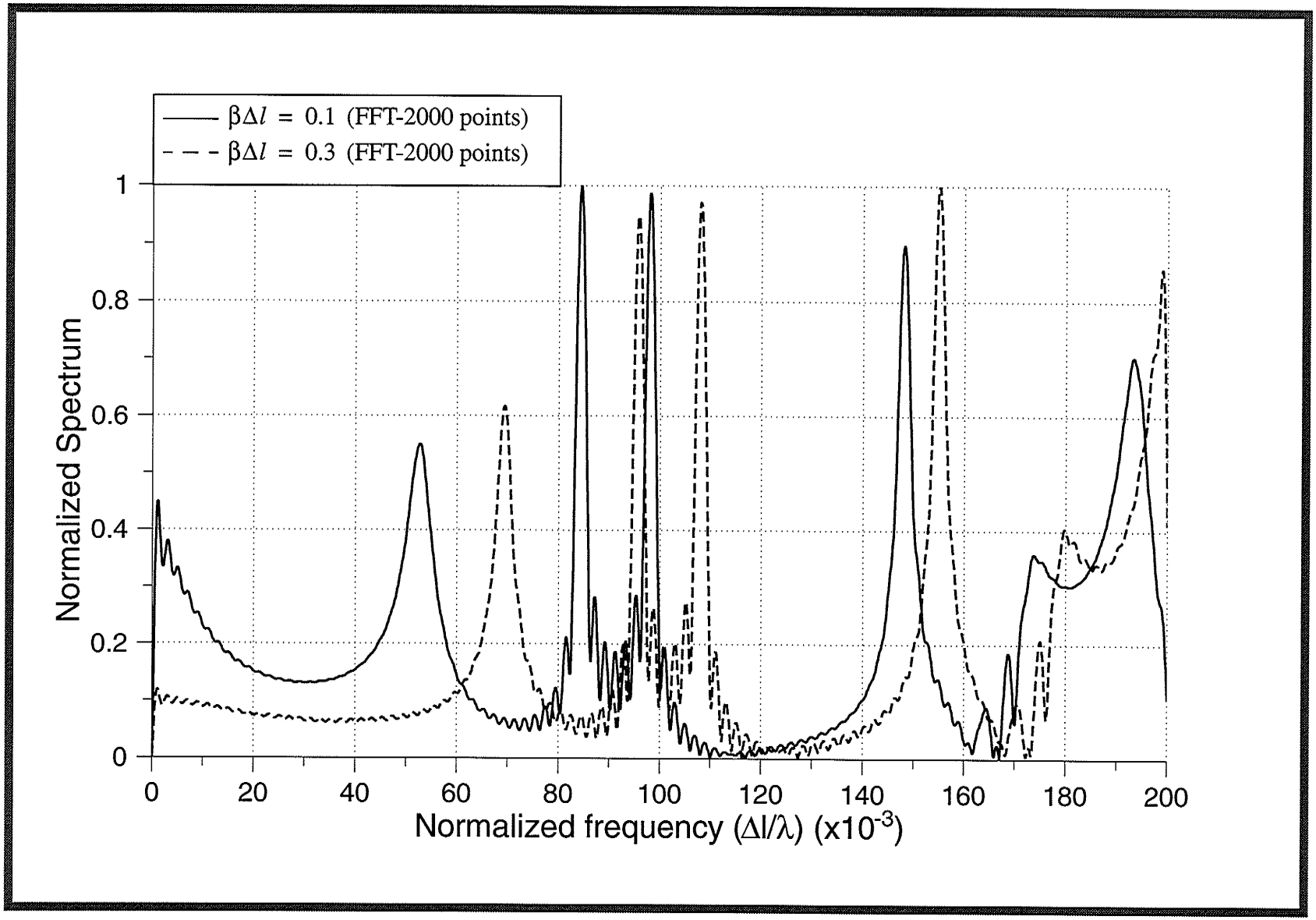

FIGURE III.10 **The Fourier spectrum (after zero padding and Hanning windowing) of the structure in Fig. III.11, corresponding to two distinct values of normalized propagation constant**

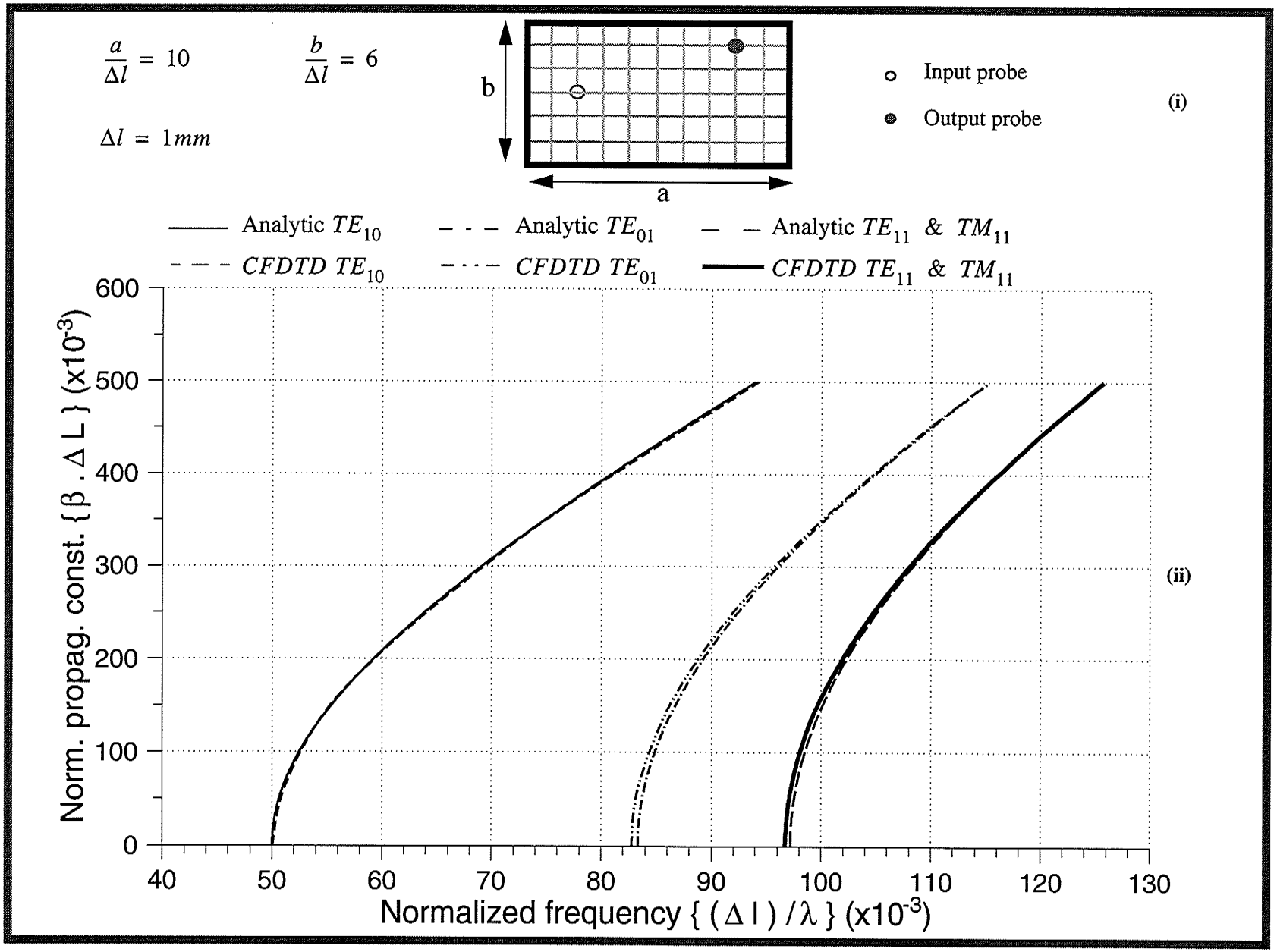

FIGURE III.11 **(i) Hollow rectangular waveguide (ii) Corresponding dispersion curves for the first four modes**

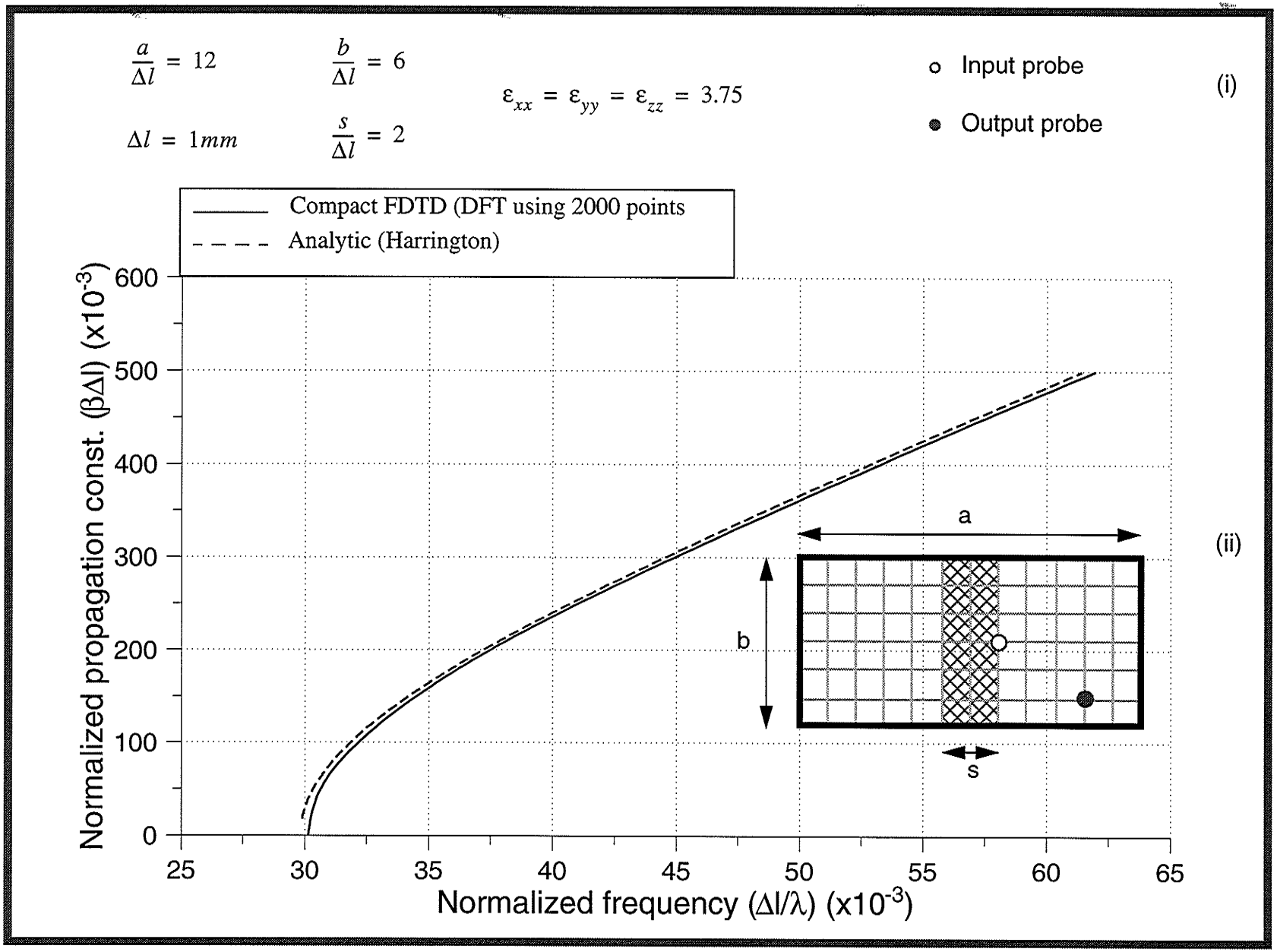

FIGURE III.12 (i) Partially-filled rectangular waveguide and (ii) Corresponding dispersion curve

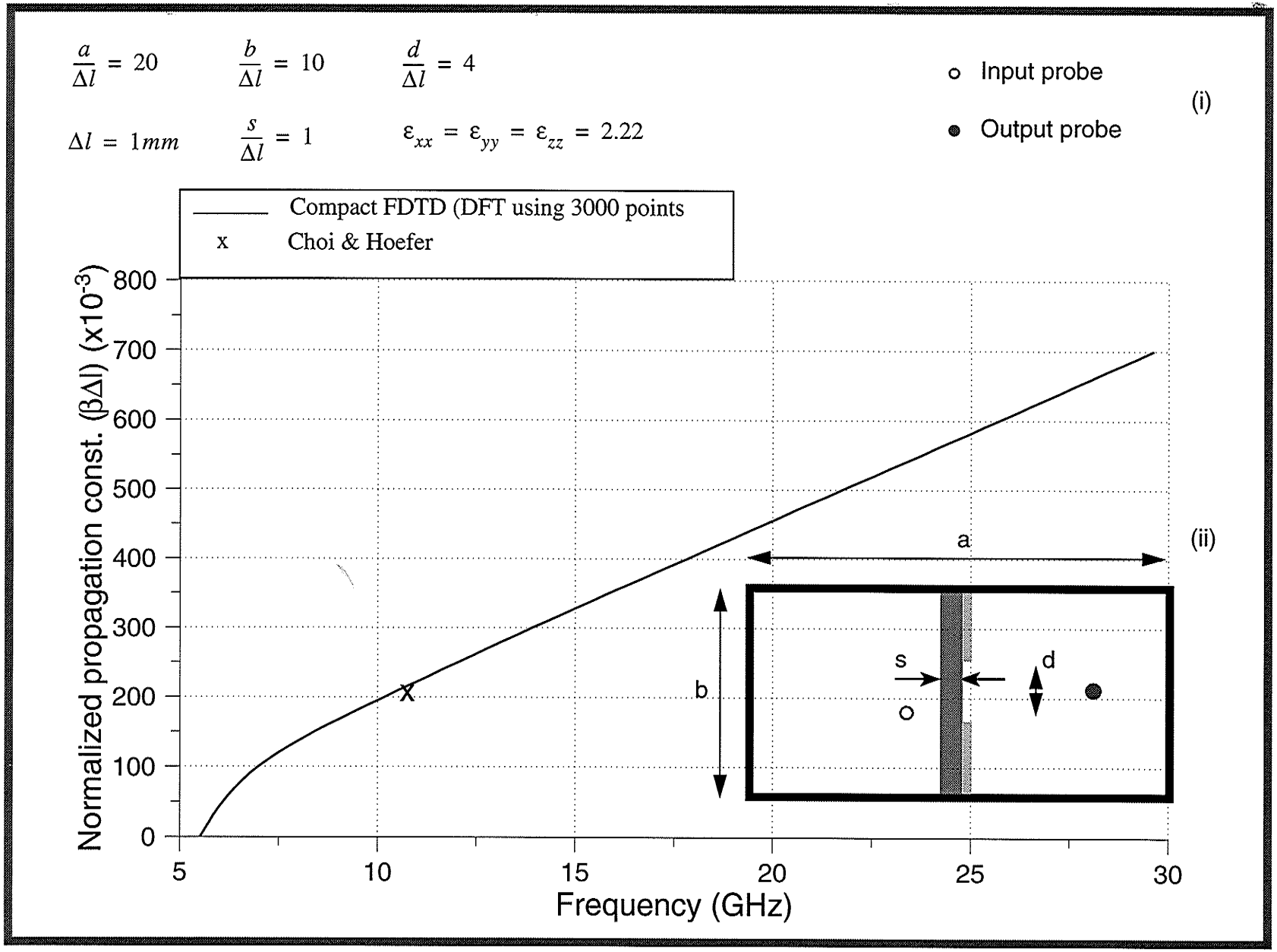

FIGURE III.13 (i) Unilateral Fin-line and (ii) Corresponding dispersion curve

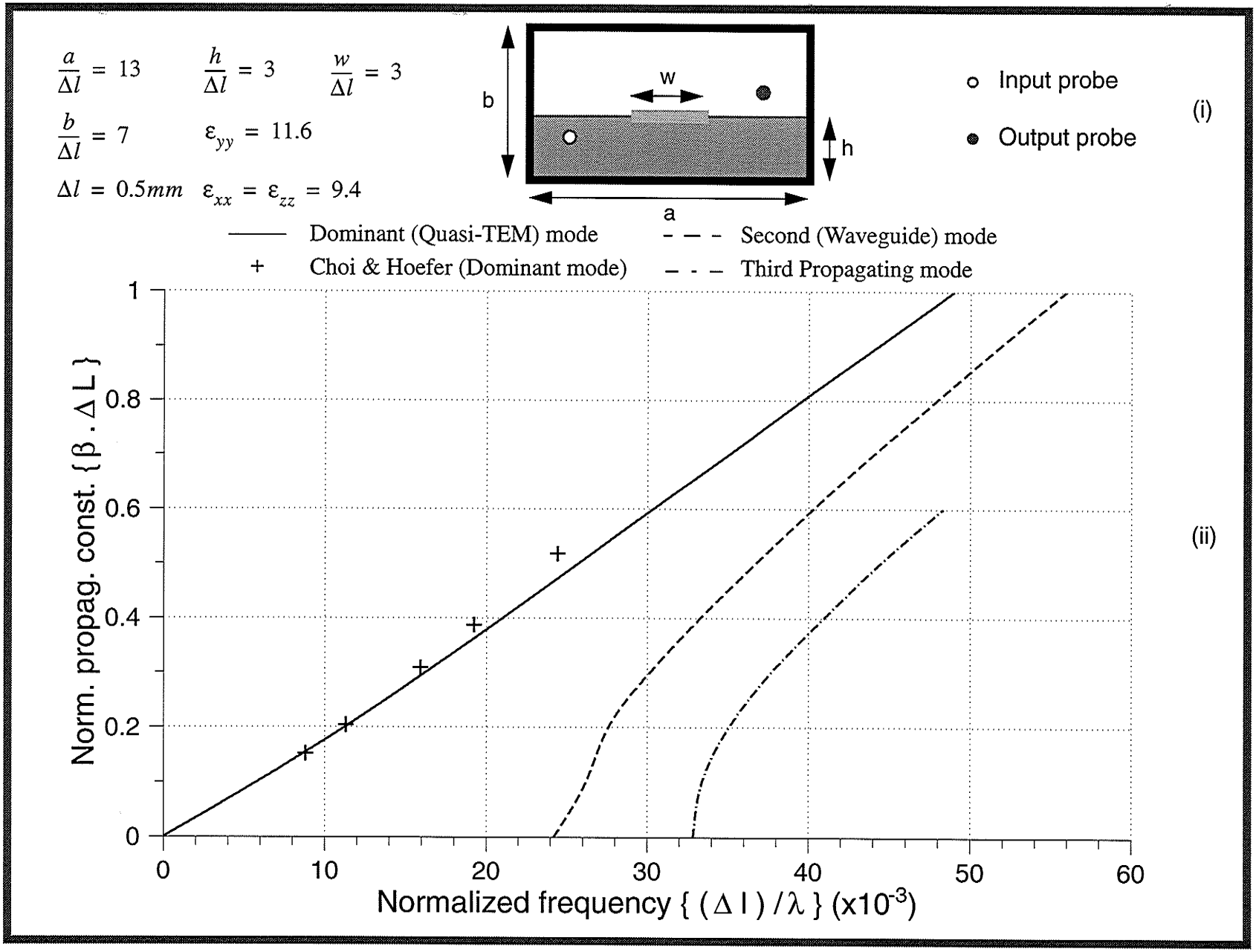

FIGURE III.14 Boxed Microstrip-line on anisotropic Sapphire and (ii) Corresponding dispersion curve for the first three modes

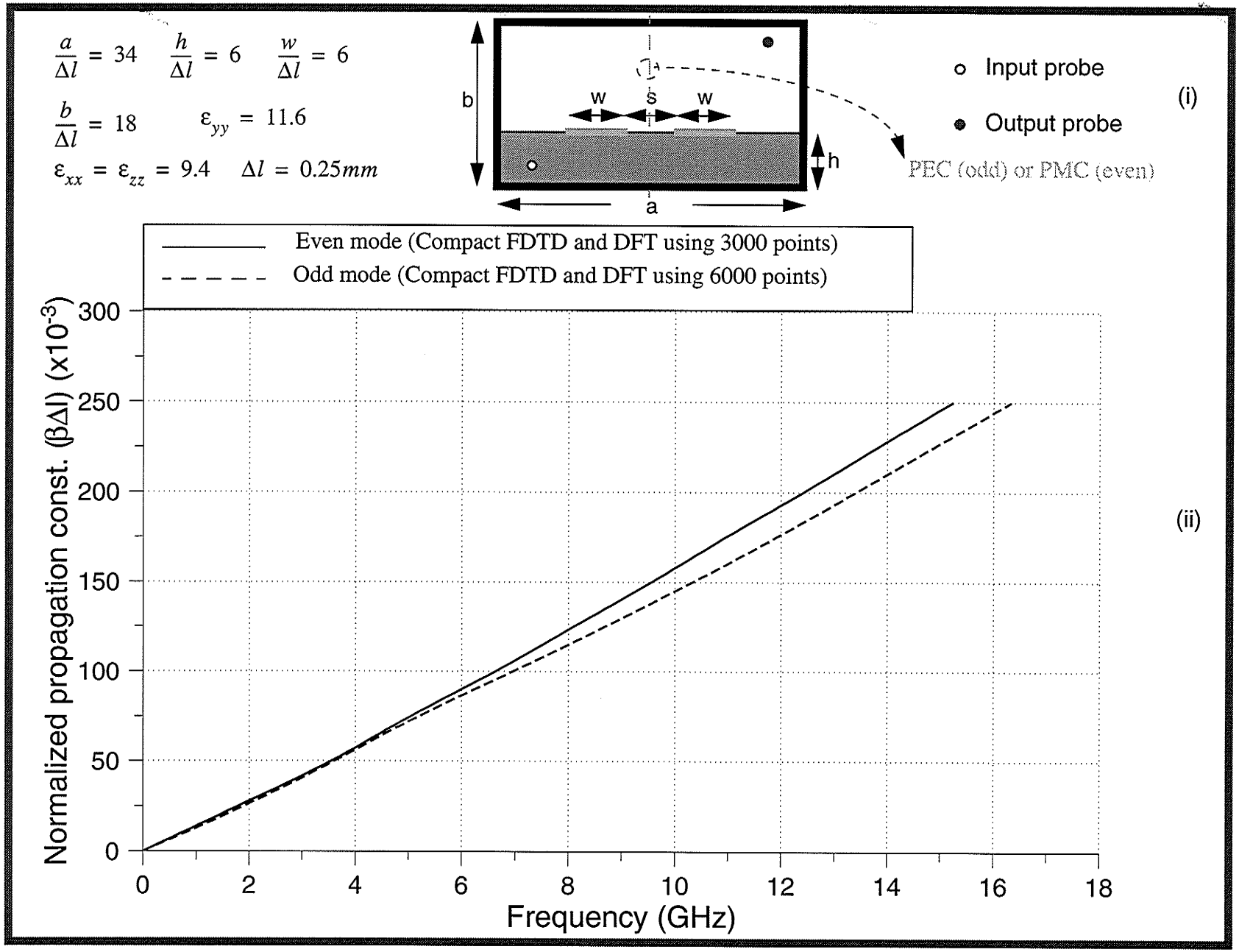

FIGURE III.15 (i) Coupled Microstrip line on anisotropic Sapphire (ii) Corresponding dispersion curves for the dominant even and odd modes

III.F. Conclusion

A NEW ***Compact 2D-FDTD*** method was proposed to determine the dispersion characteristics of guiding structures. Its speed and accuracy promises to make it the dominant method for such analyses. While it has the ***versatility*** of finite difference methods, it enjoys the ***power*** and ***speed*** of other full wave analyses.

Chapter Four

FIELD PATTERN ANALYSIS

Full Wave Finite Difference (FWFD)

IV.A. Introduction

ALTHOUGH NUMEROUS techniques are available for determining eigenvalues of microwave and optical waveguide structures, only a few are capable, or efficient in finding eigenvectors. A novel iterative FULL WAVE FINITE DIFFERENCE (FWFD) method is proposed which is capable of evaluating all six vector field components of an arbitrary shaped inhomogeneous waveguide structure simultaneously and efficiently. It is based on a new four directional finite difference treatment of Maxwell equations. For the E^{y}_{11O} mode of a shielded suspended coupled dielectric guide with a mesh discretization of 18×12, a total number of 100 iterations is adequate to achieve convergence. In this case, the entire process takes about three seconds on a Sun-Sparc10/41 workstation.

For design and analysis of waveguides one usually requires the dispersion curves and information on the field patterns. However, most of the reported papers deal with the dispersion curves and the computation of the field patterns is often neglected. This part of the thesis addresses the latter question and provides a full wave solution method for computation of the field patterns. In general, a knowledge of the dispersion curves along with the field patterns provides all the necessary information, or, means for derivation of any unknown attributes of the waveguide. Historically, a number of analytic and numerical techniques have been developed to deal with such problems. However, the analytical methods and some of the numerical ones suffer from lack of generality. The finite differ-

ence method is one of the numerical schemes which requires minimal initial assumptions and hence is applicable to almost all waveguide problems. This is therefore used in the present study for developing a full wave finite difference method.

The **Classical** finite difference method is the first version in the course of evolution of finite difference methods. It was developed for solving the **Laplace** equation which is valid only for static, i.e. zero frequency, or **Q**uasi-**TEM** modes. Since Laplace equation is just a special case of the **Helmholtz** equation, the next attempt was aimed at solving this equation. Two different strategies, Section II.C. on page 48, were reported to accomplish this task. Beaubien et al., Section II.C.1 on page 48, proposed an iterative scheme which is based on the assumption that the solution can be decomposed into two independent modes, i.e. TE_z and TM_z. This assumption is only valid for homogeneous waveguides or the inhomogeneous ones operating at cut-off frequencies. In their method, finite difference was implemented iteratively using over-relaxation in conjunction with **Rayleigh quotient** to improve the solution for eigenvalues. The second approach was implemented by Bierwirth et al., Section II.C.2. on page 58, in which the general inhomogeneous waveguides operating beyond cut-off frequencies were studied. In this method, first Helmholtz equation is discretized for both H_x and H_y components and then a homogeneous system of equations is constructed by enforcing boundary conditions between neighboring regions. In the next stage, **EISPACK** package was employed to extract the eigenvalues of the system of equations, and hence the dispersion curves of the waveguide.

It is worthwhile to make a comparison between the aforementioned finite difference techniques. Bierwirth's method is more general than Beaubien's in the sense that it is not restricted to homogeneous waveguides or inhomogeneous ones operating at cut-off. On the other hand, from the numerical point of view, Beaubien's method is more efficient. The reason for this superior numerical efficiency is twofold. First, it can be shown that the resulting matrix generated by discretization of the Helmholtz equation is sparse. Therefore, indirect methods like Beaubien's, require less **CPU** time to find the solution for such systems. Secondly, in the Bierwirth's method all the matrix elements ought to be calculated and stored before calculating the eigenvalues. This also poses an unnecessary burden on the **RAM** computer resources. In fact, in Beaubien's iterative method, only the elements of one row of the matrix need to be calculated and stored at a time.

The proposed method in this thesis, FWFD, enjoys the generality of dealing with an inhomogeneous waveguide and at the same time implements the more efficient indirect technique to extract the solution. The other important distinction between FWFD and its predecessors is in the fact that the main emphasis, here, is given to finding the eigenvectors (field patterns) rather than the eigenvalues (dispersion curves). On the other hand, due to mathematical correlation, calculation of an eigenvector requires a prior knowledge of the corresponding eigenvalue. However, the eigenvalue calculation can be performed more efficiently by the Compact FDTD (CFDTD) method, Section III.E. on page 82. In FWFD, this computed eigenvalue is used to calculate the eigenvector or field patterns. This procedure is illustrated in Fig. IV.1.

FIGURE IV.1 Flowchart of a complete CAD tool based on CFDTD and FWFD

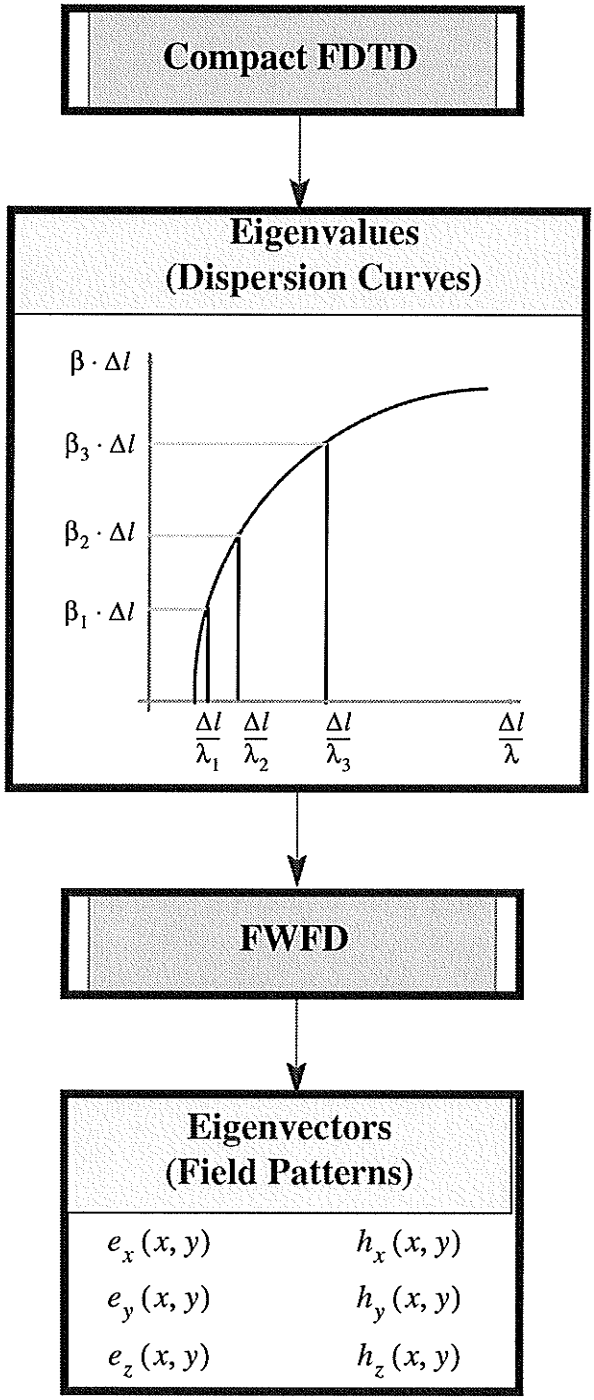

The aforementioned discussion provided a comparison between the FWFD, based on Maxwell equations, and different versions of classical finite difference methods which were all based on the Helmholtz equation. Another important comparison can also be made between the FWFD and Time Domain methods. Such a comparison is postponed to section IV.E. where a more detailed study on the application of time domain methods for calculating field patterns is conducted.

Mathematical derivation of the FWFD is described in section IV.B. Since the method is based on a four directional operator at all interior points, boundary conditions pose a problem for FWFD in the sense that at the boundaries only the information of three neighboring points are available. To overcome the problem, a boundary condition treatment, which is based on a three directional operator, is discussed in section IV.C. Details of the time domain based methods are addressed in section IV.E. The results of applying the algorithm for the case of hollow rectangular waveguide and a shielded suspended coupled dielectric guide operating at E^{y}_{11O} mode are presented in section IV.F., followed by the conclusion in section IV.G.

IV.B. Formulation

IN AN INHOMOGENEOUS waveguide carrying a wave of arbitrary frequency, all six field components are generally present. Starting from Maxwell's equations for a loss-less non-magnetic medium:

$$\vec{\nabla} \times \vec{H} = \varepsilon_0 \varepsilon_r \frac{\partial \vec{E}}{\partial t} \qquad \textbf{(IV.1.a)}$$

$$\vec{\nabla} \times \vec{E} = -\mu_0 \frac{\partial \vec{H}}{\partial t} \qquad \textbf{(IV.1.b)}$$

$$\vec{\nabla} \bullet \left(\varepsilon_r \cdot \vec{E} \right) = 0 \qquad \textbf{(IV.1.c)}$$

$$\vec{\nabla} \bullet \vec{H} = 0 \qquad \textbf{(IV.1.d)}$$

in which ε_0, μ_0 and ε_r represent free space permittivity, permeability and relative permittivity, respectively. Assuming no discontinuity in the z direction, the variation of all field components with respect to z and t can be represented by the term $e^{j(\omega t - \beta z)}$. Therefore the transformations $\frac{\partial}{\partial t} \rightarrow j\omega$ and $\frac{\partial}{\partial z} \rightarrow -j\beta$ are warranted, and Maxwell's equations can be expanded as:

$$\omega e_x = \frac{1}{\varepsilon_0 \varepsilon_r} \left(\beta h_y + \frac{\partial h_z}{\partial y} \right) \qquad \textbf{(IV.2.a)}$$

$$\omega e_y = \frac{1}{\varepsilon_0 \varepsilon_r} \left(-\beta h_x - \frac{\partial h_z}{\partial x} \right) \qquad \textbf{(IV.2.b)}$$

$$\omega e_z = \frac{1}{\varepsilon_0 \varepsilon_r}\left(\frac{\partial h_x}{\partial y} - \frac{\partial h_y}{\partial x}\right) \qquad \textbf{(IV.2.c)}$$

$$\frac{\partial\left(\varepsilon_r e_x\right)}{\partial x} + \frac{\partial\left(\varepsilon_r e_y\right)}{\partial y} + \beta \varepsilon_r e_z = 0 \qquad \textbf{(IV.2.d)}$$

$$\omega h_x = \frac{1}{\mu_0}\left(-\beta e_y - \frac{\partial e_z}{\partial y}\right) \qquad \textbf{(IV.2.e)}$$

$$\omega h_y = \frac{1}{\mu_0}\left(\beta e_x + \frac{\partial e_z}{\partial x}\right) \qquad \textbf{(IV.2.f)}$$

$$\omega h_z = \frac{1}{\mu_0}\left(\frac{\partial e_y}{\partial x} - \frac{\partial e_x}{\partial y}\right) \qquad \textbf{(IV.2.g)}$$

$$\frac{\partial h_x}{\partial x} + \frac{\partial h_y}{\partial y} + \beta h_z = 0 \qquad \textbf{(IV.2.h)}$$

in which Eqs. (IV.2.a)-(IV.2.c) and (IV.2.e)-(IV.2.g) are derived from (IV.1.a) and (IV.1.b), while Eqs. (IV.2.d) and (IV.2.h) from (IV.1.c) and (IV.1.d), respectively. All information contained in Maxwell's equations is transferred to the final algorithm. Also the following conventions are adopted:

$$E_x(x, y, z, t) = -j e_x(x, y) \bullet e^{j(\omega t - \beta z)} \qquad \textbf{(IV.3.a)}$$

$$E_y(x, y, z, t) = -j e_y(x, y) \bullet e^{j(\omega t - \beta z)} \qquad \textbf{(IV.3.b)}$$

$$E_z(x, y, z, t) = e_z(x, y) \bullet e^{j(\omega t - \beta z)} \qquad \textbf{(IV.3.c)}$$

$$H_x(x, y, z, t) = -j h_x(x, y) \bullet e^{j(\omega t - \beta z)} \qquad \textbf{(IV.3.d)}$$

$$H_y(x, y, z, t) = -jh_y(x, y) \bullet e^{j(\omega t - \beta z)} \quad \textbf{(IV.3.e)}$$

$$H_z(x, y, z, t) = h_z(x, y) \bullet e^{j(\omega t - \beta z)} \quad \textbf{(IV.3.f)}$$

Note that in Eqs. (IV.3.a) to (IV.3.f) the phasor field variables in the transverse and axial directions are defined 90° out of phase. These phase differences are introduced initially so that the final equations are in the real domain, to improve the computational efficiency in both time and RAM memory space.

Eqs. (IV.2.a)-(IV.2.h) constitute a system of equations for six two dimensional functions and their first derivatives with respect to x and y coordinates. To derive required expressions, we select e_x component and provide the details of the procedure. It may be extracted directly from Eqn. (IV.2.f). Unfortunately, this will result in an off-diagonal dominant system of equations and therefore yields a highly unstable iterative algorithm. The correct strategy is in selecting only those equations that contain $\frac{\partial e_x}{\partial x}$ and $\frac{\partial e_x}{\partial y}$ terms, i.e. (IV.2.d) and (IV.2.g), and calculate e_x by breaking down the derivatives.

Expanding Eqn. (IV.2.d) into its finite difference form yields:

$$\begin{aligned} &\varepsilon_r\left(i+\frac{1}{2}, j\right)e_x(i,j) - \varepsilon_r\left(i-\frac{1}{2}, j\right)e_x(i-1,j) \\ &= \varepsilon_r\left(i, j-\frac{1}{2}\right)e_y(i,j-1) - \varepsilon_r\left(i, j+\frac{1}{2}\right)e_y(i,j) - \hat{\beta}\varepsilon_r(i,j)\, e_z(i,j) \end{aligned} \quad \textbf{(IV.4)}$$

in which $\hat{\beta} = \beta \cdot \Delta l$ is the normalized propagation constant along the z direction and other notations are defined according to Fig. IV.2.

FIGURE IV.2 Configuration of field components in FWFD

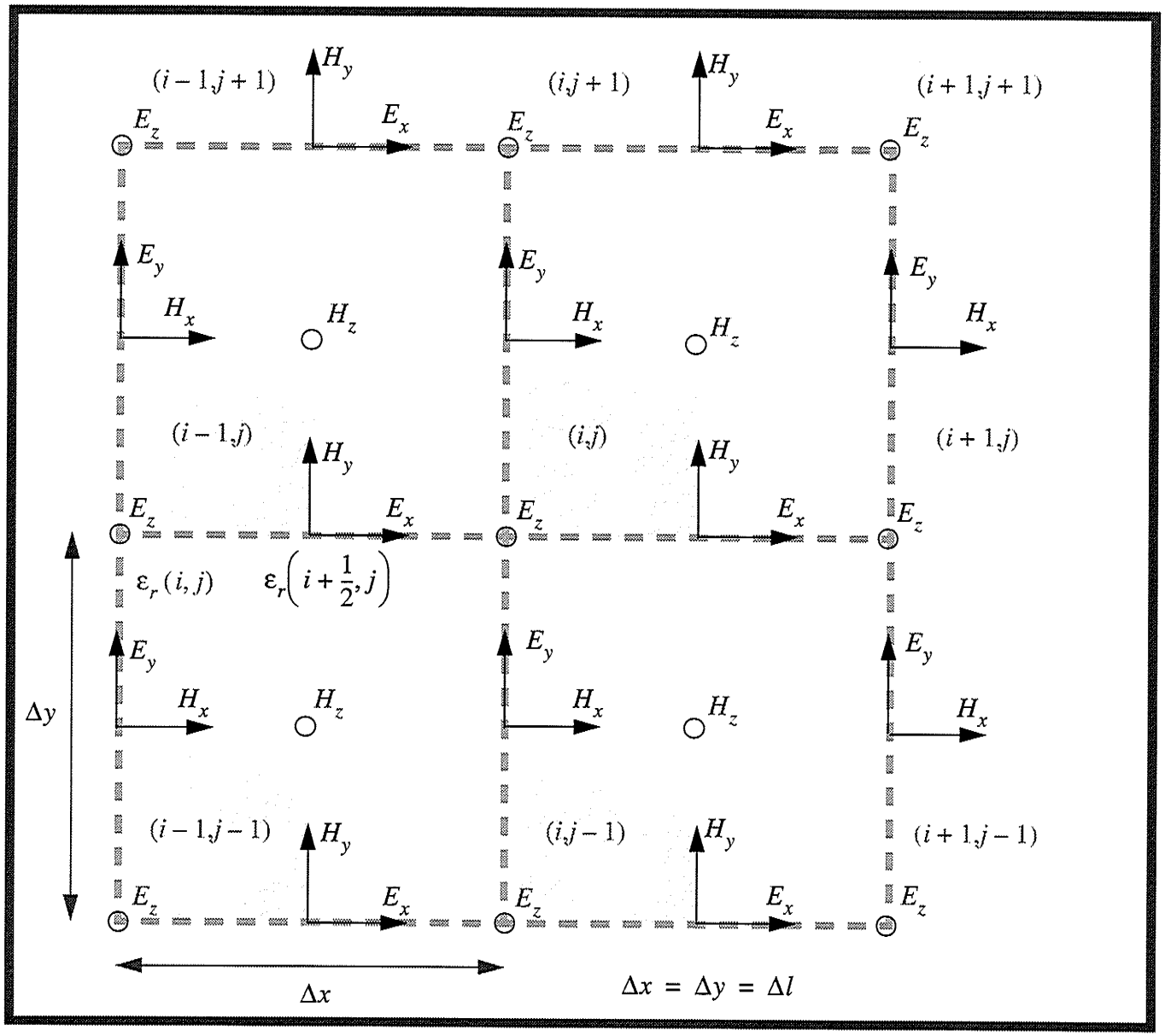

Calculating for $e_x(i,j)$ gives:

$$e_x(i,j) = \frac{1}{\varepsilon_r\left(i+\frac{1}{2},j\right)}\left\{\varepsilon_r\left(i-\frac{1}{2},j\right)e_x(i-1,j)\right. \qquad \textbf{(IV.5.a)}$$
$$\left. +\varepsilon_r\left(i,j-\frac{1}{2}\right)e_y(i,j-1) - \varepsilon_r\left(i,j+\frac{1}{2}\right)e_y(i,j) - \hat{\beta}\varepsilon_r(i,j)\,e_z(i,j)\right\}$$

and replacing i with $i+1$ in Eqn. (IV.4) and again sorting for $e_x(i,j)$ provides:

$$e_x(i,j) = \frac{1}{\varepsilon_r\left(i+\frac{1}{2},j\right)}\left\{\varepsilon_r\left(i+\frac{3}{2},j\right)e_x(i+1,j) - \varepsilon_r\left(i+1,j-\frac{1}{2}\right)e_y(i+1,j-1)\right.$$
$$\left. +\varepsilon_r\left(i+1,j+\frac{1}{2}\right)e_y(i+1,j) + \hat{\beta}\varepsilon_r(i+1,j)\,e_z(i+1,j)\right\} \qquad \textbf{(IV.5.b)}$$

Similarly, $\frac{\partial e_x}{\partial y}$ in Eqn. (IV.2.g) yields:

$$e_x(i,j+1) - e_x(i,j) = -Ah_z(i,j) + e_y(i+1,j) - e_y(i,j) \qquad \textbf{(IV.6)}$$

in which $A = \omega\mu_0\Delta l = 2\pi\left(\frac{\Delta l}{\lambda}\right)Z_0$ and gives $e_x(i,j)$ as:

$$e_x(i,j) = e_x(i,j+1) + Ah_z(i,j) - e_y(i+1,j) + e_y(i,j) \qquad \textbf{(IV.7.a)}$$

and by replacing j with $j-1$ in Eq. (IV.6) provides:

$$e_x(i,j) = e_x(i,j-1) - Ah_z(i,j-1) + e_y(i+1,j-1) - e_y(i,j-1) \qquad \textbf{(IV.7.b)}$$

Eqs. (IV.5.a), (IV.5.b), (IV.7.a), (IV.7.b) constitute a set of finite difference equations expressing the x component of electric field in terms of its values at four neighboring nodes. Adding them provides a single expression relating the field value at each point to its four adjacent nodes. Final expression for e_x can be found as:

$$e_x(i,j) = \frac{1}{4}\delta_{xx}^{ee} + \frac{1}{4}\delta_{xy}^{ee} + \frac{A}{2}\delta_{xz}^{eh} + \frac{\hat{\beta}}{2}\delta_{xz}^{ee} \qquad \textbf{(IV.8.a)}$$

in which:

$$\delta_{xx}^{ee} = e_x(i,j+1) + e_x(i,j-1) \qquad \textbf{(IV.8.b)}$$

$$+ \frac{1}{\varepsilon_r\left(i+\frac{1}{2},j\right)}\left[\varepsilon_r\left(i-\frac{1}{2},j\right)e_x(i-1,j) + \varepsilon_r\left(i+\frac{3}{2},j\right)e_x(i+1,j)\right]$$

$$\delta_{xy}^{ee} = \left\{e_y(i,j) + e_y(i+1,j-1)\right. \qquad \textbf{(IV.8.c)}$$

$$+ \frac{1}{\varepsilon_r\left(i+\frac{1}{2},j\right)}\left[\varepsilon_r\left(i,j-\frac{1}{2}\right)e_y(i,j-1) + \varepsilon_r\left(i+1,j+\frac{1}{2}\right)e_y(i+1,j)\right]\Bigg\}$$

$$- \Bigg\{e_y(i+1,j) + e_y(i,j-1)$$

$$+ \frac{1}{\varepsilon_r\left(i+\frac{1}{2},j\right)}\left[\varepsilon_r\left(i,j+\frac{1}{2}\right)e_y(i,j) + \varepsilon_r\left(i+1,j-\frac{1}{2}\right)e_y(i+1,j-1)\right]\Bigg\}$$

$$\delta_{xz}^{eh} = h_z(i,j) - h_z(i,j-1) \qquad \textbf{(IV.8.d)}$$

$$\delta_{xz}^{ee} = \frac{1}{\varepsilon_r\left(i+\frac{1}{2},j\right)}\left[\varepsilon_r(i+1,j)\,e_z(i+1,j) - \varepsilon_r(i,j)\,e_z(i,j)\right] \qquad \textbf{(IV.8.e)}$$

and $\frac{A}{2}\delta_{xz}^{eh}$ represents the contribution of h_z to e_x.

To help in understanding equation (IV.8.a), the following cases are considered.

- *Inside a homogeneous medium* $\delta_{xy}^{ee} = 0$ *and Eq. (IV.1.a) takes a simplified form:*

$$e_x(i,j) = \frac{1}{4}\left[e_x(i,j+1) + e_x(i,j-1) + e_x(i-1,j) + e_x(i+1,j)\right] + \frac{A}{2}\left[h_z(i,j) - h_z(i,j-1)\right] + \frac{\hat{\beta}}{2}\left[e_z(i+1,j) - e_z(i,j)\right] \qquad \textbf{(IV.9)}$$

- *The first bracket in Eq. (IV.9) represents an averaging scheme for the field components at neighboring points. This averaging term appears in all other equations as well. Its presence can be understood from the finite difference solution of Laplace equation, i.e.* $\nabla_t^2\Phi = 0$, *in which* $\nabla_t^2 = \frac{\partial^2}{\partial x^2} + \frac{\partial^2}{\partial y^2}$. *In that case, the solution is expressed as:*

$$\Phi(i,j) = \frac{1}{4}\left[\Phi(i+1,j) + \Phi(i-1,j) + \Phi(i,j+1) + \Phi(i,j-1)\right] \qquad \textbf{(IV.10)}$$

It can easily be verified that Eq. (IV.10) is a special case of Eq. (IV.9), when the criteria $(\omega = 0) \Rightarrow A = 0$ at $\hat{\beta} = 0$ is met. In fact, this is the same criteria for the validity of Laplace equation, i.e. Quasi-TEM or TEM assumptions.

- *It is known that inside a homogeneous waveguide, all the field components can be generated by superposition of two TE and TM modes. This is verified by Eqs. (IV.9), in which* δ_{xz}^{eh} *and* δ_{xz}^{ee} *can be viewed as the contributions of* TE_z *and* TM_z *based modes, respectively. Note that for the inhomogeneous case, an extra term,* δ_{xy}^{ee}*, is also required which diminishes everywhere except at the interface of two media with different permittivities.*

- *Eq. (IV.10) cannot be derived simply by adding Eqs. (IV.5.a), (IV.5.b), (IV.7.a) and (IV.7.b) and dividing them by four. The presence of* $\frac{1}{2}$ *multiplication factor for* δ_{xz}^{ee} *and* δ_{xz}^{eh} *in lieu of* $\frac{1}{4}$ *can be understood by studying an extreme case of a one dimensional problem. Suppose, the solution for the* TE_{10} *mode in a hollow rectangular waveguide is desired. In this case, assuming the longer edge of the waveguide in the* x *direction, all the field components are a function of* x *only and* $\frac{\partial}{\partial y} = 0$*. Eqs. (IV.2.a)-(IV.2.h) reduce to:*

$$\omega e_y = \frac{1}{\varepsilon_0}\left(-\beta h_x - \frac{\partial h_z}{\partial x}\right) \qquad \textbf{(IV.11.a)}$$

$$\omega h_z = \frac{1}{\mu_0}\left(\frac{\partial e_y}{\partial x}\right) \qquad \textbf{(IV.11.b)}$$

$$\frac{\partial h_x}{\partial x} + \beta h_z = 0 \qquad \textbf{(IV.11.c)}$$

From Eq. (IV.2.a):

$$h_z(i,j) = h_z(i-1,j) - Be_y(i,j) - \hat{\beta} h_x(i,j) \qquad \textbf{(IV.12.a)}$$

in which $B = \omega\varepsilon_0\Delta l = 2\pi\left(\frac{\Delta l}{\lambda}\right)\frac{1}{Z_0}$.

and performing the $i \rightarrow i+1$ transformation gives:

$$h_z(i,j) = h_z(i+1,j) + Be_y(i+1,j) + \hat{\beta} h_x(i+1,j) \qquad \textbf{(IV.12.b)}$$

and finally, by adding Eqs. (IV.3.a) and (IV.3.b) and dividing by two provides:

$$h_z(i,j) = \frac{1}{2}\left[h_z(i+1,j) + h_z(i-1,j)\right] + \frac{B}{2}\left[e_y(i+1,j) - e_y(i,j)\right] + \frac{\hat{\beta}}{2}\left[h_x(i+1,j) - h_x(i,j)\right] \qquad \textbf{(IV.13.a)}$$

Other two components can similarly be obtained as:

$$e_y(i,j) = \frac{1}{2}\left[e_y(i+1,j) + e_y(i-1,j)\right] + \frac{A}{2}\left[h_z(i-1,j) - h_z(i,j)\right] \qquad \textbf{(IV.13.b)}$$

$$h_x(i,j) = \frac{1}{2}\left[h_x(i+1,j) + h_x(i-1,j)\right] + \frac{\hat{\beta}}{2}\left[h_z(i,j) - h_z(i-1,j)\right] \qquad \textbf{(IV.13.c)}$$

After confirming the validity of the Eqs. (IV.13.a), (IV.13.b) and (IV.13.c) by comparing its computer generated results to the analytical ones, it can act as a benchmark to examine the final equations. It can be easily verified that the aforementioned equations for the TE_{10} mode are the same as those obtained from the final equations, assuming $\frac{\partial}{\partial y} = 0$ or in finite difference terms $f(i,j) = f(i,j+1) = f(i,j-1)$.

IV.B.1 Complete derivation of FWFD

FINAL EQUATIONS of the FWFD method.

- e_x

$$e_x(i,j) \quad \blacktriangleright \quad \text{(IV.8.a), (IV.8.b), (IV.8.c), (IV.8.d) \& (IV.8.e)} \qquad \textbf{(IV.14)}$$

- e_y

$$e_y(i,j) = \frac{1}{4}\delta_{yy}^{ee} + \frac{1}{4}\delta_{yx}^{ee} + \frac{A}{2}\delta_{yz}^{eh} + \frac{\hat{\beta}}{2}\delta_{yz}^{ee} \qquad \textbf{(IV.15.a)}$$

$$\delta_{yy}^{ee} = e_y(i+1,j) + e_y(i-1,j) \qquad \textbf{(IV.15.b)}$$

$$+\frac{1}{\varepsilon_r\left(i,j+\frac{1}{2}\right)}\left[\varepsilon_r\left(i,j-\frac{1}{2}\right)e_y(i,j-1) + \varepsilon_r\left(i,j+\frac{3}{2}\right)e_y(i,j+1)\right]$$

$$\delta_{yx}^{ee} = \left\{e_x(i,j) + e_x(i-1,j+1)\right. \qquad \textbf{(IV.15.c)}$$

$$\left.+\frac{1}{\varepsilon_r\left(i,j+\frac{1}{2}\right)}\left[\varepsilon_r\left(i-\frac{1}{2},j\right)e_x(i-1,j) + \varepsilon_r\left(i+\frac{1}{2},j+1\right)e_x(i,j+1)\right]\right\}$$

$$-\left\{e_x(i,j+1) + e_x(i-1,j)\right.$$

$$\left.+\frac{1}{\varepsilon_r\left(i,j+\frac{1}{2}\right)}\left[\varepsilon_r\left(i+\frac{1}{2},j\right)e_x(i,j) + \varepsilon_r\left(i-\frac{1}{2},j+1\right)e_x(i-1,j+1)\right]\right\}$$

$$\delta_{yz}^{eh} = h_z(i-1,j) - h_z(i,j) \qquad \textbf{(IV.15.d)}$$

$$\delta_{yz}^{ee} = \frac{1}{\varepsilon_r\left(i,j+\frac{1}{2}\right)}\left[\varepsilon_r(i,j+1)\,E_z(i,j+1) - \varepsilon_r(i,j)\,E_z(i,j)\right] \qquad \textbf{(IV.15.e)}$$

- e_z

$$e_z(i,j) = \frac{1}{4}\delta_{zz}^{ee} + \frac{A}{2}\left(\delta_{zx}^{eh} + \delta_{zy}^{eh}\right) + \frac{\hat{\beta}}{2}\left(\delta_{zx}^{ee} + \delta_{zy}^{ee}\right) \qquad \textbf{(IV.16.a)}$$

$$\delta_{zy}^{eh} = e_z(i+1,j) + e_z(i-1,j) + e_z(i,j+1) + e_z(i,j-1) \qquad \textbf{(IV.16.b)}$$

$$\delta_{zx}^{eh} = h_x(i,j) - h_x(i,j-1) \qquad \textbf{(IV.16.c)}$$

$$\delta_{zy}^{eh} = h_y(i-1,j) - h_y(i,j) \qquad \textbf{(IV.16.d)}$$

$$\delta_{zx}^{ee} = e_x(i,j) - e_x(i-1,j) \qquad \textbf{(IV.16.e)}$$

$$\delta_{zy}^{ee} = e_y(i,j) - e_y(i,j-1) \qquad \textbf{(IV.16.f)}$$

- h_x

$$h_x(i,j) = \frac{1}{4}\delta_{xx}^{hh} + \frac{B}{2}\delta_{xz}^{he} + \frac{\hat{\beta}}{2}\delta_{xz}^{hh} \qquad \textbf{(IV.17.a)}$$

$$\delta_{xx}^{hh} = h_x(i+1,j) + h_x(i-1,j) + h_x(i,j+1) + h_x(i,j-1) \qquad \textbf{(IV.17.b)}$$

$$\delta_{xz}^{he} = \varepsilon_r(i,j)\,e_z(i,j) - \varepsilon_r(i,j+1)\,e_z(i,j+1) \qquad \textbf{(IV.17.c)}$$

$$\delta_{xz}^{hh} = h_z(i,j) - h_z(i-1,j) \qquad \textbf{(IV.17.d)}$$

- h_y

$$h_y(i,j) = \frac{1}{4}\delta_{yy}^{hh} + \frac{B}{2}\delta_{yz}^{he} + \frac{\hat{\beta}}{2}\delta_{yz}^{hh} \quad \textbf{(IV.18.a)}$$

$$\delta_{yy}^{hh} = h_y(i+1,j) + h_y(i-1,j) + h_y(i,j+1) + h_y(i,j-1) \quad \textbf{(IV.18.b)}$$

$$\delta_{yz}^{he} = \varepsilon_r(i+1,j)\, e_z(i+1,j) - \varepsilon_r(i,j)\, e_z(i,j) \quad \textbf{(IV.18.c)}$$

$$\delta_{yz}^{hh} = h_z(i,j) - h_z(i,j-1) \quad \textbf{(IV.18.d)}$$

- h_z

$$h_z(i,j) = \frac{1}{4}\delta_{zz}^{hh} + \frac{B}{2}\left(\delta_{zx}^{he} + \delta_{zy}^{he}\right) + \frac{\hat{\beta}}{2}\left(\delta_{zx}^{hh} + \delta_{zy}^{hh}\right) \quad \textbf{(IV.19.a)}$$

$$\delta_{zz}^{hh} = h_z(i+1,j) + h_z(i-1,j) + h_z(i,j+1) + h_z(i,j-1) \quad \textbf{(IV.19.b)}$$

$$\delta_{zx}^{he} = \varepsilon_r\left(i+\frac{1}{2},j\right)e_x(i,j) - \varepsilon_r\left(i+\frac{1}{2},j+1\right)e_x(i,j+1) \quad \textbf{(IV.19.c)}$$

$$\delta_{zy}^{he} = \varepsilon_r\left(i+1,j+\frac{1}{2}\right)e_y(i+1,j) - \varepsilon_r\left(i,j+\frac{1}{2}\right)e_y(i,j) \quad \textbf{(IV.19.d)}$$

$$\delta_{zx}^{hh} = h_x(i+1,j) - h_x(i,j) \quad \textbf{(IV.19.e)}$$

$$\delta_{zy}^{hh} = h_y(i,j+1) - h_y(i,j) \quad \textbf{(IV.19.f)}$$

IV.C. Boundary conditions

TWO POSSIBLE BOUNDARY conditions, i.e. **Dirichlet** or **Neumann**, might be encountered when treating a field component for the points located exactly on the boundaries. The Dirichlet boundary condition can be easily satisfied just by resetting the field component at the boundary nodes to zero. The Neumann boundary condition, on the other hand, can be fulfilled by resetting to zero the normal derivative of the field component at the boundary. In this study we have accomplished this by assuming identical values for the field component at the two adjacent points at opposite sides of the boundary node. This insures nullifying the central difference derivative of that component.

To be specific, an example of treating the e_x component of a waveguide structure is presented. Suppose that two **PEC** (Perfect Electric Conductor) walls are placed at $x = 0$ and $y = 0$, and two **PMC** (Perfect Magnetic Conductor) walls at $x = a\Delta l$ and $y = b\Delta l$. Therefore, the boundary conditions at $x = a\Delta l$ and $y = 0$ are Dirichlet type, i.e. $e_x(a,j) = 0$ and $e_x(i,0) = 0$. And, because of the Neumann boundary condition at $x = 0$ and $y = b\Delta l$, Eq. (IV.9) converts into:

$$e_x(0,j) = \frac{1}{4}[2e_x(0+1,j) + e_x(0,j+1) + e_x(0,j-1)] + \frac{A}{2}[h_z(0.j) - h_z(0,j-1)] + \frac{\hat{\beta}}{2}[e_z(0+1,j)] \qquad \textbf{(IV.20)}$$

$$e_x(i,b) = \frac{1}{4}[e_x(i-1,b) + e_x(i+1,b) + 2e_x(i,b-1)] + \frac{A}{2}[-h_z(i,b-1)] + \frac{\hat{\beta}}{2}[e_z(b+1,j) - e_z(b,j)] \qquad \textbf{(IV.21)}$$

Note that, in Eqs. (IV.20) and (IV.21), valid boundary conditions on e_z and h_z were taken into account. Another scheme is also tried for this class of problems which imposes only the Dirichlet boundary condition and handles the Neumann one using a one directional operator as of Eq. (IV.5.a). Maxwell's equations automatically adjust the field values, even at the Neumann boundary nodes.

IV.D. FWFD flowchart

THE FLOWCHART of FWFD is illustrated in Fig. IV.3. First, the eigenvalue information is fed into the algorithm. Like any other iterative scheme for solving system of linear equations, an initial guess is required. In most cases, the speed of convergence is dependent on starting with a good initial guess. At this stage, FWFD formulation, i.e. Eqs. (IV.8.a)-(IV.8.e), (IV.15.a)-(IV.15.e), (IV.16.a)-(IV.16.f), (IV.17.a)-(IV.17.d), (IV.18.a)-(IV.18.d) and (IV.19.a)-(IV.19.f); must be implemented iteratively to update the field values. There have been two updating strategies reported in the literature, i.e. Jacobi and Guass-Siedel. It is found that FWFD does not converge to the correct results using either of these methods. Only a combination of the two was found to be successful. In the combined method, first the electric field values at all nodes are calculated and then updated. The same procedure is applied to the magnetic field components. In other words, calculation of electric field components follows a Jacobi procedure, while the overall updating of electric and magnetic fields is a Guass-Siedel one. The reason for this special updating mechanism goes back to the essence of the leap frog algorithm in Yee's lattice. It is known that leap frog mechanism, a half step time difference between electric and magnetic field calculation, is

required to obtain any meaningful and stable algorithm. Since in FWFD, time variable does not exist, the leap frog algorithm constitutes itself as two distinct updating stages to evaluate the electric and magnetic field components.

The other important stage of the FWFD algorithm is normalization. Normalization is required in view of the fact that for each distinct eigenvalue, there corresponds an infinite set of eigenvectors. Mathematically speaking, eigenvector problem $(A - \lambda_0) X = 0$ has a pair of unique solutions, X and $-X$, when accompanied by a constraint, $\|X\|_2 = 1$, where $\|X\|_2$ is the Euclidean norm and,

$$X = \left[e_x(1,1)\ e_y(1,1)\ e_z\ (1,1)\ h_x(1,1)\ h_y(1,1)\ h_z(1,1)\ \ldots\ h_z(M,N) \right]^T \quad \textbf{(IV.21.g)}$$

Finally, a convergence test is used to end the iterations.

FIGURE IV.3 Flowchart of FWFD

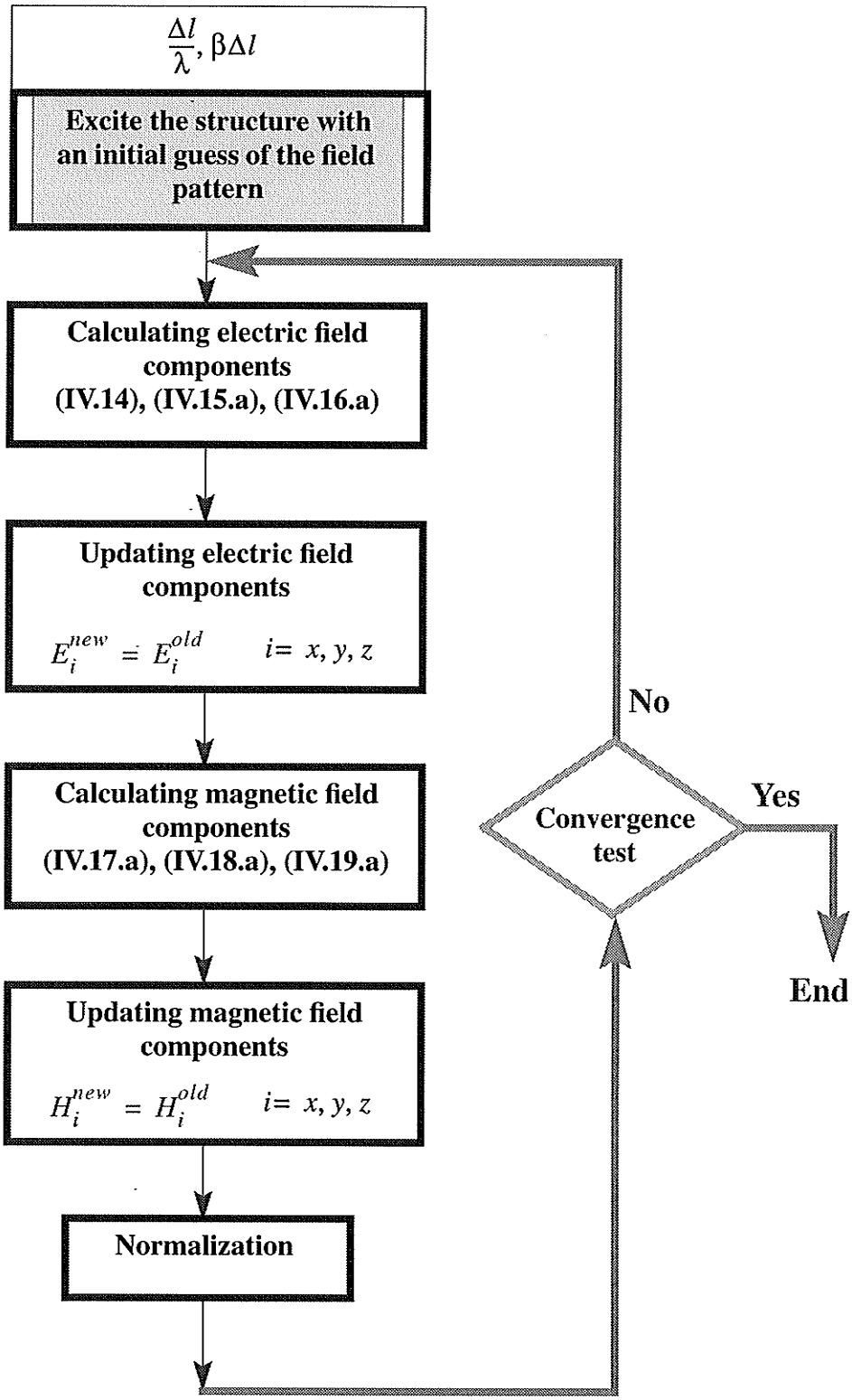

IV.E. Time Domain Techniques

AS WAS MENTIONED earlier, field patterns can be calculated using both classical and time domain based finite difference methods. Many studies have already been conducted on the classical finite difference method. And, a comparison between this class of methods and the FWFD was made in the introduction. On the other hand, time domain based method, i.e. FDTD, was used for calculating field patterns restricted to cut-off frequencies [35]. For this reason, we preferred to use time domain based methods as a benchmark for confirming the validity of the results obtained using FWFD. This way, the applicability of the time domain methods for field pattern calculations will also be elaborated which has its own merits.

Both **CFDTD** and **TLM** are capable of evaluating the dispersion curves of inhomogeneous waveguides by the Fourier transformation of their impulse responses. Theoretically, these methods can also be deployed for calculating field patterns inside a waveguide. To do this, two different strategies can be adopted. In one the structure is excited with a time impulse and evolution of all six field components (E_x, E_y, E_z, H_x, H_y, H_z) is recorded at each individual node in the mesh. A Fourier transformation of the nodal field time history provides the desired field distributions. This method, i.e. impulse-FFT analysis, though feasible, is a rather tedious and inefficient approach. The second method [13] is based on the steady state analysis of the structure. In this approach, the structure is excited with a sinusoidal waveform at an arbitrary point. After sufficient iterations, the transient response decays and what is left is the steady state response. But, this information still has an undesirable time dependency. In fact, the average of the absolute values of the time history of

the fields can better serve the purpose. This, in turn will result in the loss of relative phase information of the field components.

The flowcharts of the two different time domain algorithms, steady state and impulse-FFT analyses, are depicted in Figs. IV.4.a and IV.4.b, respectively. Compact FDTD is selected as the main engine for both. In the steady state analysis, a relatively long waiting period is required for the transient response to damp out. This waiting period is one of the main disadvantages of steady state method in addition to losing the phase information due to the presence of absolute value operator in the algorithm. Impulse-FFT, on the other hand, relies on large computer resources. The results of applying steady state and impulse-FFT analysis on a coupled waveguide are presented in the next section.

FWFD, is capable of providing the amplitude and phase information of all six field components simultaneously and through one single analysis. The algorithm starts with a crude guess of the field distribution and then proceeds with an iterative scheme to converge to the correct results.

FIGURE IV.4 (a) Flowchart of steady state algorithm, (b) Flowchart of impulse-FFT algorithm.

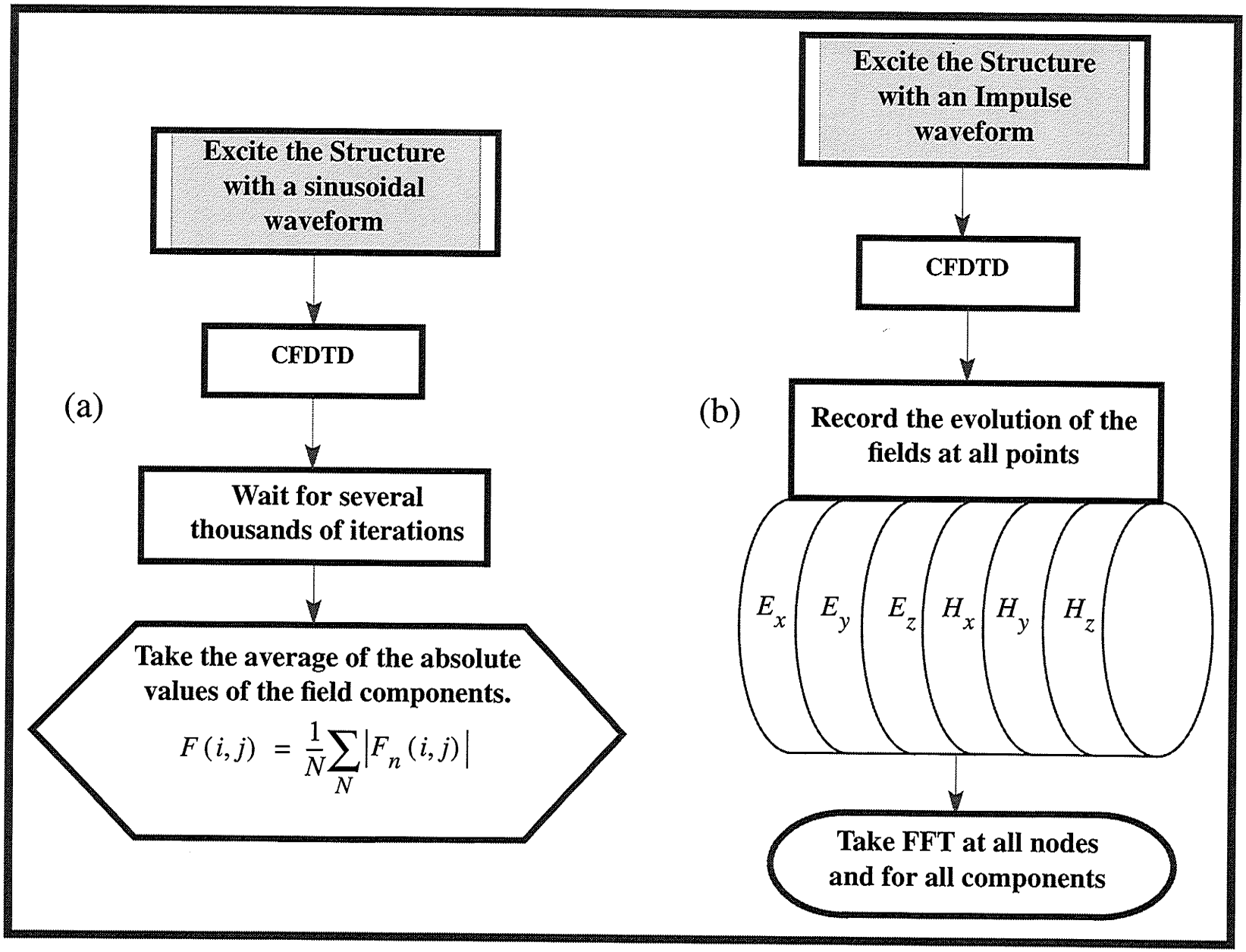

IV.F. Applications

IN THIS SECTION, the results of applying the proposed method to a hollow rectangular waveguide, consisting of four PEC walls, and a shielded suspended coupled dielectric guide are presented. Like any other iterative method for solving linear system of equations, a good initial guess, can noticeably enhance the speed of convergence. However, to show the power of **FWFD** and the fact that the field patterns for arbitrary waveguides are not generally known, a simple initial field distribution is selected, by uniformly setting e_z to unity and resetting the remaining components to zero.

IV.F.1 Hollow Rectangular Waveguide

The first case is a hollow rectangular waveguide of dimensions $18\Delta l \times 12\Delta l$. The objective, here, is calculating the field patterns corresponding to TM_{31} mode. The eigenvalue information of this structure for the mn th mode can be obtained from:

$$\frac{\Delta l}{\lambda} = \frac{1}{2}\sqrt{\left(\frac{m}{k_a}\right)^2 + \left(\frac{n}{k_b}\right)^2 + \left(\frac{\beta\Delta l}{\pi}\right)^2} \qquad \textbf{(IV.22)}$$

in which $k_a = \frac{a}{\Delta l} = 18$, $k_b = \frac{b}{\Delta l} = 12$, $m = 3$ and $n = 1$. From this, the corresponding eigenvalue to $\beta\Delta l = 0.1$ is calculated as $\frac{\Delta l}{\lambda} = 0.0945$. Next, this pair of values is fed to FWFD. The field patterns, i.e. eigenvectors, are obtained after 250 iterations. These patterns are in close agreement with those obtainable from an analytical solution. Normalized pattern of h_x component, with respect to $|h_x|_{max}$, is illustrated in Fig. IV.5 in which

both amplitude and phase information are contained. The normalized amplitudes of all field components, with respect to $|e_z|_{max}$, are also calculated and compared with those obtained from the exact solution. Table **I** summarizes the results of this comparison.

FIGURE IV.5 Normalized h_x field pattern of a TM_{31} in a hollow rectangular waveguide

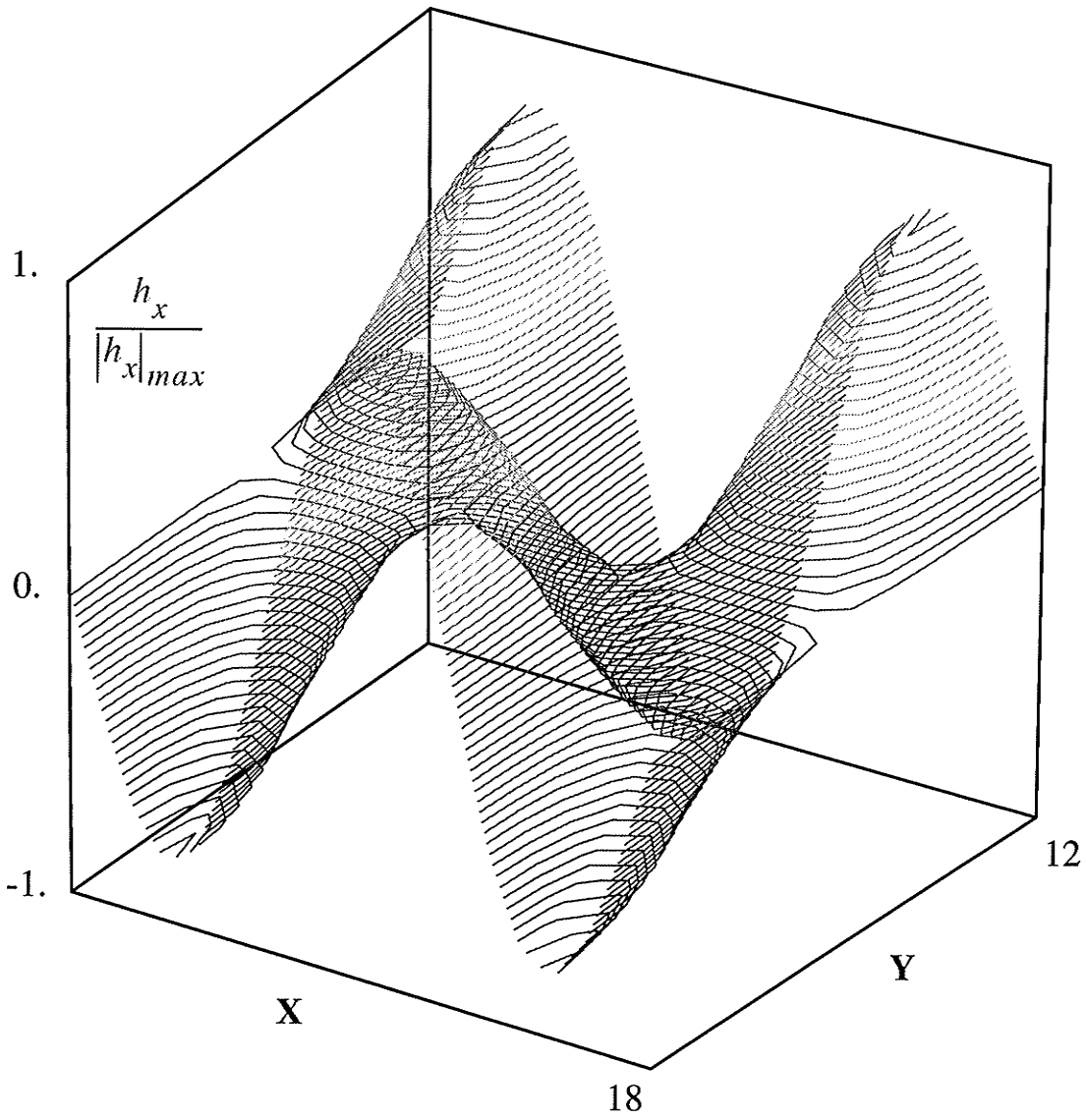

TABLE I. TM_{31} **normalized modal fields, with respect to** $|e_z|_{max}$ **in a rectangular waveguide**

	$\|e_x\|$	$\|e_y\|$	$\|e_z\|$	$\|h_x\|$	$\|h_y\|$	$\|h_z\|$
Exact	0.15	$7.6e^{-2}$	1.00	$1.2e^{-3}$	$2.4e^{-3}$	0.
FWFD	0.14	$6.8e^{-2}$	1.00	$1.1e^{-3}$	$2.1e^{-3}$	$6.7e^{-11}$

IV.F.2 Shielded Suspended Coupled Dielectric Guide [48]

The study of dominant E_y^{11O} mode in a shielded suspended coupled dielectric guide, Fig. IV.6, constitutes our second example. Since the coupled dielectric waveguide is symmetric, its propagating modes can be decomposed into two sets of even and odd modes. Odd or even mode analysis can be performed by placing a PEC (Perfect Electric Conductor) or PMC (Perfect Magnetic Conductor) on the plane of symmetry, respectively. For demonstration purposes, only the odd mode analysis is presented here. In any event, only analysis of half of the structure suffices. This configuration was already analyzed using mode matching technique [46] and an older version of CFDTD [47]. Using our CFDTD routine, normalized eigenvalue pair is calculated as $\frac{\Delta l}{\lambda} = 0.02644$ corresponding to $\beta\Delta l = 0.1$. By choosing $\Delta l = \frac{1}{3}$ mm, the physical dimension as of [46] can be obtained. In this case, the eigenvalue pair would be $f = 23.8$ GHz at $\frac{\beta}{\beta_0} = 0.6$. For convenience, FWFD is formulated in terms of normalized quantities, and so it is the normalized pair that

is actually used here. To initialize, the structure is excited by setting e_y to unity uniformly all across the waveguide, except at the boundaries. This crude initial guess is made with the only available information, i.e. an E_y^{11O} would definitely have an e_y component. Since, no other information is available, a uniform distribution is assumed for excitation. Of course, if any other information is accommodated, a smarter choice and faster convergence can be achieved. For this configuration, field patterns were calculated in 100 iterations. On a Sun-Sparc 10/41, this is equivalent to about 3 seconds computational time.

FIGURE IV.6 Shielded suspended coupled dielectric guide

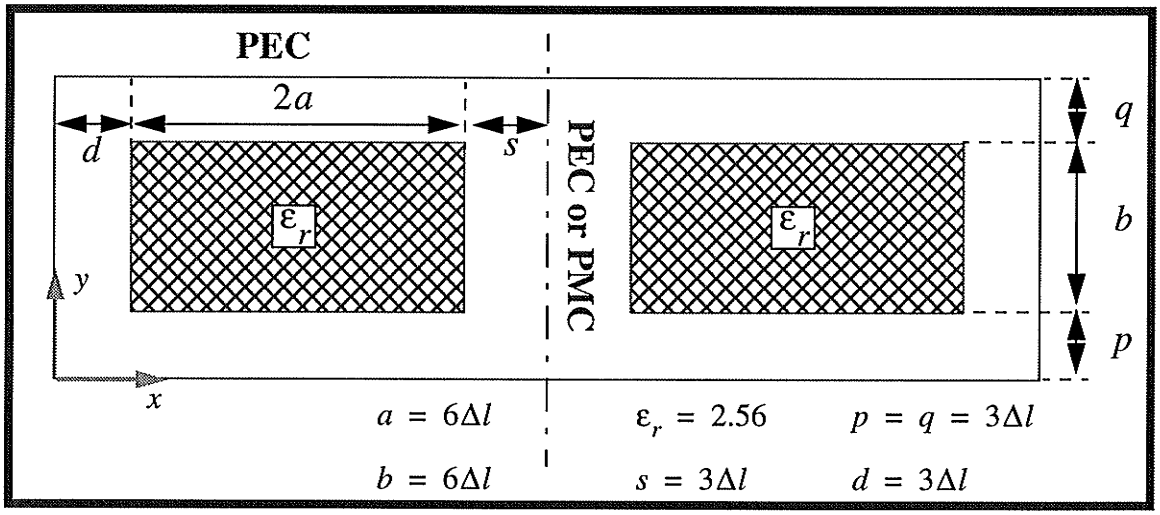

To prove the validity of FWFD results, both steady state and impulse-FFT were tried. For the sake of brevity only the patterns for normalized e_y are illustrated. Figs. IV.7.a and IV.7.b are generated by steady and impulse-FFT methods, respectively. The patterns for other field components are in close agreement with each other regardless of the method,

steady state or impulse-FFT. For the impulse-FFT method, a uniform excitation of e_y all across the waveguide was used. While for the steady state analysis, a point excitation of e_y at the node $(4, 3)$ was implemented. Obviously since the field distribution is unknown, one cannot excite the entire structure steadily with a uniform distribution. The drawback of using point excitation is evident in Fig, IV.7.a; the field pattern is distorted exactly at the location of excitation. Also the calculated field patterns using FWFD are presented in Figs. IV.8.a to IV.8.e, and, as expected are in good agreement with those of the other methods.

FIGURE IV.7.a Normalized e_y field pattern of E^y_{11O} mode using steady state method.

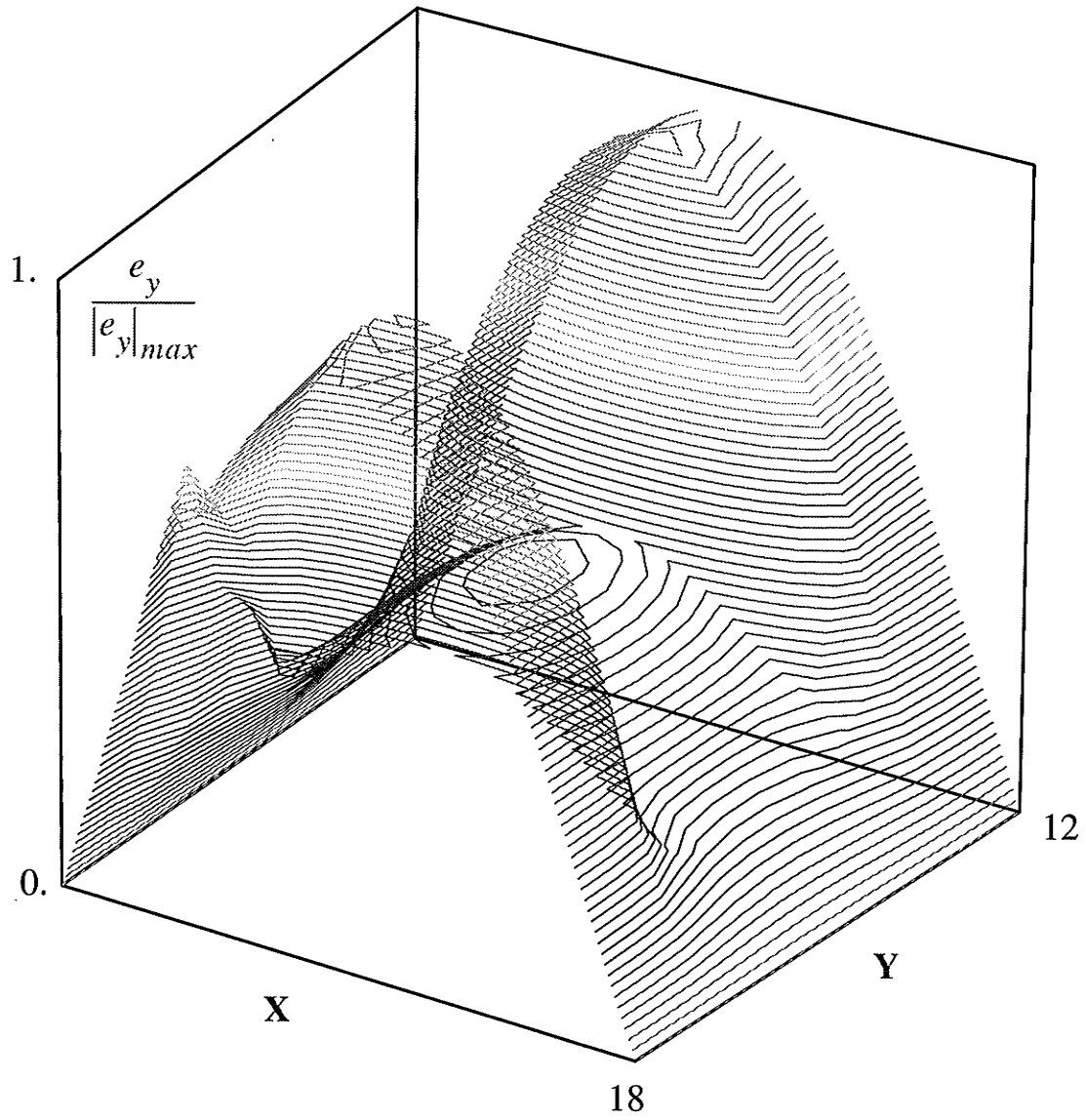

FIGURE IV.7.b **Normalized e_y field pattern of E^y_{11O} mode using impulse-FFT method.**

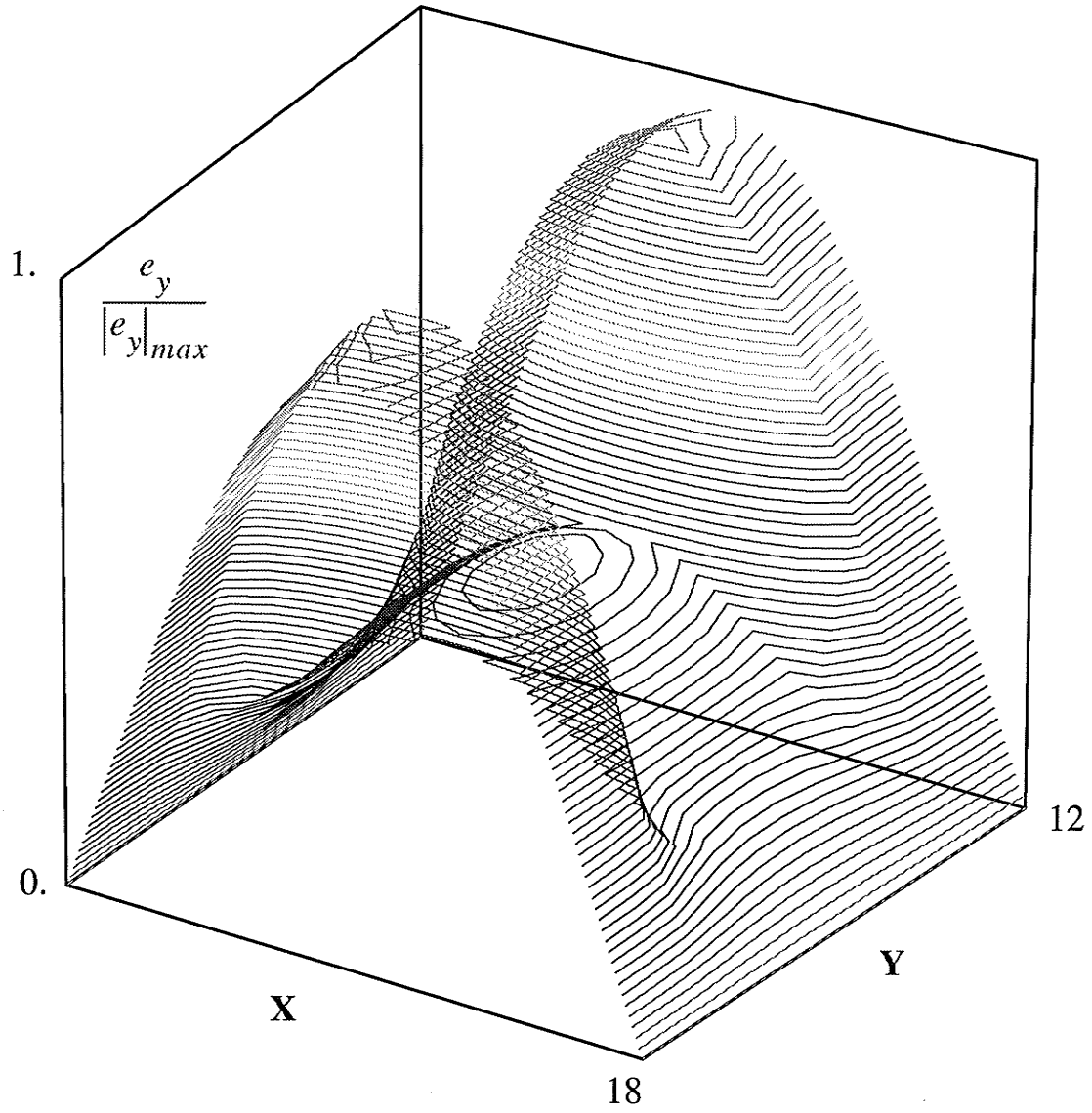

FIGURE IV.8.a **Normalized e_x field pattern of E^y_{11O} mode using FWFD.**

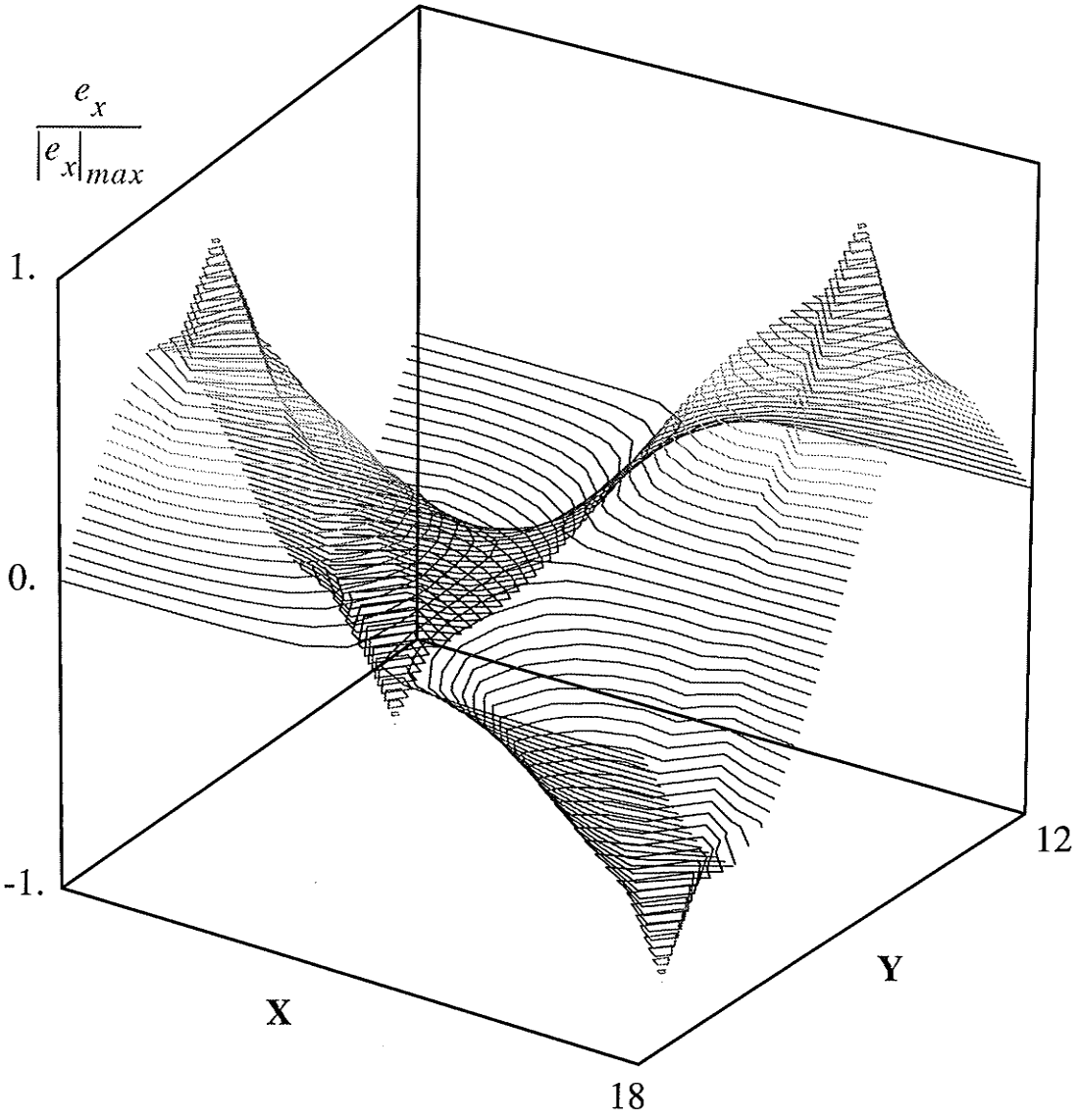

FIGURE IV.8.b **Normalized e_y field pattern of E^y_{11O} mode using FWFD.**

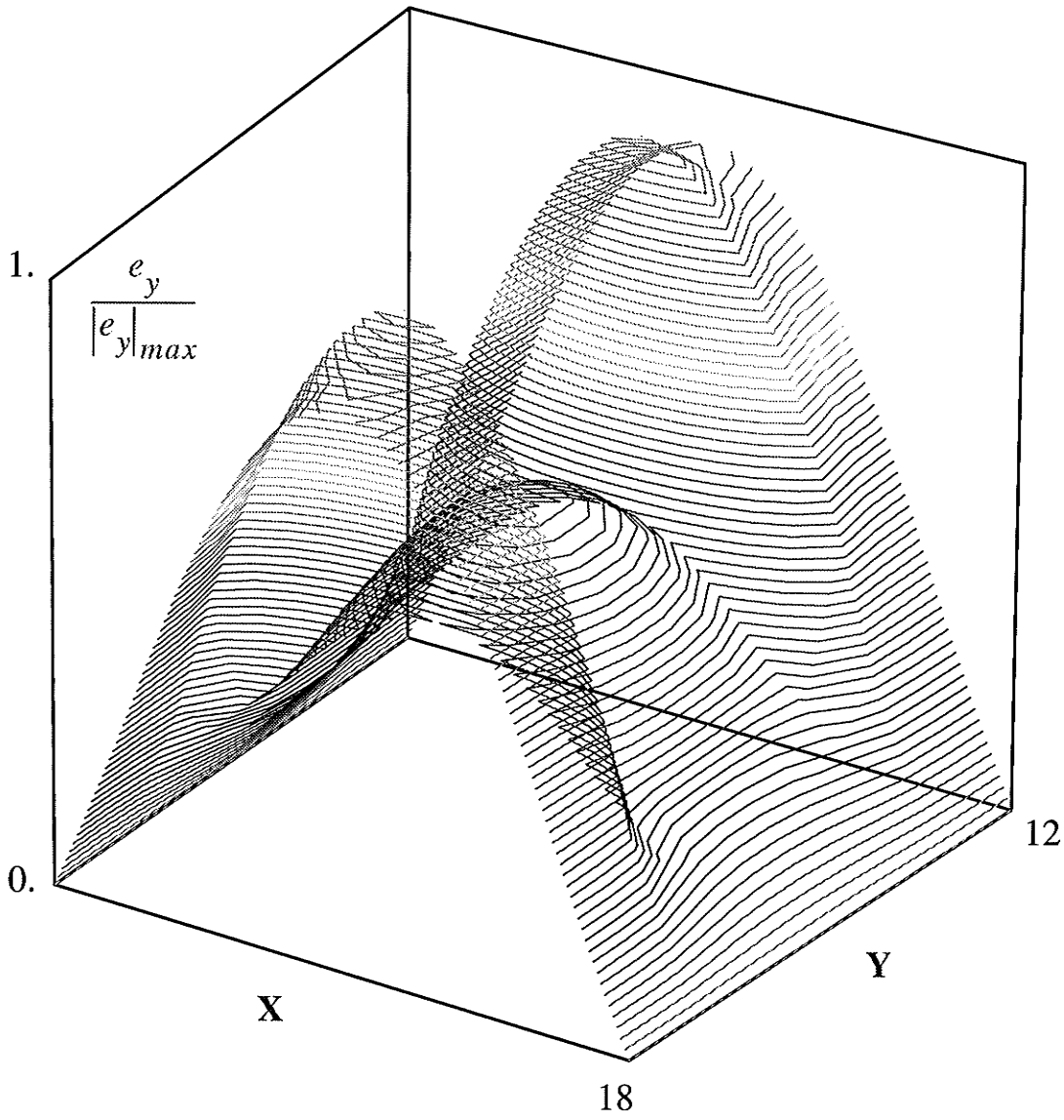

FIGURE IV.8.c **Normalized e_z field pattern of E^y_{11O} mode using FWFD.**

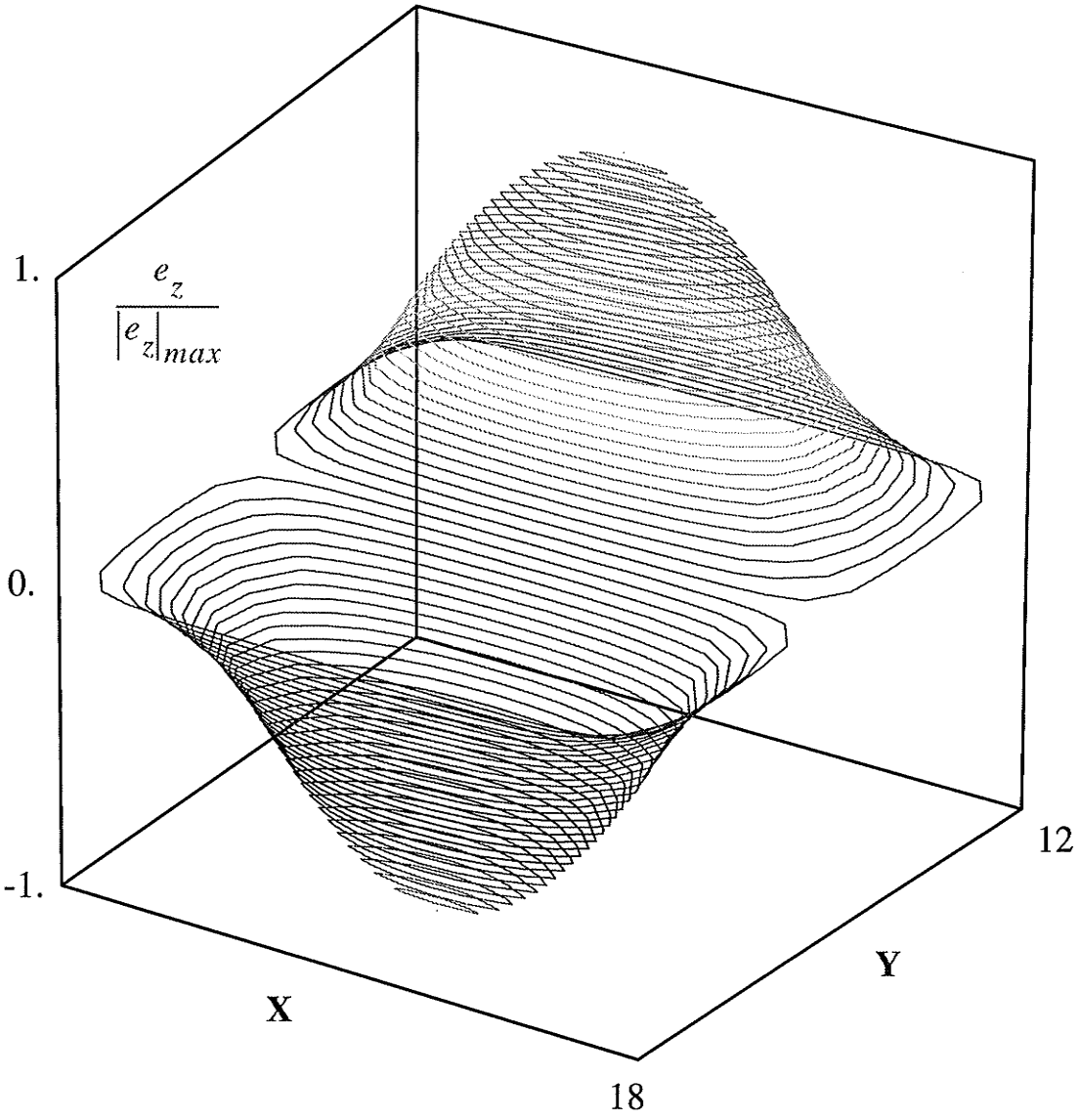

FIGURE IV.8.d Normalized h_x field pattern of E^y_{11O} mode using FWFD.

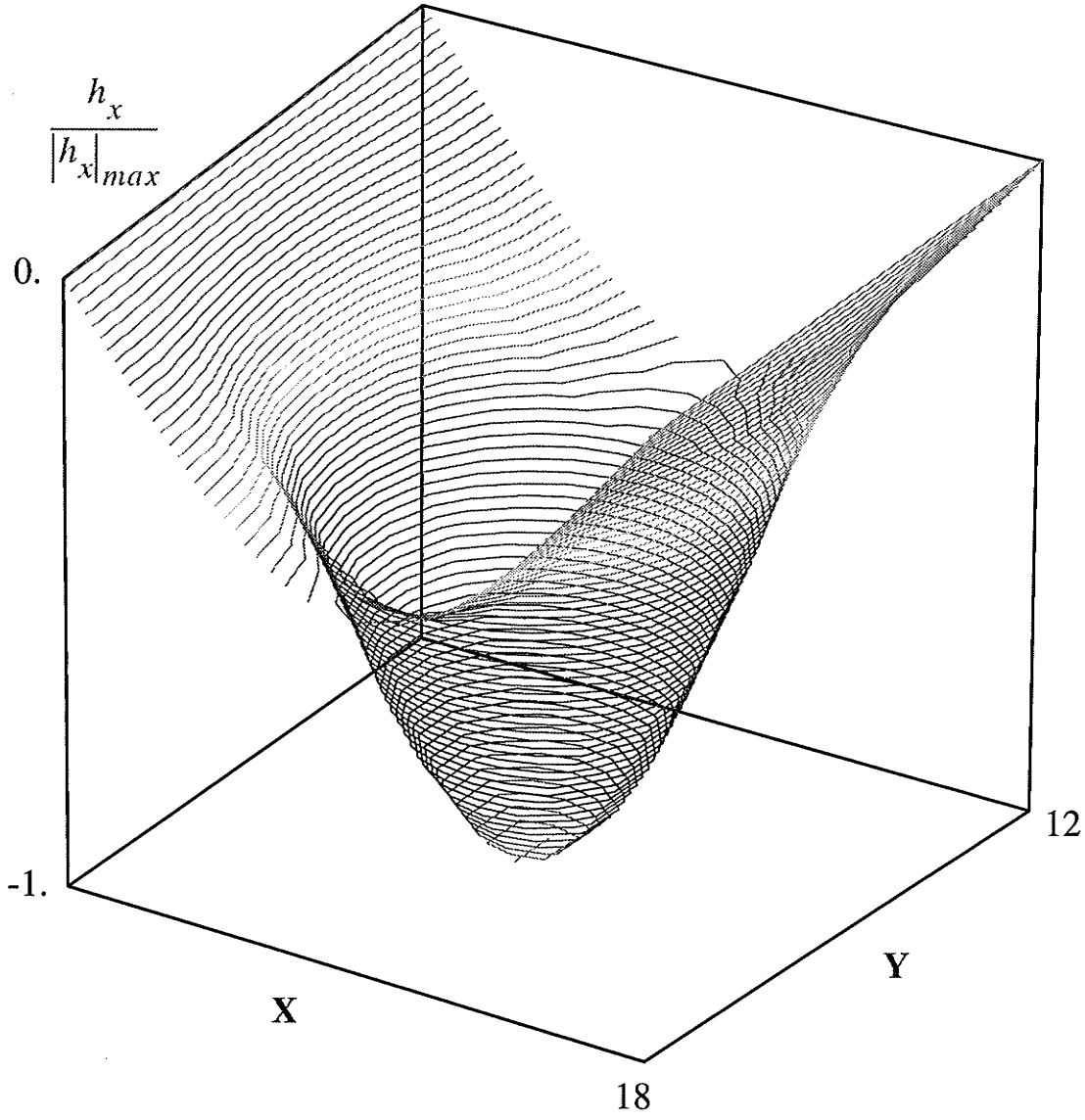

FIGURE IV.8.e **Normalized h_z field pattern of E^y_{11O} mode using FWFD.**

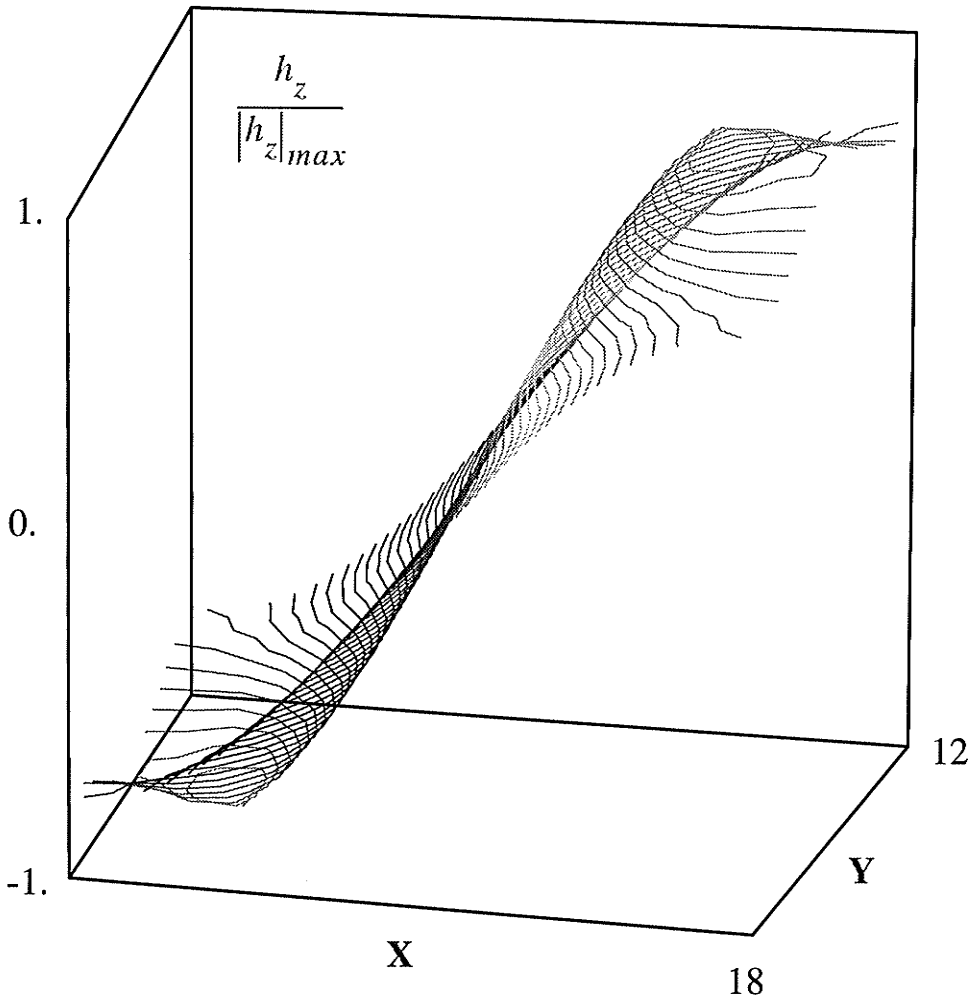

IV.F.3 Unilateral Fin-line [49]

As the next example, the study of field patterns inside a unilateral fin-line operating at cut-off frequency is selected. Fig. IV.9 depicts the fin-line structure under investigation.

FIGURE IV.9 ***TM mode in a Unilateral Fin-line***

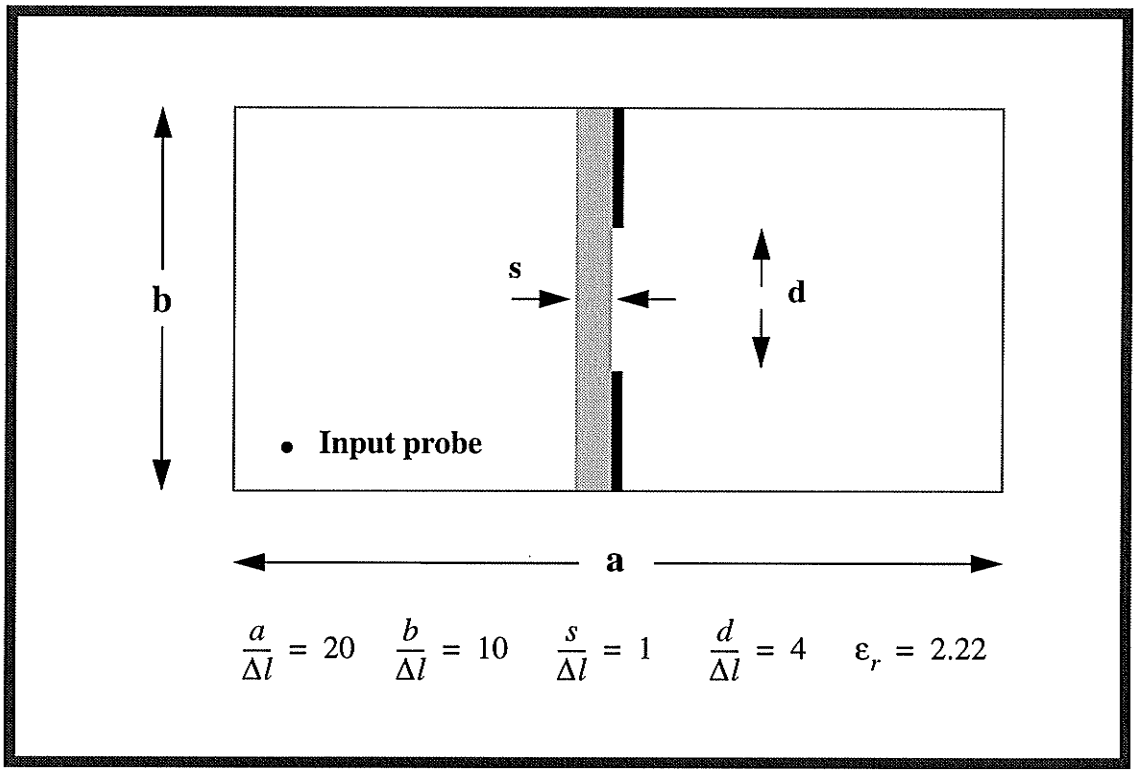

For the dominant **TM** mode of this fin-line with a mesh discretization of 20×10, a total number of 250 iterations is quite adequate to achieve an error less than 1% in convergence accuracy. In this case, the entire process takes about two seconds on a Sun-Sparc10/41 workstation. Corresponding field patterns for e_z, h_x and h_y components are illustrated in Figs. IV.10.a, IV.10.b and IV.10.c, respectively.

FIGURE IV.10.a **Normalized e_z field pattern of the dominant mode inside a unilateral fin-line.**

$$\frac{e_z}{|e_z|_{max}}$$

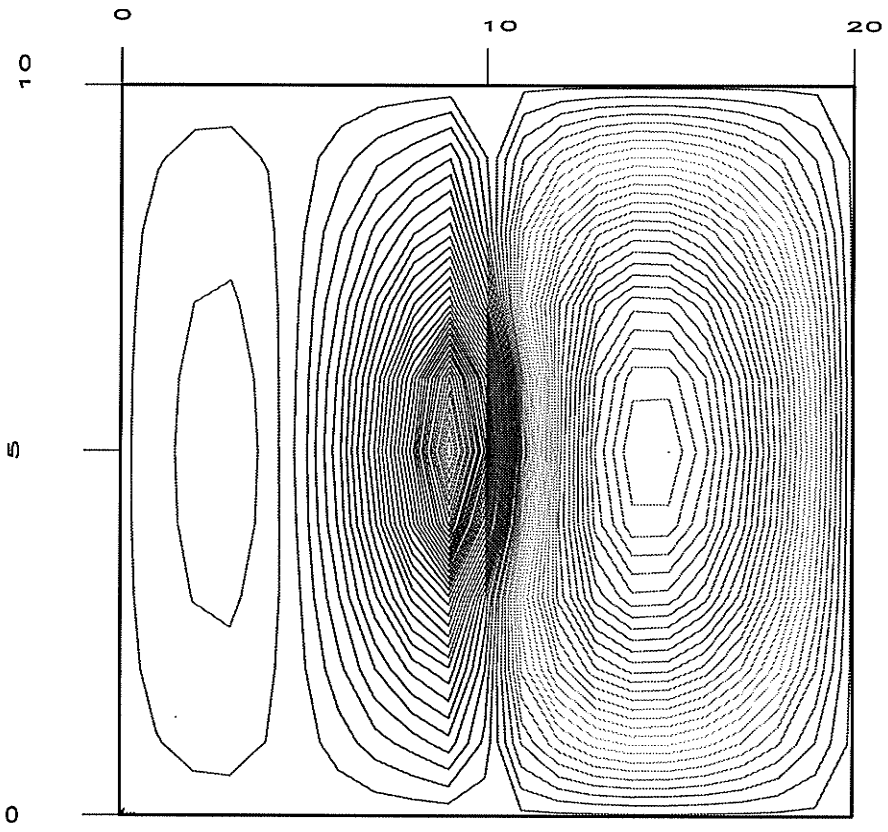

FIGURE IV.10.b **Normalized h_x field pattern of the dominant mode inside a unilateral fin-line.**

$$\frac{h_x}{|h_x|_{max}}$$

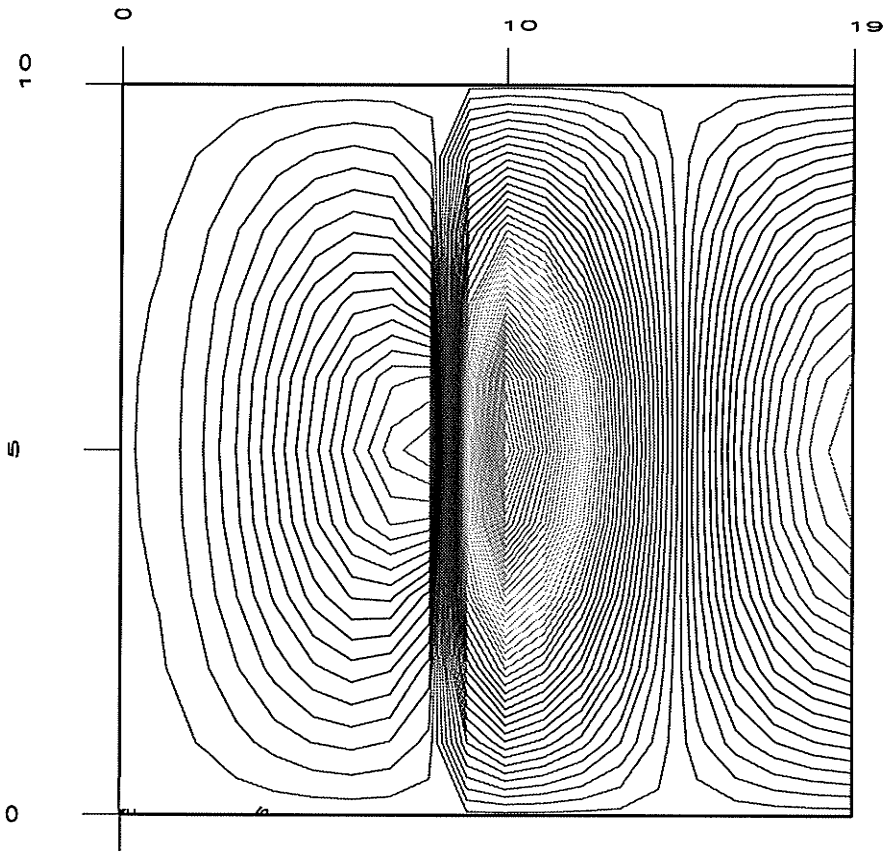

FIGURE IV.10.c Normalized h_y field pattern of the dominant mode inside a unilateral fin-line.

$$\frac{h_y}{|h_y|_{max}}$$

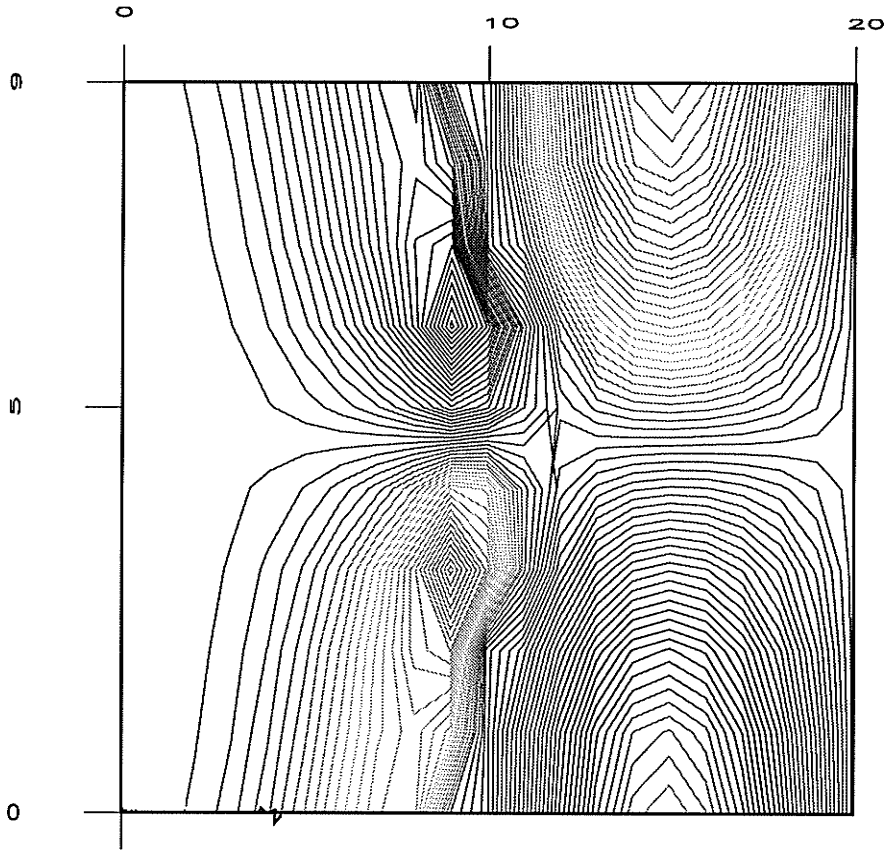

IV.F.4 Boxed Microstrip Line [50]

Finally, as the last example, the study of field patterns inside a boxed microstrip line operating at cut-off frequency is selected. Fig. IV.11 depicts the specifics of the structure under investigation. Also, the corresponding field pattern for the dominant **TM** mode at cut-off frequency is illustrated in Fig. IV.12.

FIGURE IV.11 Boxed microstrip line

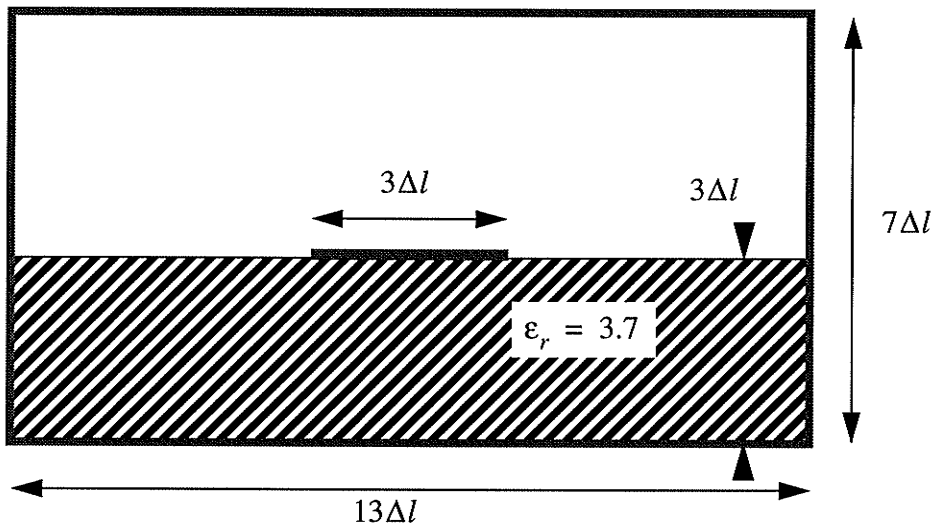

FIGURE IV.12 **Normalized h_y field pattern of the dominant mode inside a unilateral fin-line.**

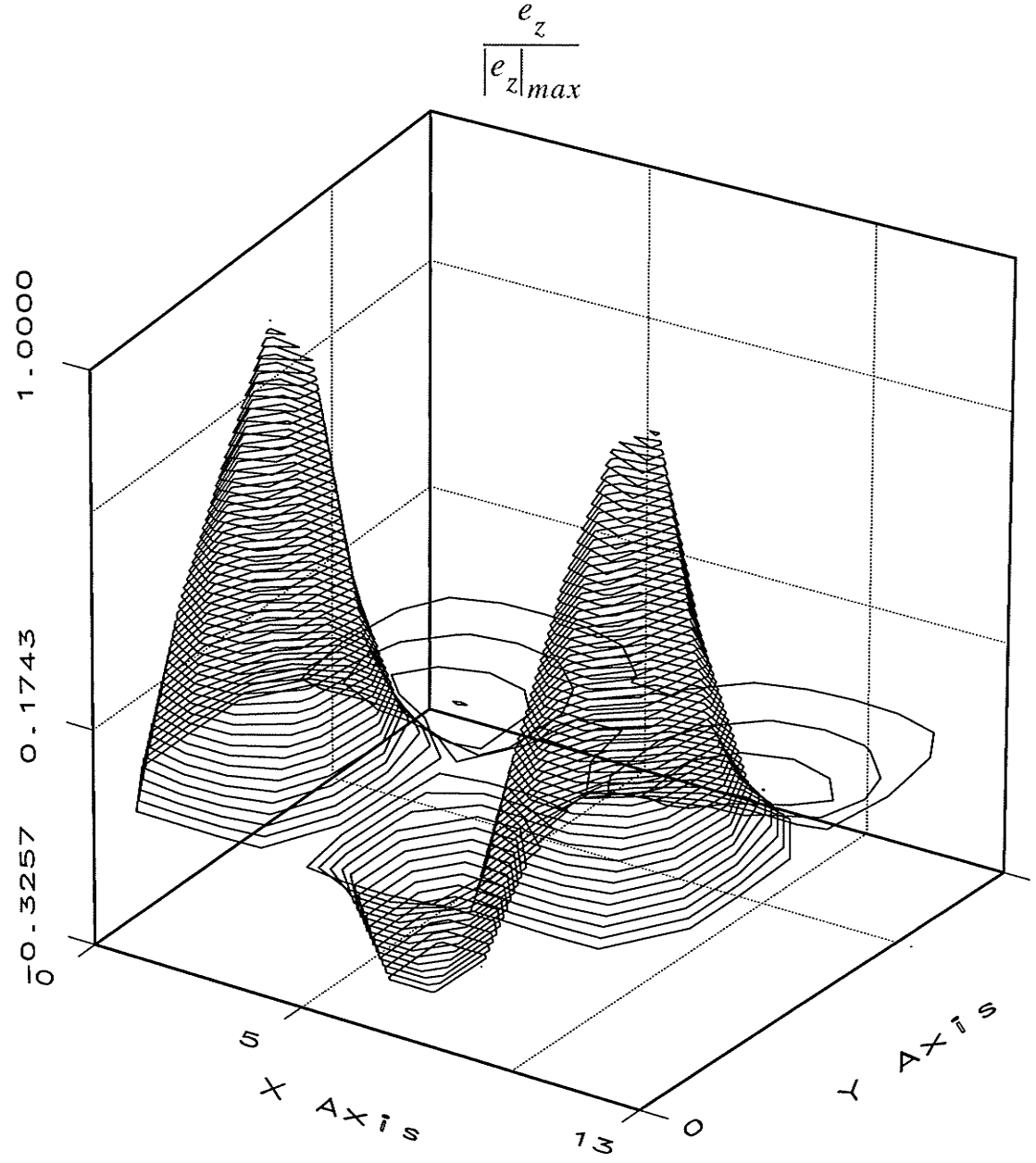

IV.G. Conclusion

A NOVEL FULL WAVE FINITE DIFFERENCE, FWFD, technique for calculating field patterns of guided wave structures is proposed. It is based on a four directional finite difference treatment of Maxwell equations. Classical finite difference methods are derived from the Helmholtz equation and therefore are restricted to dealing with just a single field component. Even though this is a desirable feature for calculating eigenvalues, it lacks the power to provide the field pattern information for all six vector field components. FWFD, on the other hand, has no such limitation and therefore is a powerful CAD tool for calculating field patterns efficiently and simultaneously.

Chapter Five

SPECTRAL ESTIMATION

V.A. Introduction

IN PREVIOUS CHAPTERS different time domain techniques were discussed. All these methods have a common requirement, they need to go the frequency domain in order to determine eigenvalues at the final stage of the analysis. For most applications, the impact of using an advanced spectral technique, alone, on saving **CPU** time can be as significant as using the Compact **FDTD** for the first part of the analysis. In fact, by using advanced spectral analysis techniques, one can use far fewer iterations in the time domain to extract information than is needed to achieve the same degree of accuracy using a less efficient spectral technique. Generally speaking, it is known that time domain simulation (**FD-TD**, **TLM**, **Bergeron**'s method) of Electromagnetic problems suffers from one major drawback, considerable **CPU** time. This means that for obtaining reliable information from the time domain simulation, the program must run for several thousand iterations. From a Signal Theory point of view, the simplest way to accomplish this task is the use of the **D**iscrete Fourier Transform (**DFT**). But, due to its slow performance, most problems are usually handled by a much faster technique, the **F**ast **F**ourier **T**ransform (**FFT**). The term **DFT** in the context of this thesis refers to taking the Fourier transform of discrete time samples, while frequency can still be assumed as a continuous variable. This definition is somewhat different from that found in standard literature in which this term implies discrete frequency domain as well.

This chapter begins with the basic spectral techniques and gradually proceeds to the most advanced available ones. Along this thread, a brief discussion of the **D**iscrete **F**ourier **T**ransform (**DFT**) and **F**ast **F**ourier **T**ransform (**FFT**) is presented in sections V.C. and

V.D., respectively. In fact, the very first concept of frequency domain had been originated from the Fourier transformation definition. Sections V.E. and V.F. will discuss **A**uto-**R**egressive (**AR**) and **Maximum Entropy Method** (**MEM**), respectively. Both these algorithms belong to the same family and are based on the same concepts. Finally, **Prony's** method is the subject of V.G.. **Prony-Hildebrand** accompanied with its modified version are presented in V.H. and V.I., respectively.

V.B. The best method and numerical noise

ONE MAY ASK: "What is the best available spectral technique?". Answering this question is not as easy as it may look. The reason is behind the empirical nature of the spectral analysis science. In fact, each of the spectral analysis techniques are based on a certain set of assumptions, either about the basic characteristics of the signal or the embedded noise. The problem becomes more critical when the signal under study contains some noise with unspecified statistical characteristics, which is usually the case. Ideally, one can give an accurate answer to the above mentioned question if and only if all the characteristics of the noise for a particular problem are a priori known. One may still argue about the source of noise in the current problem, dispersion analysis, truncation and round-off errors.

Here the problem is approached numerically; there is no background noise present in the output time domain data. But, on the other hand, due to the limitations of the digital computer and the algorithm, the data is contaminated with several numerical noises. The origin of the first noise is the round off error which is an inherent property of any digital computer calculations. Even though, the round off error has a deterministic nature, i.e. it

can be determined for any particular operation, it must be kept in mind that for just one single analysis, hundreds of thousands of mathematical operations may be required. One can easily see that for a problem of this extent, the round off error of the entire operation will exhibit a random behavior and so can be considered as a source of noise. The second source of noise is due to the approximations that have been made in the derivation of eqs. (III.22.a) to (III.22.f). It has already been stated that those equations are valid (in approximate sense) if and only if $\Delta l \to 0$ or when $\frac{\Delta l}{\lambda} \ll 1$. The exact amount of the error introduced by using a $\Delta l \neq 0$, in a single operation can be determined quite accurately. But, yet again, one is dealing with hundreds of thousands of operations of this kind and this can easily make the truncation error behave like a random variable.

In conclusion, to determine the superiority of a particular spectral analysis method for a specific problem, one has to experimentally apply each of these methods and then make the final judgement. The desirable qualities of a good technique can be summarized as follows:

- Stability
- Higher resolution
- Less **CPU** time
- Less required computer memory space
- Less complexity

V.C. Discrete Fourier Transform (DFT)[51]

DISCRETE FOURIER TRANSFORM is the first, most important and most inefficient method for transforming the time domain data to its frequency domain counterpart. Due to its simplicity, it was the method of choice for researchers utilizing time domain methods like **TLM**.

Suppose that x_n represents a time domain data sequence. Then, the **DFT** for such a discrete signal, $X\left(\frac{\Delta l}{\lambda}\right)$, is defined as:

$$X\left(\frac{\Delta l}{\lambda}\right) = \sum_{k=1}^{N} x_n \cdot e^{-j2\pi k\frac{\Delta l}{\lambda}} \qquad \textbf{(V.1)}$$

In some literatures, the **DFT** is defined by a plus sign in the exponent and its Inverse **DFT (IDFT)** by a minus sign in the exponent. The only important issue is to use different signs to define **DFT** and **IDFT**. Here, $\frac{\Delta l}{\lambda}$ is the normalized frequency. Equivalently:

$$X\left(\frac{\Delta l}{\lambda}\right) = \sum_{k=1}^{N} x_n \cdot \cos\left(2\pi k\frac{\Delta l}{\lambda}\right) \qquad \textbf{(V.2)}$$

$$X\left(\frac{\Delta l}{\lambda}\right) = -\sum_{k=1}^{N} x_n \cdot \sin\left(2\pi k\frac{\Delta l}{\lambda}\right) \qquad \textbf{(V.3)}$$

V.D. Fast Fourier Transform (FFT)[41][51]

AS IT HAS BEEN stated, **DFT** in its original form is a very straightforward but inefficient method. Fortunately, a careful inspection of eq. (V.1) depicts that for a complete calculation cycle, the exponent and its harmonics have to be calculated repeatedly. Inspired by this observation, a variety of different algorithms have been introduced to reduce the **CPU** time drastically. While there is evidence of contributions by many researchers to the development of **FFT**, a concise paper by Jim Cooley and John Tukey focused the attention of the digital processing community. The proposed algorithms can reduce the proportionality of the **CPU** time from N^2 to $N\log_2 N$.

V.D.1 Drawbacks of FFT

IN ACHIEVING the higher speed of the **FFT**, one usually has to compromise the resolution. This means that while there is no theoretical barrier for increasing the resolution in the **DFT**, it is positively restricted to a certain theoretical limit in the case of the **FFT**. This theoretical limit is always set by $\frac{1}{N\Delta}$, in which N is the number of time domain iterations or samples (which of course has to be zero-padded or truncated to an integer power of 2) and Δ is the sampling interval in the time simulation. The other problem of both the **DFT** and the **FFT** is the fact that they implicitly apply a window to the time domain data by taking the Fourier summation as Σ_0^N instead of Σ_0^∞ or equivalently multiplying the input sequence by a rectangular window. This in turn means that the actual frequency domain

spectrum is being convolved with $\frac{\sin(\pi f)}{\pi f}$. The impact of such an assumption on the frequency domain is twofold. First, it limits the resolution of Fourier transform operation to (at most) the bandwidth of the main lobe of $\frac{\sin(\pi f)}{\pi f}$ function. Second, it causes leakage of energy from one main lobe to another through the side lobes. The destructive effect of this can sometimes be so severe as to mask a main lobe by a side lobe of another neighboring lobe. Even though extensive studies[52] have been conducted to alleviate this problem by other windowing schemes, in general, either the bandwidth of the main lobe or the level of side lobes must be compromised in order to achieve better performance compared to a rectangular window.

V.E. Auto-Regressive method (AR)[53]

BASED UPON what has been cited in section V.D.1, the need for having a versatile extrapolating technique, to substitute **FFT**, which also is capable of extracting the desired information by a fraction of iterations, is inevitable. As has been mentioned in section V.B., the most important features of a successful extrapolating technique can be summarized in two aspects. First, from the speed point of view, it is desirable for the proposed method to possess a speed comparable to the **FFT**, or be at least much faster than the **DFT**. Second, from the resolution point of view, it must generate results more accurate than both the **DFT** or the **FFT** even with fewer time samples.

While no extrapolating technique can overtake the speed of the **FFT** method, there is a good chance that by applying a suitable method to a particular problem, results much

more accurate and with better resolutions than those achievable by the **DFT** and the **FFT** can be obtained. In what follows, first a quick survey of the **A**uto**R**egressive (**AR**) and **M**aximum **E**ntropy **M**ethod (**MEM**) is presented, then the applications of these methods particularly to Guided Wave Structures are indicated. Finally, a few numerical results are presented.

Among the vast class of extrapolating techniques, so far, only ***Prony***'s method has been widely used for time domain simulations. The implementation of this method dealing particularly with resonant structures has already been reported by Wills[54]. Thus, it is not the intention of this thesis to question the validity or suitability of the classical Prony's method, but rather to present alternative methods which are found to be very efficient for resonant structures. A comparative study between the presented methods and Prony's, including some modifications to enhance the Prony's performance is the subject of the ongoing research by the author.

V.E.1 Mathematical formulation[55]

CONTRARY TO Prony's method in which the major objective is extrapolating the time domain samples to intervals beyond the simulation period, in the **AR**, it is the discrete auto-correlation function of a signal that is subject of extrapolation. Mathematically, the problem can be phrased as follows:

> ***"Given the discrete auto-correlation function*** $R[n]$ ***of a process for*** $|n| \leq M$***, extrapolate the values of this function for*** $|n| > M$***."***

The importance of such an odd extrapolating technique lies in the fact that according to ***Wiener-Khinchin*** theorem, there is a direct Fourier transform relationship between the auto-correlation function of a signal and its power spectrum. Using this useful property, some fast algorithms can be developed. Hence, the significance of this kind of approach is mainly due to its numerical advantages. Considering the following relationships:

$$S(\omega) = \int_{-\infty}^{\infty} R_{xx}(\tau)\, e^{-j\omega\tau} d\tau \qquad \textbf{or} \qquad S(\omega) = \sum_{n=-\infty}^{\infty} R_{xx}[n]\, e^{-jn\Delta\omega} \qquad \textbf{(V.4)}$$

in which for the discrete case $R_{xx}[n]$ can be replaced by its biased estimate[56], $\hat{R}_{xx}[n]$:

$$\hat{R}_{xx}[n] = \frac{1}{N} \sum_{m=1}^{N-n} x_{n+m} x^*_m \qquad \textbf{(V.5)}$$

FIGURE V.1 Wiener-Khinchin Theorem

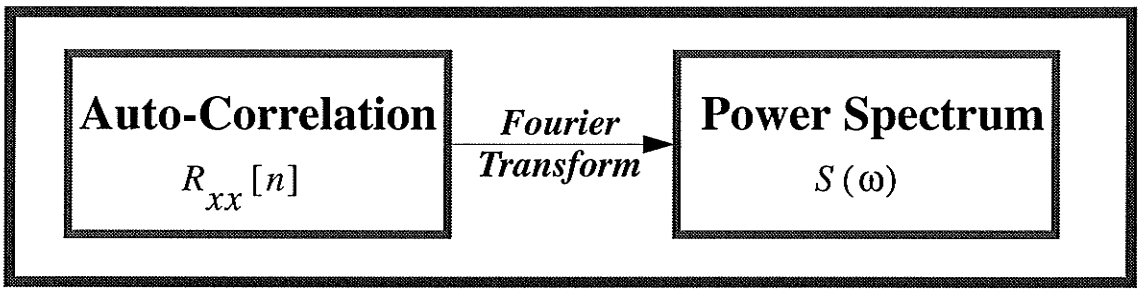

Now, let's assume that the power spectrum of a signal can be regarded as a rational function with a constant numerator, i.e. a function with several poles and no zeros, such as:

$$\hat{S}(\omega) \approx \frac{b_0}{\left|1 + \sum_{k=1}^{M} b_k z^k\right|^2} \approx \sum_{j=-M}^{M} \hat{R}_{xx}[j]\, z^j \qquad z = e^{-j\omega\Delta} \qquad \textbf{(V.6)}$$

There are at least three justifications for such an assumption[56]:

- *In the* ***FDTD*** *analysis of guided wave structures, the frequency spectrum consists of several sharp peaks which respectively correspond to different modes. Therefore, a rational function with several poles appears to be a good representation of these peaks.*

- *According to Information theory, it can be readily proved that this form of extrapolation will maximize the entropy which in turn can secure the fact that the unknown parameters will have the maximum degree of freedom to fit into the data.*

- *According to* **Wold decomposition** *theorem, any stationary* **ARMA** *(***A**uto**R**egressive **M**oving **A**verage*) or* **MA** *(***M**oving **A**verage*) process of finite variance can be represented as a unique AR model of possibly infinite order.*

At this stage, the only task left to accomplish the extrapolation procedure is having an efficient algorithm for calculating the unknown coefficients b_k [47]of $\hat{S}(\omega)$ in terms of the estimated values of the discrete auto-correlation function $\hat{R}_{xx}[n]$. If one expands the left hand side of eq. (V.4) using Laurent series, one can obtain a non-linear system of equations relating b_k 's to $\hat{R}_{xx}(j)$'s. Straightforward but practically useless!!!!

Fortunately, techniques exist that can handle the problem without resorting to non-linear equations. Here, the final result of such an algorithm known as the ***Yule-Walker*** equation is presented. It is given by:

$$\begin{bmatrix} \hat{R}_{xx}[0] & \hat{R}_{xx}[1] & \hat{R}_{xx}[2] & \dots & \hat{R}_{xx}[M] \\ \hat{R}_{xx}[1] & \hat{R}_{xx}[0] & \hat{R}_{xx}[1] & \dots & \hat{R}_{xx}[M-1] \\ \hat{R}_{xx}[2] & \hat{R}_{xx}[1] & \hat{R}_{xx}[0] & \dots & \hat{R}_{xx}[M-2] \\ \dots & \dots & \dots & \dots & \dots \\ \hat{R}_{xx}[M] & \hat{R}_{xx}[M-1] & \hat{R}_{xx}[M-2] & \dots & \hat{R}_{xx}[0] \end{bmatrix} \cdot \begin{bmatrix} b_1 \\ b_2 \\ b_3 \\ \dots \\ b_M \end{bmatrix} = - \begin{bmatrix} \hat{R}_{xx}[1] \\ \hat{R}_{xx}[2] \\ \hat{R}_{xx}[3] \\ \dots \\ \hat{R}_{xx}[M] \end{bmatrix} \qquad \textbf{(V.7)}$$

As is clear, the resultant matrix is a ***Toeplitz symmetric[41]*** one for which a very efficient inverting algorithm is available. One is reported by ***Levinson-Durbin[57]*** which also employs a recursive scheme for calculating the coefficients.

Finally, after solving the above matrix equation, one may continue with an extrapolation of the power spectrum. From here on, two different strategies can be chosen for finding the eigenvalue (resonant frequency) of the structure. The first strategy is to find the roots of the denominator directly by any numerical method. The other strategy is to find locations of peaks of the extrapolated power spectrum function in a particular frequency range of interest. I have found the former strategy to be much easier and trouble free, not withstanding the fact that finding the roots of a polynomial is always considered an ill-conditioned problem; i.e., small deviation (error) in the coefficients of the polynomial can result in extreme changes in the roots.

V.E.2 Applications[53]

Since this part of the thesis is mainly aimed at signal processing part of the time domain analysis, only a simple example, a rectangular hollow waveguide, for which the analytical solution is readily available is presented. For a more sophisticated example, a boxed anisotropic microstrip line, for which this method can equally be applied, one may consult section III.E.2 or [58]. Fig. V.2 depicts the structure under study. Fig. V.3, also illustrates the final results obtained by **AR**.

FIGURE V.2 (a) The structure under study, (b) The frequency spectrum of input signal

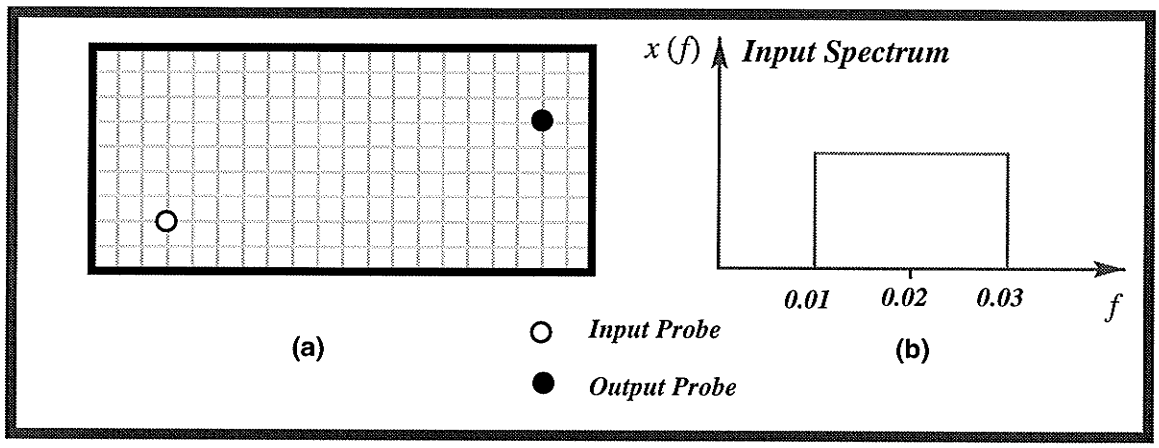

As is implied by Fig. V.2.b, a modulated $\frac{\sin x}{x}$ is used for the purpose of exciting the **FDTD** meshes. By a simple calculation, one can show that the first mode in this structure, the TE_{10} mode, will be located at $\frac{\Delta l}{\lambda} = 0.025$. For convenience, the curve is normalized to unity.

FIGURE V.3 Result generated by AR

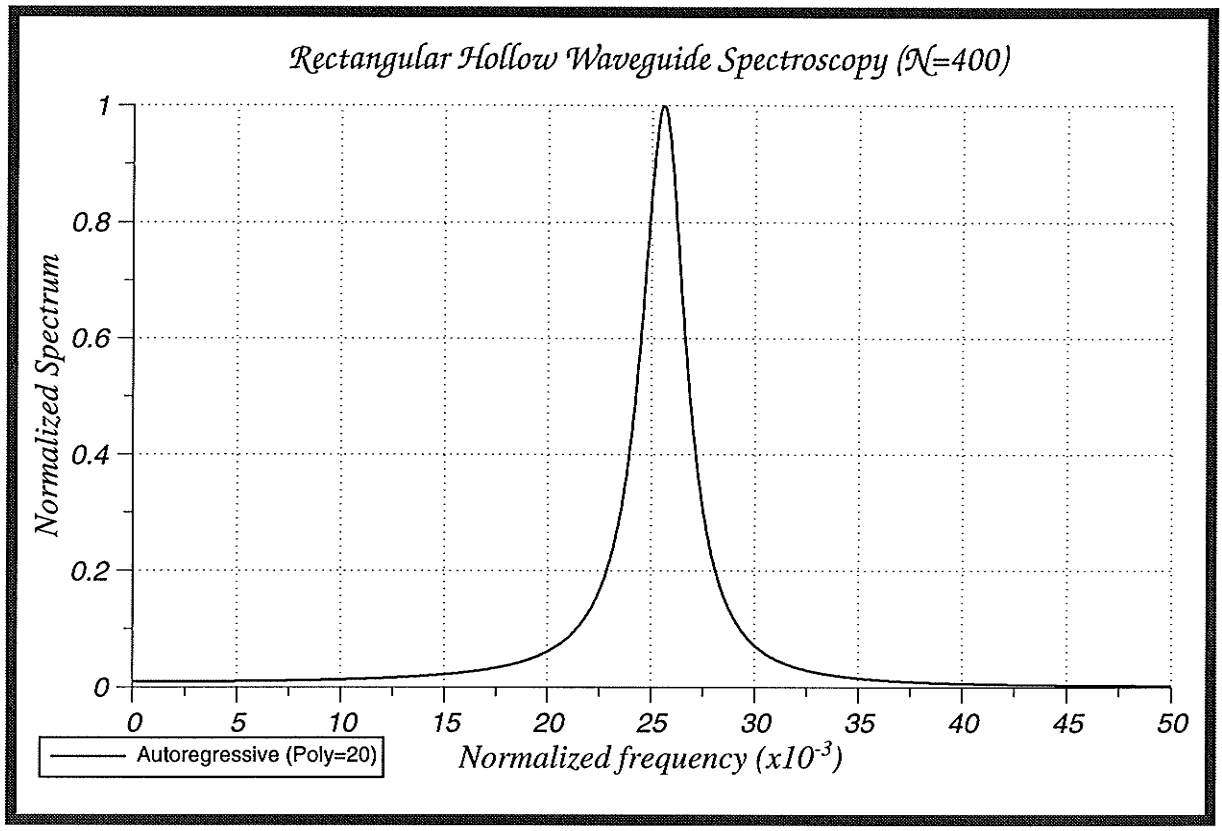

V.F. Maximum Entropy Method (MEM)[59]

DESPITE THE effectiveness and higher efficiency of the **AR** model, it still suffers from the lack of high resolution required for a successful method. The major cause of this problem stems from the fact that for most practical situations, it is the time samples that are directly available not the auto-correlation coefficients. Although eq. (V.5) seems to be a straightforward way of calculating these coefficients, this equation is obtained by assuming the ergodicity of the samples. This property permits the substitution of time averages for ensemble averages. Unfortunately, this is not always the case, especially when it comes to short data records. Hence the only way left for calculating the auto-correlation coefficients is through

statistical methods. A better solution to this problem can be found by reformulating the entire problem again in terms of the time samples themselves, not the auto-correlations. This had been done by Burg in an algorithm called after his name, **Burg**'s algorithm or **MEM**. Due to the lack of space, the mathematical details of this algorithm can not be explained here. The interested reader is referred to the literature. It is adequate to say that the essence of this algorithm is based upon a least square formulation of time samples, both known as well as those to be determined using forward and backward linear prediction theory.

One of the major weaknesses of the classic **MEM**, as presented by Burg, is its instability when detecting several peaks, i.e. biases in the frequency estimate. Another problem arises when the implementation of the method requires polynomials of higher degrees. In such a case, instead of a sharp clear peak, one obtains a peak surrounded by a set of several other peaks, i.e. spectral line splitting. This effect is particularly evident if the original data contains noise. In the present case, the origin of this noise can be attributed to the inherent round-off error of the finite difference method.

All these problems can be alleviated using a more advanced technique called **M**odified **C**ovariance **M**ethod[60]. It is believed that this algorithm can be used as a very attractive, fast as well as accurate and spurious peak free, tool in **CAD** packages.

V.F.1. Applications[53]

FIG. V.4 illustrates the results obtained respectively by the **FFT**, **DFT** and finally the classical **MEM** or **Burg**'s algorithm. For convenience, again, all the data have been normalized to unity, but it must be appreciated that neither the amplitudes nor the dimensions of the graphs are identical. To be more specific, the **DFT** and **FFT** results correspond to the frequency spectrum of the output probe signal and the **MEM** may correspond to its power spectrum.

FIGURE V.4 Results generated by FFT, DFT and classical MEM

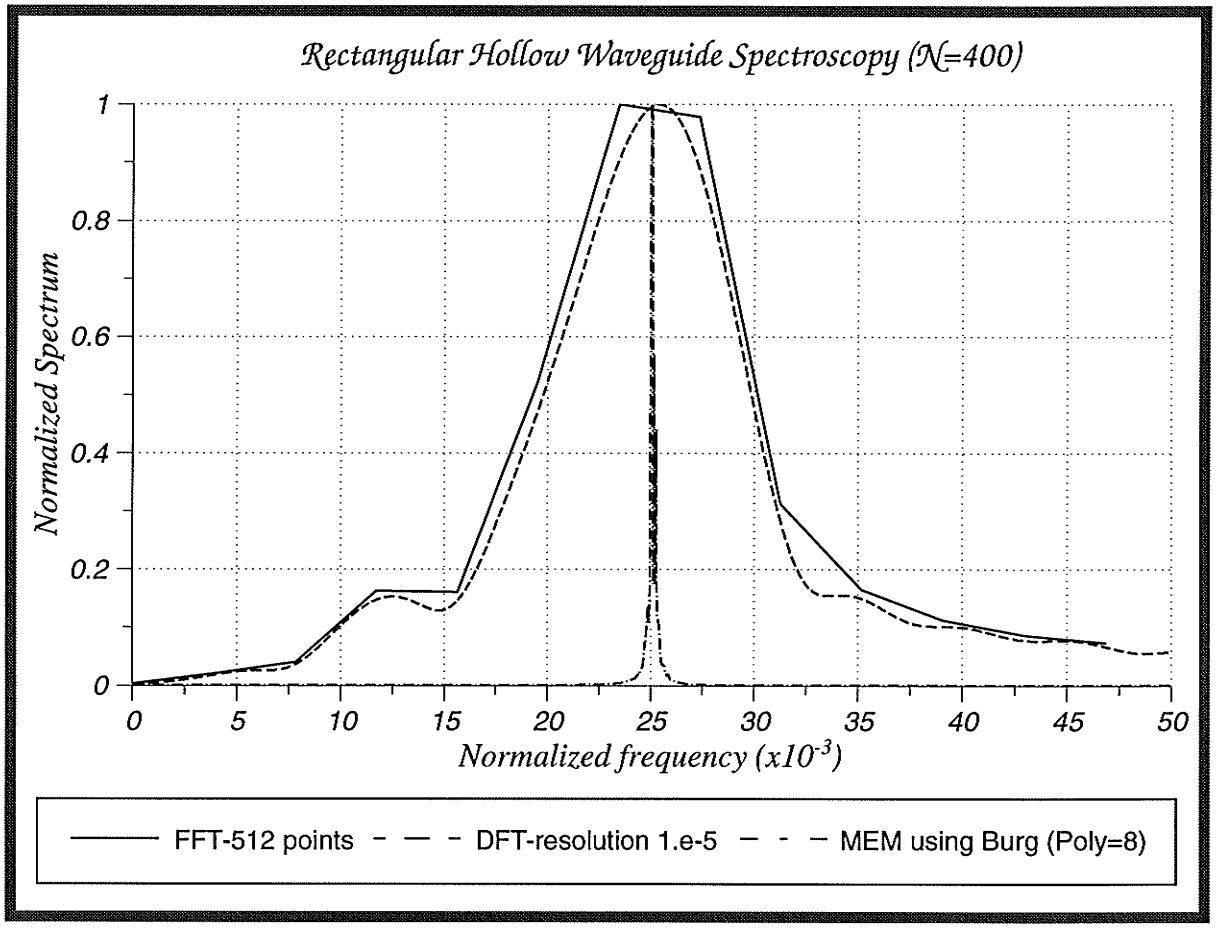

V.G. Prony's method[61]

PRONY'S METHOD and FFT are in essence similar methods; both are based on approximating the signal in terms of a polynomial of finite number of exponential functions.

$$f(x) = C_1 e^{\alpha_1 x} + C_2 e^{\alpha_2 x} + C_3 e^{\alpha_3 x} + \ldots + C_n e^{\alpha_n x} \qquad \textbf{(V.8)}$$

The only difference between these two methods is in the fact that in **FFT**, all the frequencies α_1, α_2, α_3,... are integer harmonics of a basic frequency α_1. But, in Prony's approach, all these frequencies can be chosen quite arbitrarily. And, this property makes it more suitable for approximating a general signal. In turn, one can not expect the same speed as the **FFT**.

Eq. (V.8) can be rephrased as:

$$f(x) = C_1 \mu_1^x + C_2 \mu_2^x + C_3 \mu_3^x + \ldots + C_n \mu_n^x \qquad ; \qquad \mu_k = e^{\alpha_k} \qquad \textbf{(V.9)}$$

in which, C_i's and α_i's are the unknown parameters that have to be calculated. In fact, for the specific problem in hand, only the calculation of α_i's (the resonant frequencies) is adequate. For a complete model, one needs to determine all unknown parameters.

Now, suppose that NI (**N**umber of **I**nput) discrete samples of the signal, f_0, f_1, f_2,...,f_{NI} are available, the output of the time domain **CFDTD** simulation. And also, let's assume that all these samples have been taken at equally spaced intervals of time.

$$\begin{cases} C_1 + C_2 + C_3 + \ldots + C_n = f_0 \\ C_1\mu_1 + C_2\mu_2 + C_3\mu_3 + \ldots + C_n\mu_n = f_1 \\ C_1\mu_1^2 + C_2\mu_2^2 + C_3\mu_3^2 + \ldots + C_n\mu_n^2 = f_2 \\ \qquad\qquad \vdots \\ C_1\mu_1^{NI-1} + C_2\mu_2^{NI-1} + C_3\mu_3^{NI-1} + \ldots + C_n\mu_n^{NI-1} = f_{NI-1} \end{cases} \quad \textbf{(V.10)}$$

If the values of the μ_is are known in advance, the above system of eqs (V.10) would be linear one, otherwise it is a nonlinear system of equations!!!

Baron de Prony found an ingenious method for solving this class of problems in 1795. His method is presented in this section. Let's suppose that μ's be the roots of the following algebraic equation:

$$\mu^n + a_1\mu^{n-1} + a_2\mu^{n-2} + \ldots + a_{n-1}\mu + a_n = 0 \quad \textbf{(V.11)}$$

Now, if the first equation of the system of eqs. (V.10) is multiplied by a_n, the second one by a_{n-1}, and so on..., and then be added up all together, one will come up with:

$$f_n + a_1 f_{n-1} + a_2 f_{n-2} + \ldots + a_n f_0 = 0 \quad \textbf{(V.12)}$$

Repeating the same procedure but starting from a different point, the following system of equations can be generated:

$$\begin{cases} f_n + a_1 f_{n-1} + a_2 f_{n-2} + \ldots + a_n f_0 = 0 \\ f_{n+1} + a_1 f_n + a_2 f_{n-1} + \ldots + a_n f_1 = 0 \\ f_{n+2} + a_1 f_{n+1} + a_2 f_n + \ldots + a_n f_2 = 0 \\ \vdots \\ f_{NI-1} + a_1 f_{NI-2} + a_2 f_{NI-3} + \ldots + a_n f_{NI-n-1} = 0 \end{cases} \quad \textbf{(V.13)}$$

The resultant matrix also enjoys nice symmetrical Toeplitz property which has a noticeable effect on reducing CPU elapsed time and required computer memory space. This can be solved exactly if $NI = 2n$, or approximately (in the least square sense) if $NI \neq 2n$. After calculating all a_i's from eq. (V.13), one can proceed to eq. (V.11) to evaluate μ_i's. At this stage, our problem is completely solved. But, if one may wish, he can proceed to solve eq. (V.10) for all the values of C_i's and hence completing the model.

V.H. Prony-Hildebrand approach[62]

IF THE STUDY of an unattenuated periodic signal is what is desired (like the case of this study), then there is a more efficient approach to solve the problem. First, suppose that the signal can be described (approximated) by the following equation (NF stands for the **N**umber of constituting **F**requencies):

$$f(x) = \sum_{i=1}^{NF} (A_i \cos \omega_i x + B_i \sin \omega_i x) \quad \textbf{(V.14)}$$

One can easily realize that **P**rony-**H**ildebrand is just the same as classical Prony's method with one major distinction that here, all the values of α_i's are pure imaginary and also they appear in conjugate pairs. Since, in this case, all the roots of eq. (V.11) are required to occur in the form of $\left(e^{j\omega_k}, e^{-j\omega_k} \right)$, it follows that eq. (V.11) must be invariant under the substitution of $\frac{1}{\mu}$ for μ, so that we must have $\alpha_{2NF} = 1$, $\alpha_{2NF-1} = a_1$,..., $a_{NF+1} = a_{NF-1}$. Thus, with $\mu = e^{j\omega}$, eq. (V.11) becomes:

$$e^{j2NF\omega} + a_1 e^{j(2NF-1)\omega} + \ldots + a_{NF-1} e^{j(NF+1)\omega} + a_{NF} e^{jNF\omega} + a_{NF-1} e^{j(NF-1)\omega} + \ldots + a_1 e^{j\omega} + 1 = 0 \quad \textbf{(V.15)}$$

or equivalently:

$$e^{jNF\omega}\left[\left(e^{jNF\omega} + e^{-jNF\omega} \right) + a_1\left(e^{j(NF-1)\omega} + e^{-j(NF-1)\omega} \right) + \ldots + a_{NF-1}\left(e^{j\omega} + e^{-j\omega} \right)\right] = 0 \quad \textbf{(V.16)}$$

and finally:

$$2\cos(NF\omega) + 2a_1 \cos[(NF-1)\omega] + \ldots + 2a_{NF-1}\cos\omega + a_{NF} = 0 \quad \textbf{(V.17)}$$

Since $\cos(k\omega)$ can be expressed in terms of a **Chebychev** polynomial, the final equation can be rewritten in terms of a transcendental equation of the following form:

$$T_{NF}(\cos\omega) + a_1 T_{NF-1}(\cos\omega) + \ldots + a_{NF-1} T_1(\cos\omega) + \frac{1}{2} a_{NF} = 0 \quad \textbf{(V.18)}$$

in which the coefficients of this equation, a_i, can be calculated from:

$$
\begin{cases}
f_0 + f_{2NF} + (f_1 + f_{2NF-1})\, a_1 + (f_2 + f_{2NF-2})\, a_2 + \ldots + (f_{NF-1} + f_{NF+1})\, a_{NF-1} \\
\qquad\qquad + f_{NF} a_{NF} = 0 \\
f_1 + f_{2NF+1} + (f_2 + f_{2NF})\, a_1 + (f_3 + f_{2NF-1})\, a_2 + \ldots + (f_{NF} + f_{NF+2})\, a_{NF-1} \\
\qquad\qquad + f_{NF} a_{NF} = 0 \\
\vdots \\
f_{NI-2NF-1} + f_{NI-1} + (f_{NI-2NF} + f_{NI-2})\, a_1 + (f_{NI-2NF+1} + f_{NI-3})\, a_2 + \ldots \\
\qquad + (f_{NI-NF-2} + f_{NI-NF})\, a_{NF-1} + f_{NI-NF-1} a_{NF} = 0
\end{cases}
\tag{V.19}
$$

In accordance with the fact that the approximation of eq. (V.14) contains $3NF$ unknowns, NF of A_is, NF of B_is and finally NF of ω_is; one must have at least $NI \geq 3NF$ in order to be able to solve the problem exactly or approximately (in the least square sense). This is exactly the same number of equations required for solving the system of eqs. (V.19). Because the above system of equations contains $NI - 2NF$ equations and NF unknowns, so we must have $NI - 2NF \geq NF$ or equivalently $NI \geq 3NF$.

After solving the system of eqs. (V.19), one can insert the calculated values of a_i's in eq. (V.18) to solve for the unknown frequencies. Once again, the current problem is solved at this stage, but if one is interested, he can easily solve for the other unknown parameters of the model A_i's and B_i's, as explained in section V.G.

V.I. SVD based Prony-Hildebrand's method [63]

ACCORDING TO what have been explained in section V.H., in a noise free simulation, exactly $3NF$ number of equally spaced samples of a signal suffices to determine the constituting frequencies of that signal. But, of course, in most practical situations (like the present problem), this is not the case and the data is contaminated with noise in one way or another. Under these circumstances, it is not wise to consent just to the $3NF$ number of data samples. In fact, if a stable and accurate result is desired, it is much better to use as many data samples as are available in calculating the model parameters.

Strictly speaking, for solving a general problem, one has to generate the system of equations of (V.19) using all available data, and proceed to solve the resultant system of equations in the least square sense. My proposed method to accomplish this task is **S**ingular **V**alue **D**ecomposition (**SVD**).

Still, there is another major advantage in using **SVD** (which is in fact one of the other contributions that have been made in this thesis). And that is the ability to exactly determine the number of required frequencies for a model. One has to keep in mind, that for many practical applications, the number of model frequencies (NF), is not initially known. In the proposed method, one can run **SVD** on the non-square matrix of the system of eqs. (V.19), and thereafter find the singular values of the matrix. The number of model frequencies is exactly equal to the number of non-zero singular values. This finding is very crucial in the applicability of Prony-Hildebrand's method.

V.I.1 Application

To prove the validity of the method and its advantages to classical Prony-Hildebrand method, a signal consisting of two neighboring frequencies is considered:

$$f(t) = \cos\left[\left(\frac{2\pi}{3}\right)t\right] + \sin\left[\left(\frac{2\pi}{3.1}\right)t\right] \qquad \textbf{(V.20)}$$

As is pointed out on page 174, even sophisticated techniques such as Burg's have difficulties in distinguishing between two closely located frequencies. Let's see how the classical Prony-Hildebrand and the proposed technique handle this problem.

To run any version of Prony's method, one has to decide on the number of frequencies that the method has to look for, i.e. the number of frequencies in eqs. (V.8) or (V.14). Unfortunately, for many practical situations, this information may not be a priori known. Therefore, using conventional Prony's method, it seems that guessing the number of involved frequencies would be the only solution. Let's try this concept on the signal expressed by eq. (V.20), which has been sampled only slightly above the Nyquist level at intervals of $\Delta t = 1$. Also, let's assume that one hundred of these time samples are available.

Table V.1 illustrates the calculated frequencies by Prony-Hildebrand technique using different number of terms as the initial guess. As can be seen, for methods of orders higher than two, the correct frequencies are always detected. But, the problem still remains: How to distinguish the actual frequencies from the spurious ones?

TABLE V.1 **Detecting frequencies of $f(t) = \cos\left[\left(\frac{2\pi}{3}\right)t\right] + \sin\left[\left(\frac{2\pi}{3.1}\right)t\right]$ by Prony-Hildebrand**

Prony-Hildebrand Technique								
Order of the method	**First**	**Second**	**Third**	**Fourth**	**Fifth**	**Sixth**	**Seventh**	**Eighth**
$i = 1$	3.0499							
$i = 2$	**2.9999**	**3.1007**						
$i = 3$	**3.0000**	**3.0995**	9.2787					
$i = 4$	**2.9992**	**3.1007**	3.3794	14.005				
$i = 5$	2.3183	**2.9993**	**3.1000**	6.1279	19.712			
$i = 6$	2.2076	**3.0005**	**3.0995**	4.5789	7.9598	22.032		
$i = 7$	2.1774	**2.9999**	**3.1001**	3.2387	5.2855	8.8741	27.000	
$i = 8$	2.1371	2.5339	**2.9999**	**3.1002**	4.4075	6.2826	10.346	32.136
The desired periods are 3.0000 and 3.1000								

Now, let's see how the proposed SVD-based Prony-Hildebrand technique solves this problem. At the first run, the matrix of coefficients is generated, i.e. eq. (V.19). Then, the method proceeds to SVD decompose the resultant matrix. Again, for the first trial, an initial guess for the order of the method, large enough to cover all possible number of frequencies, is selected. Assuming $i = 8$, the following singular values are calculated.

TABLE V.2 **Singular value decomposition of the matrix represented by eq. (V.19) for $f(t) = \cos\left[\left(\frac{2\pi}{3}\right)t\right] + \sin\left[\left(\frac{2\pi}{3.1}\right)t\right]$**

Singular Value Decomposition								
Order of the method	**First**	**Second**	**Third**	**Fourth**	**Fifth**	**Sixth**	**Seventh**	**Eighth**
Singular Values	33.553	5.3551	0	0	0	0	0	0
Any singular value less than 1.e-4 is set to zero								

After performing this analysis, it is clear that only two non-zero singular values exist, table V.2. This shows that only two of the equations in the entire system of equations are linearly independent. The subsequent conclusion that can be drawn from this observation is that only two frequencies have been involved in generating the original signal.

Executing the program for a second time and assuming $i = 2$ as the order of the method, the following periods are calculated: $T_1 = 2.99999$ and $T_2 = 3.10066$. The above mentioned example proves that the proposed algorithm is not only capable of calculating the frequencies, but also picking out the right solutions from the spurious ones.

V.J. Conclusion

IN PART ONE, several techniques for analyzing the problem in the time domain have been explained. On the other hand, the raw time domain response, by itself, is not useful and usually requires another processing stage to convert it to frequency domain information. The easiest means for performing this transformation are using basic **DFT** or an advanced version of it, **FFT**. But, these are not the only possible choices. As a matter of fact, one can find a variety of techniques in digital signal processing literatures that can accomplish this task much better than **DFT** and, in some aspects, even better than **FFT**. Among these are, **AR**, **MEM**, **Prony**'s and **Prony-Hildebrand** methods, to name a few.

For the first time, the **A**uto-**R**egressive and **M**aximum **E**ntropy **M**ethods were successfully implemented for determining the cutoff frequencies of guided wave structures. While the **AR** method always provides stable results, it cannot be used in those occasions where higher resolution is the prime concern. On the other hand, **MEM** is capable of providing results with very high resolutions. The **Burg** algorithm has several problems associated with it, including spectral line splitting and biases in the frequency estimate. Both these problems can be alleviated using a more sophisticated algorithm, **Modified Covariance Method**. Still, even **AR** and **MEM** in their present forms can be used very successfully for narrow band, single mode, analysis.

Using the least square concept, a modified version of Prony-Hildebrand method has been proposed. It is believed that this new technique, **SVD-based Prony-Hildebrand**, can enhance the performance and applicability of the older version noticeably.

Chapter Six

CONCLUSIONS AND FUTURE WORKS

VI.A. Conclusions

Throughout this thesis, two novel finite difference scheme were presented. Together, they can be integrated into a very efficient CAD package for calculating the dispersion curves and field patterns of arbitrary guided wave structures.

Advantages of **Compact FDTD** compared to other methods, i.e. classical **FD**, **FDTD** and **TLM** can be summarized as follows:

- *Rendering a traditionally 3D problem to a 2D space and thereafter obtaining the entire dispersion curve, not just cut off frequencies.*
- *Compared to the 3D-TLM or 3D-FDTD, the relative efficiency of the proposed technique, the CFDTD, is estimated to be somewhere between 10 to 100 times, depending on the method and the objectives of the analysis.*
- *Elimination of the troublesome and rather time consuming direct eigenvalue and eigenvector extraction from excessively large matrices.*
- *The method provides an important physical insight to the real situation. For instance, the locations of the input and output probes have exactly the same effect as in the experimental situations.*
- *Usually information along a constant* β *axis is needed more than along a constant* k *axis. Just consider the cutoff spectrum is a special case of* $\beta = 0$.

- *All the intermediate results are quite informative. For instance one can even plot the actual field distribution of either six field components or study the evolution of a transient response.*

- *In the case of a Microwave waveguide, characteristic impedance can be easily calculated from the same analysis.*

- *Because of the implementation of all six Maxwellian equations at the same time, this method is free of spurious modes.*

- *In the case of the **3D-FDTD** or **3D-TLM** using **PECs** at the two ends of the waveguide along the z direction, all the harmonics of the main β in equation (III.7) will appear at the final spectrum which results in modes being mixed with each other, while this is not the case for the Compact **FDTD**.*

Some **disadvantages** of classical **FD** approach can be summarized as follows:

- *Normally, even for a moderately accurate study one has to consider at least a 50×100 point structure which in turn renders the problem to finding the eigenvalues of a 5000×5000 square matrix!!!!*

- *Spurious modes*

- *In lots of practical applications, finding the cut-off frequencies of a particular waveguide is of major concern. Using this method, the problem has to be completely solved to obtain this information.*

- *None of the intermediate information is useful.*

- *The operation cannot be terminated at any point for a less accurate estimate of the desired quantity.*

As it was shown, all these drawbacks can be effectively eliminated using a completely different approach, the Compact **FDTD**.

FIGURE VI.1 The procedure that generates a complete dispersion curve using classical FD method

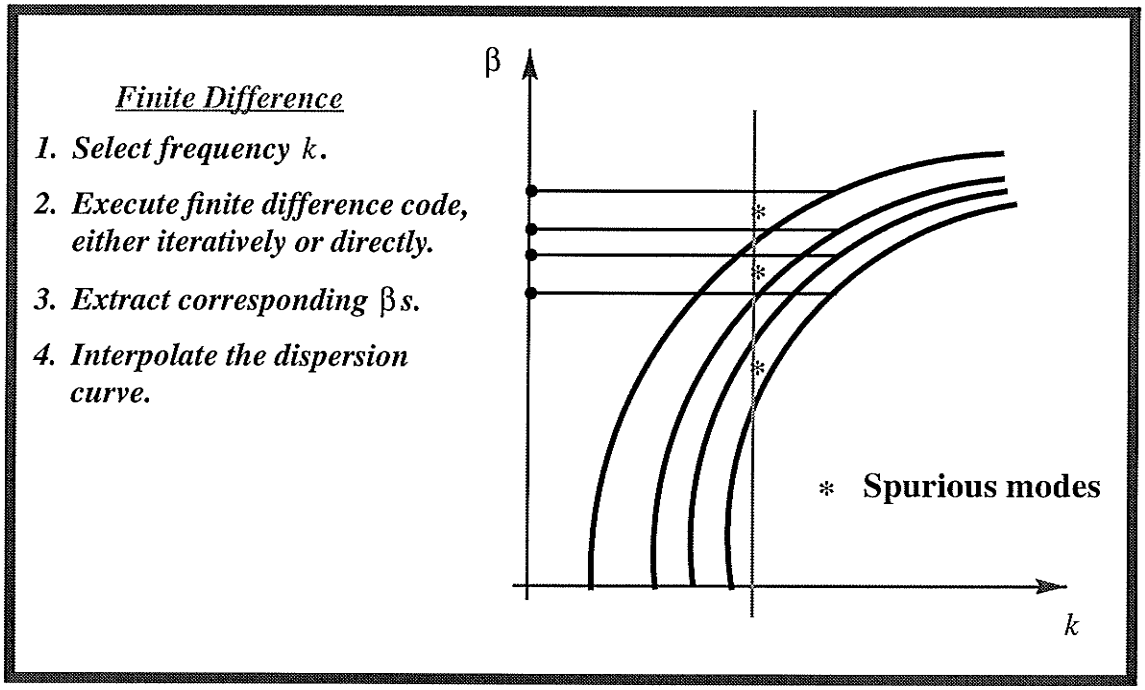

At the next stage, a novel frequency domain finite difference technique was introduced. This method, i.e. the FWFD, is based on the knowledge acquired after executing the first part of the analysis, i.e. the CFDTD. This means that after calculating the dispersion curve, the eigenvalue pairs will be passed on to the FWFD for calculating the field patterns. It has to be pointed out that the CFDTD by itself is also capable of calculating the field patterns. But, the method will be very inefficient compared to FWFD. This is due to

the presence of an unnecessary time variable in CFDTD formulation when only field pattern calculation is desired.

Finally, some new spectral estimation techniques were investigated. These techniques are far more efficient and accurate than standard DFT or FFT techniques. The application of some previously known methods, as well as proposition of a new one, were discussed in chapter five.

VI.B. Future Works

Time Domain (CFDTD)

- *Expanding the technique to generalized coordinate systems.*
- *Developing an adaptive CFDTD.*
- *A user friendly CAD package that provides the complete dispersion curves.*

Finite Difference (CFDTD)

- *Expanding the technique to generalized coordinate systems*
- *Developing an adaptive FWFD.*
- *A user friendly CAD package that provides the complete dispersion curves.*
- *Still some improvements are required to make the method more reliable and stable.*

Signal Processing Techniques

- *Performing a comparative study between AR, MEM, Prony, Prony-Hildebrand and SVD based Prony Hildebrand method.*
- *Maximum Covariance Method to improve the current problems encountered using MEM method.*

APPENDICES

Appendix A: TE-TM decomposition theorem

THEOREM:

"At cut-off frequencies, i.e. $\beta = k_z = 0$, all modes are either TE or TM"

Note that in general, in inhomogeneous and/or anisotropic waveguides, for a non-zero value of k_z, almost all the modes are of hybrid type, i.e. a mode with all six vector components present.

PROOF:

Assuming $\frac{\partial}{\partial z} = 0$ in equations (II.13.a)-(II.13.f) which is in fact equivalent to the cut-off frequency assumption, i.e. $\beta = k_z = 0$ in phasor domain, yields:

$$\frac{\partial H_x}{\partial t} = \frac{1}{\mu}\left(-\frac{\partial E_z}{\partial y} - \rho_m H_x\right) \tag{A.1}$$

$$\frac{\partial H_y}{\partial t} = \frac{1}{\mu}\left(\frac{\partial E_z}{\partial x} - \rho_m H_y\right) \tag{A.2}$$

$$\frac{\partial E_z}{\partial t} = \frac{1}{\varepsilon}\left(-\frac{\partial H_x}{\partial y} + \frac{\partial H_y}{\partial x} - \sigma E_z\right) \tag{A.3}$$

$$\frac{\partial E_x}{\partial t} = \frac{1}{\varepsilon}\left(\frac{\partial H_z}{\partial y} - \sigma E_x\right) \tag{A.4}$$

$$\frac{\partial E_y}{\partial t} = \frac{1}{\varepsilon}\left(-\frac{\partial H_z}{\partial x} - \sigma E_y\right) \tag{A.5}$$

$$\frac{\partial H_z}{\partial t} = \frac{1}{\mu}\left(\frac{\partial E_x}{\partial y} - \frac{\partial E_y}{\partial x} - \rho_m H_z\right) \qquad \textbf{(A.6)}$$

Note that in the aforementioned equations, each of them corresponds to its counterpart in the set of equations (II.13.a)-(II.13.f), except for equations (A.3) and (A.6) which have interchanged their positions.

A quick inspection of the above equations reveals the fact that these equations constitute two sets of uncoupled differential equations. The first set consists of H_x, H_y and E_z vector field components and hence is a **TM** type mode. While the second one consists of E_x, E_y and H_z vector field components and hence is a **TE** type.

It has to be emphasized that this theorem is valid for the most general case, i.e. lossy anisotropic inhomogeneous waveguide.

Appendix B: Singular value decomposition theorem [41]

SVD IS THE most robust matrix decomposition technique.

THEOREM:

Any $M \times N$ matrix A whose number of rows M is greater than or equal to its number of columns N, can be written as the product of an $M \times N$ column orthogonal matrix U, an $N \times N$ diagonal matrix W with positive or zero elements, singular values, and the transpose of an $N \times N$ orthogonal matrix V.

$$\left[\ A\ \right]_{M\times N} = \left[\ U\ \right]_{M\times N} \bullet \left[\ W\ \right]_{N\times N} \bullet \left[\ V^T\ \right]_{N\times N}$$

in which the following orthogonality relationship holds:

$$\sum_{i=1}^{M} U_{ik}U_{in} = \delta_{kn} \qquad \begin{matrix} 1 \le k \le N \\ 1 \le n \le N \end{matrix}$$

$$\sum_{j=1}^{N} V_{jk}V_{jn} = \delta_{kn} \qquad \begin{matrix} 1 \le k \le N \\ 1 \le n \le N \end{matrix}$$

The most important feature of an SVD decomposition is that it can even deal with non-square matrices. Also, the condition number of the matrix A is defined as the ratio between the largest element of the diagonal matrix W to its smallest element.

Since matrices U and V are orthonormal matrices, their inverse can be obtained by simply transposing them. Also, the inverse of the diagonal matrix W can be obtained by inverting its diagonal elements. Therefore:

$$A^{-1} = \left[U \bullet W \bullet V^T\right]^{-1} = \left[V^T\right]^{-1} \bullet W^{-1} \bullet U^{-1}$$

$$A^{-1} = V \bullet \left[diag\left(\frac{1}{w_i}\right)\right] \bullet U^T$$

This means that once the SVD decomposition is performed, the inverse of the matrix is also readily available. The only possible difficulty occurs when one or more elements of the diagonal matrix W is zero, i.e. $w_i = 0$. Obviously, having at least one zero diagonal element in matrix W means that the condition number of the original A matrix has been infinity. Therefore, unless the matrix A is a singular matrix, this situation will never occur. On the other hand, a singular matrix by definition can not have an inverse in the strict sense. This means that there has been a linear dependency between the equations from which the A matrix is originated. Eventhough, there would not be any inverse for a singular matrix, but one may still be interested in calculating the inverse in the least square sense. The beauty of the SVD decomposition is that even under such circumstances, the inverse of a singular matrix can still be achieved by simply substituting the infinite elements of W^{-1}, i.e. $\frac{1}{w_i} \to \infty$, with zero, i.e. $\frac{1}{w_i} \to 0$. The proof of this procedure can be found in the literature [64].

Appendix C: List of Publications

[1] A. Asi and L. Shafai, "**Dispersion analysis of anisotropic inhomogeneous waveguides using 2D-FDTD**," **IEE** Electronics Letters, pp. 1451-1452, 16th July 1992.

[2] A. Asi and L. Shafai, "**Extrapolating time domain data using autoregressive and maximum entropy methods**," Proceedings of ANTEM92, pp. 405-410, Aug. 5-7, 1992, Winnipeg, Canada.

[3] A. Asi and L. Shafai, "**Errata-Dispersion analysis of anisotropic inhomogeneous waveguides using 2D-FDTD**," **IEE** Electronics Letters, 1992.

[4] A. Asi, L. Shafai, "**A new time domain analysis of bounded waveguides and coupled lines**," Proceedings of **ICEE**' 93, vol.4, pp. 70-79, May 1993, Tehran, Iran.

[5] A. Asi, L. Shafai, "**Multiple mode analysis of waveguides using Compact FDTD**," **IEEE** AP-S symposium digest, vol.1, pp. 360-363, 1993, Ann Arbor, Michigan.

[6] A. Asi, L. Shafai, "**Field pattern computation of the waveguides**," **IEEE** AP-S, URSI symposium digest, pp. 462, June 1994, Seattle, Washington.

[7] A. Asi and L. Shafai, "**Field patterns inside a boxed microstrip line**," Proceedings of **ANTEM94**, pp. 345-348, Aug. 2-5, 1994, Ottawa, Canada.

[8] A. Asi and L. Shafai, "**Full Wave Finite Difference (FWFD),**" Submitted for publication to **IEEE** Microwave Theory and Techniques transaction.

[9] A. Asi and L. Shafai, "**SVD based Prony Hildebrand Technique for CFDTD Processing,**" Accepted for publication by **URSI-95** International Conference.

[10] A. Asi and L. Shafai, "**Cavity Microstrip Antenna with Radome,**" Accepted for publication by **IEEE AP-95** International Conference.

Appendix D: Major Contributions

[1] Introducing and developing a new Finite Difference Time Domain technique for calculating eigenvalues (dispersion curves) of guided wave structures, **COMPACT FDTD**.

[2] Introducing and developing a novel Finite Difference technique for calculating eigenvectors (field patterns) of guided wave structures, **FULL WAVE FINITE DIFFERENCE (FWFD)**.

[3] Applying advanced signal Processing techniques such as **AUTO REGRESSIVE** and **MAXIMUM ENTROPY METHOD** to dispersion curve analysis of guided wave structures.

[4] Introducing and enhancing a new signal processing technique, **SVD BASED PRONY-HILDEBRAND**.

REFERENCES

IX. REFERENCES

[1] S. M. Saad, ***"Review of numerical methods for the analysis of arbitrarily shaped microwave and optical dielectric waveguides"***, **IEEE** Trans. Microwave Theory Tech., vol. **MTT**-33, pp. 894-899, Oct. 1985.

[2] T. Itoh, "***Numerical techniques for microwave and millimeter wave passive structures,***" **Wiley** Interscience, 1989.

[3] T. Itoh. "***An overview on numerical techniques for modeling miniaturized passive components,***" Annales des Telecommunications, vol. 41, pp. 449-462, Sept.-Oct.1986.

[4] I. Bahl, P. Bhartia, "***Microwave solid state circuit design,***" **Wiley** Interscience, 1988.

[5] K. Bierwirth, N. Schulz, F. Arndt, "***Finite difference analysis of rectangular dielectric waveguide structures,***" **IEEE** Trans. Microwave Theory Tech., vol. **MTT**-34, pp. 1104-1114, Nov. 1986.

[6] G. Mur, "***A new time domain analysis of bounded waveguides and coupled lines,***" Proceedings of **ICEE**' 93, vol.4, pp. 70-79, May 1993, Tehran, Iran.

[7] A. W. Snyder, J. D. Love, "***Optical waveguide theory,***" **Chapman and Hall**, 1983.

[8] W. J. R. Hoefer, "***The transmission line matrix method-theory and applications,***" **IEEE** Trans. Microwave Theory Tech., vol. **MTT**-33, pp. 882-893, Oct. 1985.

[9] DA. Taflove, K. R. Umashankar, "***Review of FDTD numerical modeling of electromagnetic wave scattering and radar cross section,***" Proceedings of the **IEEE**, pp. 682-699, 1989.

[10] N. Yoshida, T. Kashiwa, N. Kukutsu, I. Fukai, "***Three dimensional formulation of time dependent wave propagation in a gyroanisotropic medium by Bergeron's method***," **Wave Motion** 10, pp. 611-626, 1988.

[11] N. Yoshida, I. Fukai and Fukuoka, "***Transient analysis of a stripline having a corner in three dimensional space***," **IEEE** Trans. Microwave Theory Tech., vol. **MTT**-32, pp. 491-498, May 1984.

[12] P. B. Johns, "***On the relationship between TLM and finite difference methods for Maxwell's equations***," **IEEE** Trans. Microwave Theory Tech., vol. **MTT**-35 (1), pp. 60-61, Dec. 1987.

[13] D.H. Choi and W.J.R. Hoefer, "***The finite difference time domain method and its application to eigenvalue problems***," **IEEE** Trans. Microwave Theory Tech., vol. **MTT**-34, pp. 1464-1470, Dec. 1986.

[14] S. Akhtarzad, "***Analysis of lossy microwave structures and microstrip resonators by the TLM method***," Ph.D. dissertation, **University of Nottingham**, May 1975.

[15] P. B. Johns, "***A new mathematical model to describe the physics of propagation***," **The Radio and Electronic Engineer**, vol. 44, pp. 657-666, Dec. 1974.

[16] A. Taflove, "***Computational Electrodynamics: the finite difference time domain method***," **Artech House**, 1995.

[17] E. Schweig, W.B. Bridges, "***Computer analysis of dielectric waveguides: A finite difference method***," **IEEE** Trans. Microwave Theory Tech., vol. **MTT**-32, pp. 531-541, May 1984.

[18] S. Seki, T. Yamanaka, K. Yokoyama, "***Two dimensional analysis of optical waveguides with a nonuniform finite difference method***," **IEE** Proceedings-J, vol. 138, pp. 123-127, Apr. 1991.

[19] C. M. Kim, R. V. Ramaswamy, "***Modeling of graded index channel waveguides using nonuniform finite difference method***," **IEEE** Journal of Light Wave Technology, vol. 7, pp. 1581-1589, Oct. 1989.

[20] M. J. Beaubien, A. Wexler, "***An accurate finite difference method for higher order waveguide modes***," **IEEE** Trans. Microwave Theory Tech., vol. **MTT**-16, pp. 1007-1017, Dec. 1968.

[21] J. B. Davies and C. A. Muilwyk, "***Numerical solution of uniform hollow waveguides with boundaries of arbitrary shape***," Proceedings of the **IEE** (London), vol. 113, pp. 277-284, Feb. 1966.

[22] M. J. Beaubien, "***An accurate finite difference method for higher order waveguide modes***," Ph.D. dissertation, **University of Manitoba**, 1970.

[23] G. F. Forsythe and W. R. Wasaw, "***Finite difference methods for partial differential equations***," **Wiley**, 1967.

[24] N. Schulz, K. Bierwirth, F. Arndt, "***Finite difference analysis of integrated optical waveguides without spurious mode solutions***," **IEE** Electronics Letters, pp. 963-965, 28th Aug. 1986.

[25] R. F. Harrington, "***Time Harmonic Electromagnetic fields***," NewYork: **McGraw-Hill**, 1961.

[26] , B. S. Garbow, J. M. Boyle, J.J. Dougarra and C.B. Moler, "***Matrix Eigensystem routines-EISPACK guide extension***," in lecture notes in Computer Science, vol. 51, Heidelberg: **Springer-Verlog**, 1977.

[27] P.B. Johns, R. L. Buerle, "***Numerical solution of two dimensional scattering problems using a transmission line matrix***," Proceedings of the **IEE**, vol. 118, pp. 1203-1208, Sept. 1971.

[28] P. B. Johns, "***The solution of inhomogeneous waveguide problems using a transmission line matrix***," **IEEE** Trans. Microwave Theory Tech., vol. **MTT**-22, No. 3, pp. 209-215, Mar. 1974.

[29] P. B. Johns, "***Application of the transmission line matrix method to homogeneous waveguides of arbitrary cross section***", Proceedings of the **IEE**, vol. 119, No.8, pp. 1086-1091, Aug. 1972.

[30] S. Akhtarzad, P. B. Johns, "***Solution of Maxwell's equations in three space dimensions and time by the T.L.M. method of numerical analysis***," Proceedings of the **IEE**, vol. 122, pp. 1344-1348, Dec. 1975.

[31] S. Akhtarzad, P. B. Johns, "***Generalized elements for TLM method of numerical analysis***," Proceedings of the **IEE**, vol. 122, pp. 1349-1352, Dec. 1975.

[32] S. Akhtarzad, P. B. Johns, "***Three dimensional transmission line matrix computer analysis of microstrip resonators***," **IEEE** Trans. Microwave Theory Tech., Vol. **MTT**-23, pp. 990-997, Dec. 1975.

[33] S. Akhtarzad, P. B. Johns, "***Dispersion characteristics of a microstrip line with a step discontinuity***," **IEE** Electronics Letters, vol. 11, pp. 310-311, 10th July, 1975.

[34] S. Akhtarzad, P. B. Johns, "***TLMRES - The TLM computer program for the analysis of microstrip resonators***," **IEEE** Trans. Microwave Theory Tech., **MTT**, pp. 675, Oct. 1976.

[35] E. A. Navarro, V. Such, "***Study of TE and TM modes in waveguides of arbitrary cross-section using an FDTD formulation***," **IEE** Proceedings ~H, **Microwaves, Antennas and Propagation**, pp. 491-494, vol. 139, no. 6, December 1992.

[36] S. Akhtarzad, P. B. Johns, "***TLM analysis of the dispersion characteristics of microstrip lines on magnetic substrates using three dimensional resonators***," **IEE** Electronics Letters, vol. 11, 20th Mar., 1975.

[37] X. Zhang, J. Fang, K.K. Mei, and Y. Liu, "***Calculations of the dispersion characteristics of microstrips by the time domain finite difference method***," **IEEE** Trans. Microwave Theory Tech., vol. **MTT**-36, pp. 263-267, Feb. 1988.

[38] A. Asi and L. Shafai, "***Dispersion analysis of anisotropic inhomogeneous waveguides using compact 2D-FDTD***", **IEE** Electronics Letters., pp. 1451-1452, 16th July 1992.

[39] A. Asi and L. Shafai, "***Errata-Dispersion analysis of anisotropic inhomogeneous waveguides using 2D-FDTD***," **IEE** Electronics Letters, 1992.

[40] Cangellaris, A. C., "***Numerical stability and numerical dispersion of a Compact 2D-FDTD method used for the dispersion analysis of waveguides***," **IEEE** Microwave and guided wave letters, vol.3, No. 1, pp. 3-5, Jan. 1993.

[41] W. H. Press, B. P. Flannery, S. A. Teukolsky, W. T. Vetterling, "***Numerical Recipes (FORTRAN)***," **Cambridge University Press**, 1990.

[42] N. G. Alexopoulos and C. M. Krowne, "***Characteristics of single and coupled microstrips on anisotropic substrates***," **IEEE** Trans. Microwave Theory Tech., vol. **MTT**-26, pp. 387-393, June 1978.

[43] W. Getsinger, "***Microstrip dispersion model***," **IEEE** Trans. Microwave Theory Tech., vol. **MTT**-21, pp. 34-39, Jan. 1973.

[44] N. G. Alexopoulos, "***Integrated-circuit structures on anisotropic substrates***," **IEEE** Trans. Microwave Theory Tech., vol. **MTT**-33, pp.847-881, Oct. 1985.

[45] A. Asi and L. Shafai, "***Multiple mode analysis of waveguides using Compact-FDTD***," **IEEE AP**-93 Digest, vol.1, pp. 360-363, June 28 - July 2, 1993, Ann Arbor, Michigan, U.S.A.

[46] A. K. Tiwari, B. Bhat and R. P. Singh, "***Generalized coupled dielectric waveguide and its variants for millimeter wave applications***," **IEEE** Trans. Microwave Theory Tech., vol. MTT-34, No. 8, pp. 869-875, Aug. 1986.

[47] S. Xiao, R. Vahldieck and H. Jin, "***Full wave analysis of guided wave structures using a novel 2D-FDTD"***, **IEEE** Microwave & Guided Wave Letters, vol.2, no.3, pp. 165-167, May 1992.

[48] A. Asi and L. Shafai, "***Full Wave Finite Difference (FWFD)***," Submitted for publication to **IEEE** Microwave Theory and Techniques transaction.

[49] A. Asi, L. Shafai, "***Field pattern computation of the waveguides***," **IEEE** AP-S, URSI symposium digest, pp. 462, June 1994, Seattle, Washington.

[50] A. Asi and L. Shafai, "***Field patterns inside a boxed microstrip line***," Proceedings of **ANTEM94**, pp. 345-348, Aug. 2-5, 1994, Ottawa, Canada.

[51] A. V. Oppenheim and R. W. Schafer, "***Digital signal processing***," Englewood Cliffs, NJ: **Prentice-Hall**, 1975.

[52] F. J. Harris, "***On the use of windows for harmonic analysis with the discrete Fourier transform***," Proceedings of the **IEEE**, vol. 66, pp. 51-83, Jan. 1978.

[53] A. Asi, L. Shafai, "***Extrapolating time domain data using autoregressive and maximum entropy methods***," Symposium on Antenna Technology and Applied Electromagnetics, Winnipeg, Canada, **ANTEM-92** Conference Proceedings, pp. 405-410, Aug. 5-7, 1992

[54] J. D. Wills, "***Spectral estimation for the transmission line matrix method***," **IEEE** Trans. on Microwave Theory and Techniques, vol. **MTT-38**, no.4, pp.448-451, Apr.1990.

[55] A. Papoulis, "***Signal Analysis***," **McGraw-Hill** 1984.

[56] S. M. Kay and S. L. Marple, "***Spectrum analysis-a modern perspective***," Proceedings of the **IEEE**, vol.69, pp.1380-1419, Nov. 1981.

[57] N. Levinson, "***The Wiener (root mean square) error criterion in filter design and prediction***," **J. Math. Phys.**, vol. 25, pp. 261-278, 1974.

[58] A. Asi and L. Shafai, "***A new time domain analysis of bounded waveguides and coupled lines***," Proceedings of **ICEE**' 93, vol.4, pp. 70-79, May 1993, Tehran, Iran.

[59] J. P. Burg, "***Maximum entropy spectral analysis***," Ph.D. dissertation, Dept. Geophysics **Stanford Univ.**, Stanford, CA, May 1975.

[60] S. L. Marple, "***Digital spectral analysis with applications***," **Prentice Hall**, 1987.

[61] M. L. Van Blaricum, R. Mittra, "***Problems and solutions associated with Prony's method for processing transient data***," **IEEE** Trans. Antennas Propagation, vol. **AP**-26, pp. 174-182, Jan. 1978.

[62] F. B. Hildebrand, "***Introduction to numerical analysis***," New York, **McGraw-Hill**, pp. 457-465, 1974.

[63] A. Asi and L. Shafai, "***SVD based Prony Hildebrand Technique for CFDTD Processing***," Accepted for publication by **URSI-95** International Conference.

[64] G. H. Golub and C. F. Van Loan, "***Matrix computations***," Baltimore, **Johns Hopkins University Press**, 1983.